

Barbara Obereigner, BSc

**Synthesis of luminescent star polymers for the  
investigation of triplet-triplet annihilation photon up-  
conversion**

**MASTERARBEIT**

zur Erlangung des akademischen Grades

Diplom-Ingenieurin

Masterstudium Technische Chemie

eingereicht an der

**Technischen Universität Graz**

Betreuer

Assoc. Prof. Dipl.-Ing. Dr. techn. Gregor Trimmel

Dr. techn. Manuel Hollauf, MSc BSc

Institute for Chemistry and Technology of Materials

Graz, Juni 2018



## Eidesstattliche Erklärung

Ich erkläre an Eides statt, dass ich die vorliegende Arbeit selbstständig verfasst, andere als die angegebenen Quellen nicht benutzt, und die den benutzten Quellen wörtlich und inhaltlich entnommenen Stellen als solche kenntlich gemacht habe. Das in TUGRAZonline hochgeladene Textdokument ist mit der vorliegenden Masterarbeit identisch.

## Affidavit

I declare that I have authored this thesis independently, that I have not used other than the declared sources/resources, and that I have explicitly indicated all material which has been quoted either literally or by content from the sources used. The text document uploaded to TUGRAZonline is identical to the present master's thesis.

---

*Datum/Date*

---

*Unterschrift/Signature*

## Abstract

The aim of this master thesis was to study triplet-triplet annihilation photon up-conversion (TTA-UC) in defined polymeric architectures. TTA-UC requires two dyes: a so-called sensitizer and an emitter to interact with each other. The absorption of light by the sensitizer molecule leads to the population of excited triplet states. The energy of the sensitizer's triplet states can be transferred radiationless to an excited triplet state of a close emitter dye via triplet-triplet energy transfer. The annihilation of two excited emitter triplet states leads to an excited singlet state of higher energy, which decays radiatively. The emission of photons of higher energy is thereby observable as anti-Stokes-fluorescence. TTA-UC is interesting for various applications such as photovoltaics, optical data storage, and bioimaging. However, TTA-UC in polymeric materials is still a rather new field of research. In this work, TTA-UC star polymers with platinized benzoporphyrins in the center and copolymers of methyl acrylate and perylene-functionalized acrylates as emitter arms were synthesized. Based on preliminary studies, a ratio of 4:1, emitter molecules to sensitizer molecules was chosen. The distance between sensitizer and emitter was varied in order to investigate the dependence of polymer arm lengths on the quantum yield. The core-first approach was chosen for star polymer synthesis by atom transfer radical polymerization (ATRP) respectively reversible addition-fragmentation chain transfer (RAFT) polymerization. From a bulk of preliminary experiments to synthesize statistical copolymers, RAFT polymerization emerged as a versatile approach. Three star polymers of different chain lengths per arm (100, 250, and 500) were prepared by RAFT polymerization using the R-group-approach. In principle, polymerization was observed but lower molecular weights than expected were found, presumably due to termination events. Therefore, the polymerization strategy has to be adapted in further studies in order to avoid early termination or further side reactions. The best TTA-UC quantum yield (1.75%) has been observed for the star polymer with the lowest theoretical arm lengths, 100 per arm, obtained by excitation by a 635 nm monochromatic laser source.

## Kurzfassung

Das Ziel dieser Masterarbeit war die Untersuchung der Triplett-Triplett-Annihilierung Photonen-Hochkonversion (TTA-UC) in definierten Polymerarchitekturen. TTA-UC erfordert das Vorhandensein von zwei Farbstoffen, dem sogenannten Sensitizer und dem Emitter, die miteinander interagieren. Die Absorption von Licht durch ein Sensitizermolekül führt zur Besetzung von angeregten Triplett-Zuständen. Die Energie der Triplett-Zustände des Sensitiveurs wird durch Triplett-Triplett Energietransfer strahlungslos an einen angeregten Triplett-Zustand eines naheliegenden Emitter-Farbstoffes übertragen. Die Annihilierung zweier angeregter Triplets des Emitters führt zu einem Singlett-Zustand höherer Energie, der unter Abgabe von Strahlung zerfällt. Infolgedessen wird bei Emission von Photonen höherer Energie Anti-Stokes-Fluoreszenz wahrgenommen. TTA-UC findet großes Interesse bei Anwendungen in verschiedenen Bereichen, z.B. für Solarzellen, optischer Datenspeicherung und Bioimaging. Dennoch ist TTA-UC in Polymeren ein relativ junges Forschungsgebiet. Im Zuge dieser Arbeit wurden TTA-UC Sternpolymere mit platinieren Benzoporphyrinen als Zentren und Copolymere aus Methylacrylat und Perylene-funktionalisierten Acrylaten als Emitter-Arme synthetisiert. Basierend auf vorhergehenden Arbeiten wurde ein Verhältnis von 4:1, Emittermolekülen zu Sensitizermolekülen, gewählt. Der Sensitizer-Emitter Abstand wurde variiert, um die Abhängigkeit der Polymerarmlängen auf die Quantenausbeute zu untersuchen. Zur Synthese der Sternpolymere wurde der „Core-first“ Ansatz gewählt, und radikalische Atom-Transfer Polymerisation (ATRP) und reversible Addition-Fragmentation Kettentransferpolymerisation (RAFT) versucht. Im Rahmen vieler Vorversuche zur Herstellung statistischer Copolymere ging die RAFT-Polymerisation als vielseitige Methode hervor. Drei Sternpolymere mit verschiedenen Kettenlängen pro Arm (100, 250 und 500) wurden mithilfe der RAFT-Polymerisation nach dem R-Gruppen-Ansatz synthetisiert. Im Wesentlichen wurde eine Polymerisation festgestellt, jedoch wurden niedrigere Molekulargewichte als erwartet erreicht, vermutlich aufgrund von Terminierungsreaktionen. Die Polymerisationsmethode sollte daher für weiteren Studien adaptiert werden, sodass frühzeitige Terminierungs- und Nebenreaktionen vermieden werden können. Die beste TTA-UC Quantenausbeute (1,75%) wurde für das Sternpolymer mit der kleinsten theoretischen Armlänge (100) beobachtet, welches mit einer 635 nm Laserdiode angeregt wurde.

## Acknowledgement

An erster Stelle würde ich gerne Prof. Gregor Trimmel danken, der die Arbeit von Anfang an unterstützt und ermöglicht hatte.

Dr. Manuel Hollauf ist ebenfalls als Mitbetreuer im Besonderen zu erwähnen, der die Arbeit mit viel Erfahrung und zahlreichen praktischen Tipps bereichert hat. Er inspirierte mich, Ergebnisse von verschiedenen Seiten zu beleuchten und neue Ansätze zu versuchen.

Außerdem sei Dr. Christian Rossner erwähnt, der seine Expertise für RAFT- Polymerisationen einbrachte, sowie Dr. Peter Zach, mit dem die TTA-UC Messungen gemeinsam durchgeführt wurden.

Im Weiteren möchte ich der Arbeitsgruppe Trimmel und dem am Institut für Chemische Technologien an Materialien beteiligten Personen danken, die für ein angenehmes Arbeitsklima sorgten, mit denen gesellige Runden verbracht werden konnten, und mit denen diese Zusammenarbeit innerhalb des Institutes ermöglicht wurde.

In diesem Zusammenhang möchte ich Fr. Ing. Hobisch, Fr. Dr. Kaschnitz und Fr. Ing. Bartl für die Durchführung von Gelpermeationschromatographie bzw. für die Instruktion bei NMR und MALDI-TOF- Massenspektrometrie danken.

Im Speziellen sei nun meinen Studienkollegen, meinen Musikvereinskollegen und meinen Freunden gedankt, mit denen ich eine wertvolle und unvergessliche Zeit hier in Graz sowie auch in Oberösterreich verbracht habe.

Und nicht zuletzt und vor allem besonders, sei meinen Eltern und meiner Verwandtschaft gedankt, die mich unterstützt haben und die Entschlossenheit meine Entscheidungen zu treffen gefördert haben, sowie meinen fünf Geschwistern, die immer wieder Erheiterung gebracht haben.

## Abbreviations

ATRP	atom transfer radical polymerization
CH	cyclohexane
CTA	chain transfer agent
DCM	dichloromethane
EA	ethyl acetate
ISC	intersystem crossing
LAM	less activated monomer
MA	methyl acrylate
MALDI-TOF	matrix assisted laser desorption ionisation – time of flight
MAM	more activated monomer
MMA	methyl methacrylate
NMP	nitroxide mediated polymerization
NMR	nuclear magnetic resonance
PDI	polydispersity index
RAFT	reversible addition fragmentation chain transfer
RDRP	reversible deactivation radical polymerization
ROMP	ring opening metathesis polymerization
St	styrene
TCT	thiocarbonylthio
TLC	thin layer chromatography
TTA-UC	triplet-triplet annihilation photon up-conversion
TTET	triplet-triplet energy transfer

# Table of Content

<b>1. Introduction .....</b>	<b>11</b>
<b>2. Theoretical Background .....</b>	<b>13</b>
2.1 Triplet-triplet annihilation photon up-conversion .....	13
2.1.1 Porphyrin as a sensitizer .....	16
2.1.2 Perylene as an emitter .....	17
2.1.3 TTA-UC in polymers.....	17
2.2 Reversible deactivation radical polymerization techniques .....	20
2.2.1 RAFT .....	21
2.2.1.1 RAFT mechanism.....	21
2.2.1.2 Selection of R and Z groups .....	23
2.2.1.3 Star polymers by RAFT .....	24
2.2.2. ATRP .....	25
2.2.2.1 Kinetics of copper-catalyzed ATRP.....	26
2.2.2.2 ARGET ATRP .....	27
2.2.2.3 Star polymers by ATRP .....	28
<b>3. Materials and Methods.....</b>	<b>29</b>
3.1 Chemicals .....	29
3.2 Equipment.....	29
<b>4. Experimental.....</b>	<b>31</b>
4.1 Dye Synthesis .....	31
4.1.1 Synthetic pathway of the benzoporphyrin dyes monomers.....	31
4.1.1.1 Zn(II) tetrabromo meso-tetraphenyl tetra(tert-butyl)benzoporphyrin (Br <sub>4</sub> TPTBTBP Zn).....	34
4.1.1.2 Tetrabromo meso-tetraphenyl tetra(tert-butyl) benzoporphyrin (Br <sub>4</sub> TPTBTBP) 35	
4.1.1.3 Pt(II) tetrabromo meso-tetraphenyl tetra(tert-butyl)benzoporphyrin (Br <sub>4</sub> TPTBTBP Pt) .....	36
4.1.1.4 Pt(II) tetrahydroxymethylphenyl meso-tetraphenyl tetra(tert-butyl)-benzoporphyrin (HMP <sub>4</sub> TPTBTBP Pt).....	37
4.1.1.5 Pt(II) tetra(2-bromopropanoatemethylphenyl) meso-tetraphenyl tetra(tert-butyl)-benzoporphyrin (BPMP <sub>4</sub> TPTBTBP Pt) .....	38
4.1.1.6 Pt(II) dibromo di(2-bromopropanoatemethylphenyl) meso-tetraphenyl tetra(tert-butyl)-benzoporphyrin (Br <sub>2</sub> BPMP <sub>2</sub> TPTBTBP Pt).....	40
4.1.1.7 Pt(II) tetra(((2-hexylthio)thioxomethyl)thiopropionatemethylphenyl) meso-tetraphenyl tetra(tert-butyl)-benzoporphyrin (HTP <sub>4</sub> TPTBTBP Pt) .....	41
4.1.1.8 Pt(II) monobromo tris(((2-hexylthio)thioxomethyl)thiopropionate methylphenyl) meso-tetraphenyl tetra(tert-butyl)-benzoporphyrin (Br HTP <sub>3</sub> TPTBTBP Pt ) .....	43

4.1.2	Synthetic pathway of PDE <sub>mon</sub> .....	45
4.1.2.1	Potassium perylene 3,9-dicarboxylate (PDC) .....	46
4.1.2.2	3-butyl 9-(6-hydroxyhexyl) perylene-3,9-dicarboxylate (PDE) .....	47
4.1.2.3	3-(6-(acryloyloxy)hexyl)9-butyl perylene-3,9-dicarboxylate (PDE <sub>mon</sub> ) ..	48
4.2	Polymer Synthesis .....	50
4.2.1	Preliminary studies and strategic considerations for RAFT polymerization 50	
4.2.1.1	Statistical perylene-MA-copolymer.....	51
4.2.1.2	Statistical perylene-MMA-copolymer.....	53
4.2.1.3	Benzoporphyrin-MA star polymer .....	54
4.2.1.4	Benzoporphyrin-MMA star polymer.....	55
4.2.1.5	Statistical benzoporphyrin-MA-perylene star polymer .....	56
4.2.1.6	Statistical benzoporphyrin-MMA-perylene star polymer .....	57
4.2.2	Preparation of star polymers .....	59
4.2.2.1	Polymer I .....	59
4.2.2.2	Polymer II .....	60
4.2.2.3	Polymer III .....	62
4.2.3	Strategic considerations for ATR polymerization .....	64
4.2.3.1	PMMA as a model substance .....	65
4.2.3.2	Copolymer of Br <sub>2</sub> BPMP <sub>2</sub> TBPTBTBP Pt and MMA as matrix monomer 66	
<b>5.</b>	<b>Results and Discussion.....</b>	<b>68</b>
5.1	Dye Characterization.....	68
5.1.1	Benzoporphyrin synthesis and characterization .....	68
5.1.1.1	Identification of HTP <sub>4</sub> TPTBTBP Pt and Br HTP <sub>3</sub> TPTBTBP Pt.....	71
5.1.1.2	Identification of BPMP <sub>4</sub> TPTBTBP Pt and Br <sub>2</sub> BPMP <sub>2</sub> TPTBTBP Pt....	72
5.1.2	Perylene diester synthesis and characterization.....	73
5.2	Polymer Characterization .....	76
5.2.1	Preliminary studies.....	76
5.2.1.1	Selection of the matrix .....	76
5.2.2	Star polymers.....	79
5.3	ATRP experiments .....	85
5.4	TTA-UC measurements .....	88
5.4.1	Quantum yields .....	90
5.4.2	Light irradiance dependent measurements.....	91
<b>6.</b>	<b>Outlook and Conclusions.....</b>	<b>93</b>
<b>7.</b>	<b>References.....</b>	<b>96</b>
<b>8.</b>	<b>List of Tables .....</b>	<b>100</b>

<b>9.</b>	<b>List of Figures.....</b>	<b>101</b>
<b>10.</b>	<b>Appendix.....</b>	<b>103</b>

## 1. Introduction

In this master thesis, defined polymeric architectures were designed to study triplet-triplet annihilation photon up-conversion (TTA-UC). The absorption of light causes the up-conversion, which is the energy conversion of photons of lower energy to photons of higher energy. TTA-UC is a process consisting of multiple steps generating photons of higher energy. Thereby, the energy of the excited sensitizer is lower than the first excited populated state of the emitter. However, many steps are preceded before fluorescence is apparent, such as absorption by the sensitizer, population of its first singlet excited state, intersystem crossing, triplet-triplet energy transfer between the sensitizer and the emitter, triplet-triplet annihilation and first singlet excited state of one of the emitters. The decay of the excited state to the ground state can be observed as anti-Stokes fluorescence. As a sensitizer, typically a metal-ligand complex<sup>1</sup> having a high quantum yield of triplet state formation is used. Pt(II) and Pd(II) complexes with *meso*-tetraphenyl-tetrabenzoporphyrins as ligands have been reported as optical oxygen sensors<sup>1,2</sup>. In the presence of oxygen, the luminescence of these metal-ligand complexes is quenched. However, the sensitivity of these Pt(II) and Pd(II) *meso*-tetraphenyltetrabenzoporphyrin complexes regarding oxygen concentration and partial pressures is low. As such, they show high molar absorption coefficients, strong phosphorescence at room temperature and large Stokes' shifts<sup>3</sup>, so they are excellent suited as sensitizers in TTA-UC. Typically, polycyclic aromatic hydrocarbons<sup>1</sup> are applied as annihilators in TTA-UC, featuring lower triplet states than the sensitizer. In our case, a perylene diester was used, which features the fluorescence maximum at 510 nm. At this wavelength, the absorption of the benzoporphyrin complexes is inefficient. As sensitizer- emitter pair, platinum(II) benzoporphyrin was used in combination with a functionalized spacer bearing the perylene diester moiety. Platinum(II) benzoporphyrin was selected as the center of a star polymer, and copolymers of methyl acrylate and perylene-functionalized acrylates as emitter arms were synthesized. In order to investigate the TTA-UC at different chain lengths, a reversible deactivation radical polymerization (RDRP) technique was chosen to achieve low polydispersity indices (PDIs). To the best of our knowledge, there has been no example reported like that before, as well as on platinum(II)-porphyrins as central cores of star polymers in coherence with

TTA-UC. As reversible deactivation radical polymerization techniques (RDRP), atom transfer radical polymerization (ATRP) and radical addition fragmentation transfer (RAFT) were tested. Even though ATRP is one of the most current and popular approaches<sup>4-7</sup> for star polymer synthesis starting from a (metal) porphyrin-core, no polymeric substance was obtained. The reasons for this are discussed in chapter 5.3. The main reason can be attributed to the fact, that only a limited number of metals can be used inside the porphyrin core (i.e. Zn<sup>II</sup>, Pd<sup>II</sup>)<sup>4-6</sup> in order to perform ATRP. This is due to the interactions of these metals with the copper catalyst. In addition, it was reported that the subsequent removal of the copper catalyst was challenging and often lead to the decomposition of the polymer.<sup>8</sup> However, by using RAFT polymerization for star polymer synthesis via R-group approach, a polymer was yielded. This is consistent as RAFT is a metal-free living radical system, which has been proven to be compatible with a wide range of monomers.<sup>4</sup> As explained in the latter chapters (2.2.1.3; 5.2), star polymer synthesis by RAFT polymerization via R-group approach is also challenging due to termination reactions. Numerous literature examples were studied in order to find comparable strategies. There were some examples found about the RDRP of a perylene moiety (ATRP, RAFT, NMP)<sup>9-11</sup>, but there was no research found about the copolymerization of a perylene moiety with a platinum(II)- porphyrin by RDRP. Based on the recent study Hollauf et al. presented on the successful synthesis of terpolymers<sup>12</sup> by ring opening metathesis polymerization (ROMP), the preparation of starpolymers by RDRP techniques and investigation of TTA-UC was the consequential goal of this master thesis.

## 2. Theoretical Background

### 2.1 Triplet-triplet annihilation photon up-conversion

Photon up-conversion<sup>13–15</sup>, which is the observation of photon emission, accomplished through sensitized TTA was first reported by Parker and Hatchard (15) in 1962. Parker and Hatchard prepared donor/acceptor solutions<sup>15</sup> containing phenanthrene/naphthalene and reported the observations as delayed fluorescence.

Photon up-conversion is the process observed of photons having a higher energy than the excitation energy. Another term relevant to this topic is anti-Stokes fluorescence<sup>13,16</sup>, which confers to the wavelengths and is defined as the excitation at lower energy (longer wavelength) with the subsequent population of excited states at higher energy (shorter wavelength). Due to many possible applications, such as photovoltaics, artificial photosynthesis, photocatalysis, and optics, up-conversion is an attractive phenomenon to research.

There is a large quantity of up-converting processes, such as second- or third-harmonic generation and two-photon absorption emission. In order to trigger them, coherent, high power light is required. This is, for example produced by lasers. In contrast to that, photon up-conversion by triplet–triplet annihilation (TTA-UC) is already feasible with non-coherent, polychromatic excitation. In contrast to that, TTA-UC is accomplishable at much lower power densities. As the Shockley–Queisser solar power conversion limit can be conquered, the part of the solar spectrum beyond a solar cell's bandgap<sup>16</sup> can be recovered. Therefore, TTA-UC is a promising tool to use the otherwise-wasted lower-energy range of the solar spectrum<sup>17</sup> for potential applications in photovoltaics, optoelectronics and security devices. However, the absorption of the emitter often limits the application in photovoltaics.

TTA-UC-systems consist of a sensitizer and an annihilator alias emitter. The sensitizer, typically a metal-ligand complex absorbs the incident light. The emitter<sup>1</sup> is usually a polycyclic aromatic hydrocarbon with the triplet state located lower than that of the sensitizer. By the excitation of a sensitizer molecule, the energy is

transferred by multiple steps to the emitter and delayed fluorescence<sup>18</sup> is observed, as seen in Figure 1.

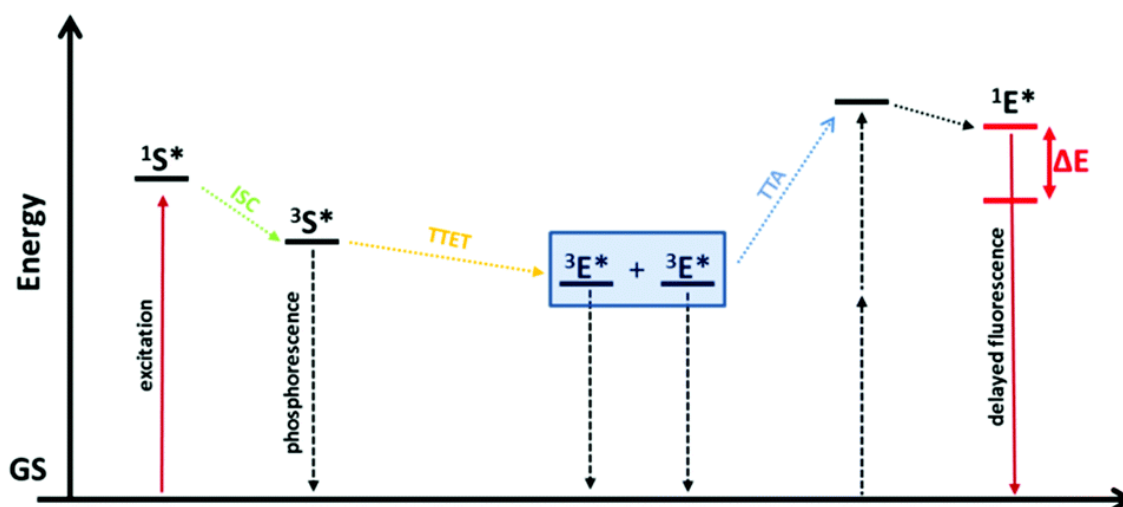


Figure 1. Scheme of the steps involved in the TTA-UC.<sup>12</sup>

In Figure 1, the overall TTA up-conversion process is depicted as a qualitative Jablonski Diagram. As the sensitizer absorbs the excitation energy, the first singlet excited state of a sensitizer ( $1S^*$ ) gets populated. After spin-forbidden intersystem crossing<sup>19</sup> (ISC), the photons relax to the triplet excited state ( $3S^*$ ). The intersystem crossing (ISC) rate increases due to the presence of heavy atoms<sup>20</sup>, thus producing a large number of triplet states from which energy is transferred to the triplet state emitter. The triplet excited state has a longer lifetime than that of the singlet excited state. Consequently, the energy is transferred from the sensitizer to an emitter ( $3E^*$ ) via triplet–triplet energy transfer (TTET). Triplet–triplet annihilation<sup>19</sup> (TTA) of two emitter triplets populate the emitter first singlet excited state ( $1E^*$ ) which is of higher energy, then the first excited singlet state of the sensitizer. The radiative decay of this excited state is visible as fluorescence. It has to be considered, that TTA-UC contains Dexter-type energy transfer, which occurs under close proximity of the molecules.<sup>13,18</sup>

For an efficient up-conversion process, several factors are required, such as the concentration of triplet states, the power density of the incident light, molecular

mobility and distance of the chromophores. Considering these factors, as well as potential obstacles under ambient conditions<sup>19</sup> like reabsorption of the up-converted emission or quenching by oxygen, it is rather complex to acquire the optical conditions for TTA-UC. Therefore, TTA-UC suffers from low external quantum efficiency<sup>17</sup>, especially in solid systems due to the lack of molecular mobility.

Significant UC emission<sup>18</sup> was observed in liquid solutions as well as rubbery polymers, even at low dye concentrations, on account of appreciable translational mobility of the chromophores in such systems. However, in contrast to that, glassy materials need high dye contents to accomplish up-conversion. The lack of molecular mobility in these materials is dealt with by diffusion of the excitons between the densely packed chromophores. Even so, using the same chromophores, the TTA-UC quantum yields for dilute liquid solutions were reported to be generally higher than for solid state materials. This was reasoned by the different molecular diffusion rate<sup>18,21</sup>.

As TTA-UC is well implemented for solutions, the acquisition of TTA-UC to solid matrices is favorable for innovative applications<sup>16,18</sup>, ranging from soft actuators, display techniques, to solar harvesting, and in vivo bioimaging. As low excitation power densities ( $1 \text{ kWm}^{-2}$ , AM 1.5 global spectrum) are required for TTA-UC, this can be used for organic and inorganic photovoltaic devices, and therefore harvesting energy from the solar spectrum<sup>20</sup>.

### 2.1.1 Porphyrin as a sensitizer

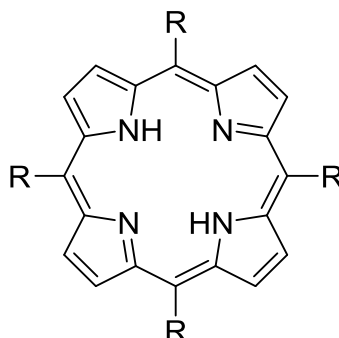


Figure 2. General structure of porphyrin.

Porphyrins<sup>6</sup> are characterized by their aromatic planar macrocycle, exhibiting a cavity. Regarding electronics, it consists of a delocalized 18-electron cloud, linked by four pyrrolic subunits and four methine bridges. (Figure 2). The porphyrin cavity has an inherent high affinity for metal complexation, which is the reason that porphyrins are used as organometallic ligands. Porphyrins are interesting precursors for hybrid materials<sup>22</sup>, and are, as such, used in many devices. Porphyrins show optical properties and have high molar absorption coefficients. Metalloporphyrins can efficiently harvest sunlight<sup>6</sup>. These properties can be changed by adding electron-donating or electron-withdrawing substituents<sup>23</sup> on the meso- and/or  $\beta$ -pyrrole positions, subsequently influencing spectra and electrochemical properties of the compound. However, the solubility of porphyrins in many polymers may be low, and aggregation and/or poor dispersion may arise. This may result in quenching, poor sensitivity, and/or failure of reproducibility in local pressure measurements.<sup>5</sup> One attempt to improve solubility and dispersibility of porphyrins is the attachment of polymerizable groups in thin film preparation, in order to establish covalent bonds.

### 2.1.2 Perylene as an emitter

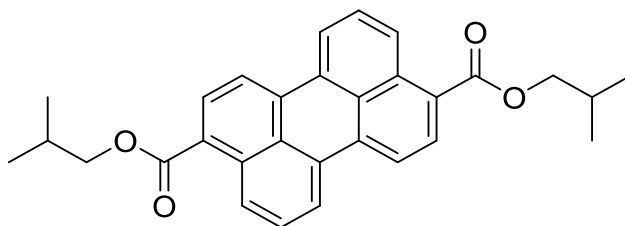


Figure 3. Structure of diisobutyl perylene-3,9-dicarboxylate (Solvent Green 5).

Diisobutyl perylene-3,9-dicarboxylate (Solvent Green 5, Figure 3) is a dye<sup>24</sup> used in industries for coloring plastics, oils and resins. Due to its Stokes shift and high fluorescent quantum yields in purified form, it has been recommended as fluorescent collector. Fluorescent collectors act like chemical lenses in order to concentrate the absorbed light and emit the fluorescent light. Therefore, potential applications are solar cells, clocks, charging equipment, illuminated signs, or displays.<sup>24</sup> Recent publications are concerned with the optimization of the energy state energy levels to increase TTA efficiency by extending the  $\pi$ -conjugation framework.<sup>25,26</sup>

### 2.1.3 TTA-UC in polymers

Since its discovery<sup>16</sup> in the 1960s, TTA-UC was realized in liquid solutions, as molecular mobility and diffusion of the chromophores facilitated the intermolecular energy transfer steps.

The first experiments to operate TTA-UC in polymers were performed with physical mixtures of sensitizers in conjugated polymers. Blends of suitable chromophores containing a rubbery polymer matrix were produced. The goal was to obtain polymer-like systems with mechanical properties. Aggregation of sensitizer

and the emitter respectively was avoided by keeping the concentration below 0.001 wt% and 0.02 wt%.<sup>16</sup>

A well-investigated model system was based on the Pd(II)octaethylporphyrin (PdOEP) as light absorber and sensitizer, and on the 9,10-diphenylanthracene (DPA) as emitter. Solution-casting was chosen as a method to incorporate small amounts of PdOEP and DPA into an ethyleneoxide/epichlorohydrin copolymer matrix. It was shown that the up-converted fluorescence intensity was highly dependent on the temperature and decreased dramatically below the glass transition temperature ( $T_g$ ) of the polymer.<sup>27</sup>

Many other techniques were developed to facilitate TTA-UC in polymers, such as the confinement of chromophores in (nano)particles, soft/liquid core–hard shell assemblies, nanostructured films, or attempts of embedding the sensitizer into a polymeric emitter.<sup>28</sup>

However, the covalent binding<sup>12</sup> of one dye to a polymeric matrix was shown in recent studies, considering a short distance between emitter and sensitizer to establish TTET and TTA (Figure 1). The covalent tethering of a suitable chromophore pair to a polymeric backbone has been observed by Boutin et al. (29), Lee et al. (27) and Hollauf et al. (12). Boutin et al. (29) prepared star polymers containing Ru(bpy)<sub>3</sub> as a sensitizer and 9,10-diphenylanthracene (DPA) as multiple emitter units by RAFT polymerization. They polymerized with 0.2 equ. AIBN for 6-armed polymers at a temperature of 70°C for 24 h. The resulting polymers were depicted in Figure 4. The obtained quantum yield.<sup>29,30</sup> for these polymers was  $1.8 \times 10^{-3}$  (2-armed star polymer) and  $1.9 \times 10^{-3}$  (6-armed star polymer) respectively. For their experiments, a continuous-wave frequency-doubled Nd:YAG laser was selected and excitation was at 532 nm. They measured in deaerated chloroform solution at a concentration of 75  $\mu$ M.

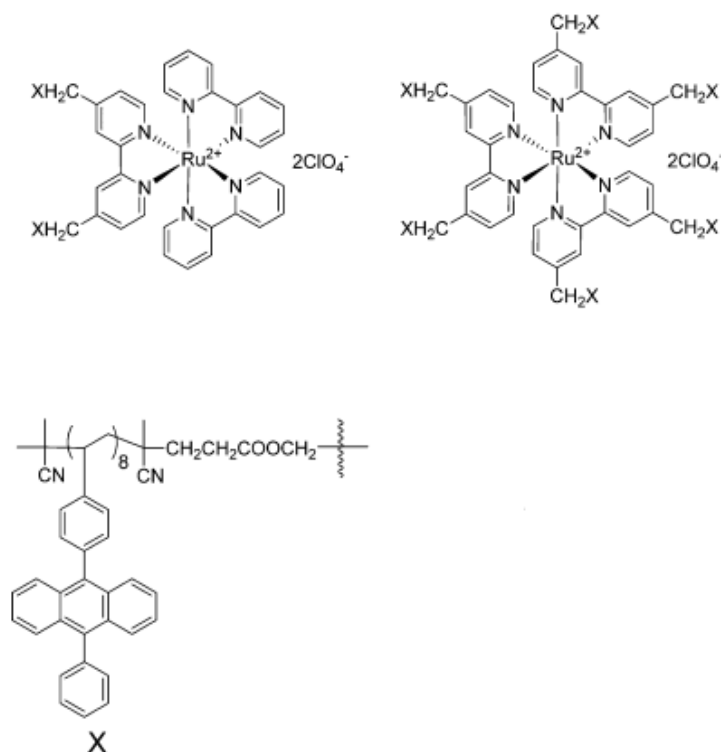


Figure 4. Polymers prepared by RAFT polymerization, carrying Ru(bpy)<sub>3</sub> and DPA units.<sup>29</sup> Copyright (2013) Elsevier.

Lee et al. copolymerized the monomer palladium meso-phenoxy-tris(heptyl)porphyrin-ethylmethacrylate (PdmPH3PMA), with a diphenylanthracene methacrylate (DPAMA) as the emitter-bearing monomer, and methyl methacrylate (MMA) as an optically inert comonomer (Figure 5).<sup>27</sup> They performed conventional free radical polymerization by using AIBN as an initiator. Higher sensitizer contents did not lead to better up-conversion. Instead, a considerable decrease of both sensitizer fluorescence quantum yield and delayed fluorescence intensity was observed. The results indicated that the decay of up-converted emission was due to the formation of nonradiative dye complexes. However, there was an overlap of the absorption and emission spectra of the sensitizer and emitter, which indicates reabsorption of the emitted light.<sup>27</sup> The excitation was at 532 nm with a Nd:YAG laser.

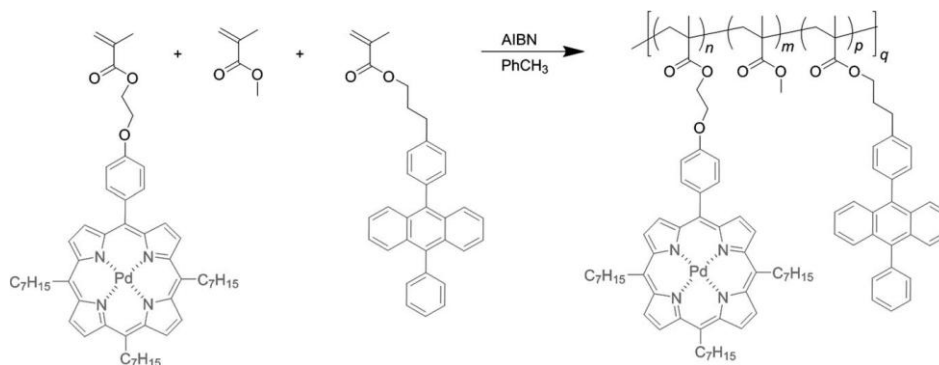


Figure 5. Covalent attachment of PdmPH3PMA, MMA and DPAMA.<sup>27</sup> Copyright (2015) John Wiley and Sons.

Hollauf et al. prepared polymers by ROM polymerization 3-(6-((-Bicyclo[2.2.1]hept-5-ene-2-carbonyl)oxy)hexyl)9-butyl perylene-3,9-dicarboxylate (PDE<sub>mon</sub>), Platinum(II) *meso*-tetraphenyl tetra(*tert*-butyl)benzo porphyrin monomer (TPTBTBP Pt<sub>mon</sub>) and dimethyl-5-norbornene-2,3-dicarboxylate (N-DME) as polymer backbone (Figure 6).<sup>12</sup> The highest quantum yield was achieved for a statistically distributed sensitizer and emitter in an inert matrix, with a value of 3%. It was measured in 1,4-dioxane solution and excitation was at 635 nm with a laser diode.<sup>12</sup>

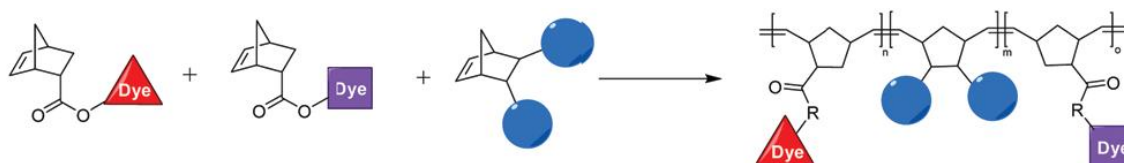


Figure 6. Covalent attachment of PDE, TPTBTBP Pt and DME by Hollauf and Zach.<sup>12</sup>

## 2.2 Reversible deactivation radical polymerization techniques

According to IUPAC, a living polymerization is “a chain polymerization from which irreversible chain transfer and irreversible chain termination (deactivation) are absent”.<sup>31</sup> For a “controlled/living polymerization”, the initiator should be depleted at

an early stage and the equilibrium between active and dormant species should shift fast. However, it is clear that termination events are unavoidable in (radical) polymerization reactions and that side reactions can occur. Therefore, the new term launched by IUPAC for describing controlled radical polymerizations, such as ATRP, NMP, or RAFT was reversible deactivation radical polymerization (RDRP). RDRPs employ dynamic equilibria between active and dormant chains. They are well-suited for block copolymers and sophisticated architectures, which can be available in biomedicine and industry for future applications.

## 2.2.1 RAFT

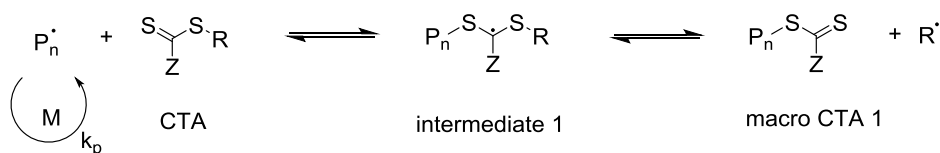
The reversible addition-fragmentation chain transfer (RAFT) polymerization was first reported by the working group of Rizzardo<sup>32</sup> in 1998. The method was exceptional, due to its applicability to a wide range of monomers and reaction conditions. Due to usage of the thiocarbonylthio group (TCT) as a side or end group, complex architectures were easily accessible. Moreover, controlled molecular weights and narrow polydispersity indices could be obtained. Thiocarbonylthio (TCT) compounds were used in combination with conventional initiators, such as azo or peroxy initiators, for instance N,N-azobisisobutyronitril (AIBN) or dibenzoyl peroxide (BPO). Thiocarbonylthio compounds such as dithioesters, dithiocarbamates, trithiocarbonates and xanthates have been well-established as chain transfer agents. However, the appropriate selection of a chain transfer agent (CTA) or RAFT agent, which acts in the mechanism as the dormant species, is essential.

### 2.2.1.1 RAFT mechanism

Basically, the RAFT mechanism is depicted as equilibrium between an active and a dormant species (Figure 7). The RAFT reaction is facilitated by the chain transfer agent (CTA) or RAFT-agent. The CTA bears the R and Z group, whereas the R group is the fragmenting group, and the Z group is the stabilizing group. After

initiation, the radical formed reacts with a monomer with the propagation rate constant  $k_p$ , yielding the propagating radical ( $P_n^\cdot$ ). The propagating radical encounters the “pre”-equilibrium as the active species and adds to the reactive double bond of the dormant thiocarbonylthio function. The newly formed intermediate radical cleaves off the fragmenting group  $R^\cdot$ , which is able to reinitiate with a monomer to yield a second propagating radical ( $P_m^\cdot$ ). The  $P_m^\cdot$  as the active species reacts with the macro CTA 1 (dormant species); after this addition reaction and the subsequent fragmentation reaction, the macro CTA 2 is formed and the  $P_n^\cdot$  is released. As indicated in the reaction scheme, the reactions are reversible. The position of the main equilibrium<sup>33</sup> is controlled by the rate coefficients  $k_{add}$  (addition rate constant) and  $k_{frag}$  (fragmentation rate constant). The combination of  $P_n^\cdot$  and  $P_m^\cdot$  can lead to termination, producing dead chains which cannot react any further. The general mechanism, which is shown here, is well-established. However, the detailed kinetics and side reactions<sup>31</sup> are disputed.

**“pre”-equilibrium:**



**“main”-equilibrium:**

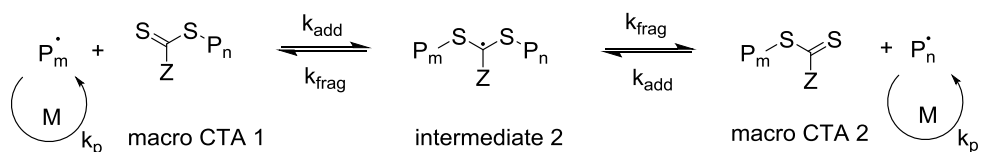


Figure 7. Mechanism of RAFT polymerization.<sup>33</sup>

### 2.2.1.2 Selection of R and Z groups

Two functional groups can be distinguished in RAFT agents (Figure 8). The leaving group (R group) and the stabilizing group (Z group).

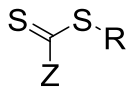


Figure 8. Structure of a thiocarbonylthio RAFT agent.

The leaving group (R group) is generally easily cleavable, because it determines selectivity and accomplishes re-initiation. Therefore, the bond between the S–R functionality is weak and the radical species  $\text{R}^{\bullet}$  has better leaving group abilities than the propagating radical<sup>34</sup> ( $\text{P}_n^{\bullet}$ ) in the pre-equilibrium. The R group leaving ability is influenced by steric and electronic effects.<sup>35</sup>

Moreover, the Z group, or stabilizing group, has an important role. On the one hand, it activates the thiocarbonyl function in order to obtain a high addition rate. On the other hand, it stabilizes the intermediate radical, but only as little as possible in order to obtain a high fragmentation rate. However, the more the thiocarbonyl function is activated, the more the intermediate radical<sup>34</sup> gets stabilized.

In an ideal RAFT polymerization, the rate of addition ( $k_{\text{add}}$ ) should be higher than the rate of propagation ( $k_{\text{p}}$ ) or at least compete. Though, the addition reaction should not be so favored to such a degree that the (reverse) fragmentation reaction is inhibited<sup>36</sup>. Moreover, the ability to react with monomers is similarly crucial to consider: Two classes of monomers can be distinguished, the “more-activated” monomers (MAMs) and “less activated” monomers (LAMs). MAMs such as methyl methacrylate (MMA), methyl acrylate (MA), styrene (St), acrylonitrile (AN) and acrylamide (AM)<sup>31</sup> react with CTAs such as dithioesters (Z = aryl or alkyl) or trithiocarbonates (Z = alkylthio) in a controlled fashion. However, polymers of dithioesters or trithiocarbonates with LAMs such as vinyl acetate (VAc), *N*-vinylpyrrolidone (NVP), and *N*-vinylcarbazole (NVC)<sup>31</sup> cannot be maintained.

Therefore, the selection of the R and Z groups has a great influence, as they determine the progress of the polymerization. However, it also provides control of the polymerization, as the rates of propagation, addition, and fragmentation<sup>37</sup>

can be altered by the structure of the CTA. The careful selection of the appropriate CTA is extremely important and the support of precise kinetic data<sup>36</sup> can be helpful.

### 2.2.1.3 Star polymers by RAFT

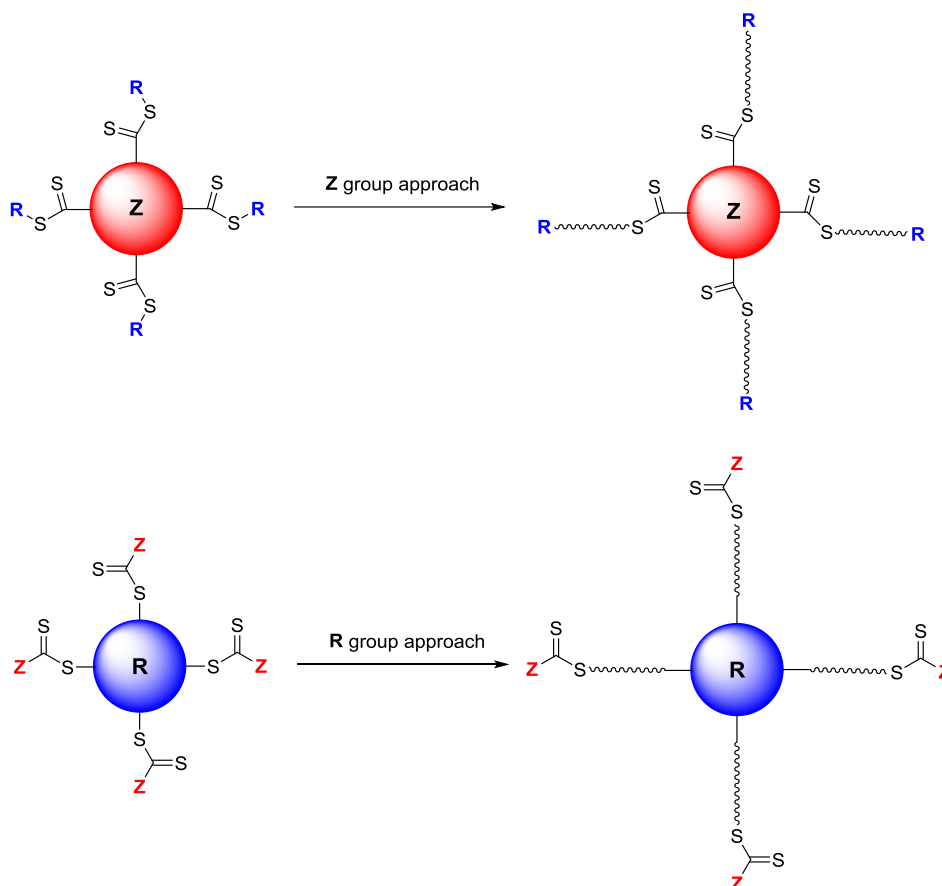


Figure 9. Star polymer synthesis following Z group approach (above) and R group approach (below) respectively.

Star polymers can be synthesized by RAFT polymerization either by the arm-first or by the core-first approach. Core-first RAFT star polymers can be synthesized via two strategies, the Z group approach and the R group approach (Figure 9). In Z star polymers<sup>38,39</sup>, the RAFT-agent remains attached to the core, while in R star polymers<sup>4,40</sup> these moieties are the end groups. The position of the RAFT agent onto the core determines the mechanism<sup>41</sup> and outcome.

Z star polymer synthesis benefits from the low possibility of star–star coupling<sup>31</sup>. However, the Z group approach suffers from the sterically inaccessibility by further reaction progress. The star polymer synthesis via R-group approach is very similar to other RDRP techniques, such as ATRP or NMP. Star-star coupling is a possible bi-radical termination event. Also, for other star polymerizations, such as with core-first ATRP and NMP star-star coupling has been frequently observed. Star polymerization is therefore restricted to the low monomer conversion regime<sup>38</sup> and hampers the formation of long chains and high molecular masses.

Cleavage reactions<sup>4,31,41</sup> of the end-groups (RAFT-agents) that do not destroy the star structure can also occur. The thiocarbonylthio (TCT) function can be lost, consequently linear living chains are found in solution. Due to the inhomogeneity in the star polymer structure, molecular weight distributions are multimodal<sup>38</sup> and broad. A further event, the loss of an active arm could possibly lead to star-chain couplings.<sup>41</sup> Even though, there are several issues associated with the R-group approach, there are several indications<sup>42</sup> that it is more efficient and controlled than the Z group approach. Boschmann et al. reported the formation of high molecular weight compounds by Z group approach<sup>38</sup>, which was attributed to star-star coupling events.

### 2.2.2. ATRP

Another favored RDRP technique to obtain defined macromolecular architectures and functionalities is ATRP. Functional polymeric materials can be established with ATRP, obtaining well-defined structures<sup>43</sup>, such as block copolymers, stars, and combs. As it is common for RDRPs, this is achieved by utilizing dynamic equilibrium between propagating species (free radicals) and dormant species (alkyl halides). ATRP is controlled by an interchange<sup>44</sup> between a metal complex and the organic polymeric chain ends. Due to the well-controlled features, polymers with predictable molecular weights and low polydispersity indices (PDIs) can be obtained. There are many metal complexes reported in the literature, such as with elements of the groups 4 (Ti), 6 (Mo), 7 (Re), 8 (Fe, Ru, Os), 9 (Rh, Co), 10 (Ni, Pd), and 11 (Cu). However, complexes of copper have been found to be

the most efficient catalysts in the ATRP of a broad range of monomers in diverse media.<sup>45</sup>

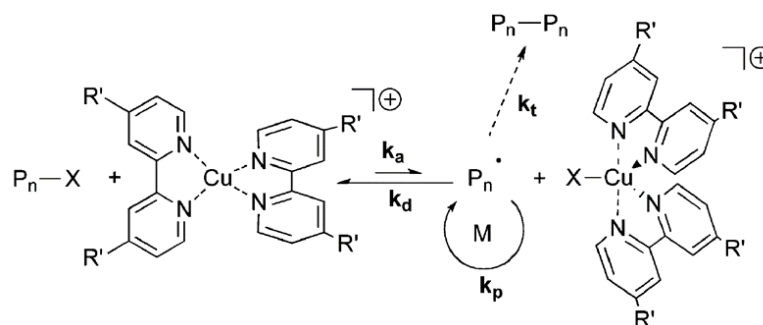


Figure 10. General ATRP mechanism of copper/2,2'-bipyridine.<sup>45</sup> Copyright (2008) Royal Society of Chemistry.

Figure 10 illustrates the general mechanism of ATR polymerization mediated by copper and 2,2'-bipyridine as a ligand.  $Cu^I$  acts as a catalyst in this reaction and is coordinated by the bidentate bipyridine ligand. The equilibrium is strongly determined by the  $Cu^I$  complex, which cleaves the alkyl halide bond ( $P_nX$ ), to coordinate with the halogen atom and forms a higher oxidation state complex ( $Cu^{II}$ ). The organic radical ( $P_n$ ) established in this reaction, acts as a living species and has the possibility either to propagate with the monomer ( $k_p$ ) or terminate ( $k_t$ ). Afterwards, the  $Cu^{II}$  complex is reversibly deactivated ( $k_d$ ) and the chain is dormant again, capped with the halide. This activation-propagation-deactivation cycle proceeds until all the monomer is consumed.<sup>45</sup>

### 2.2.2.1 Kinetics of copper-catalyzed ATRP

A successful ATRP process should meet several requirements. First, the initiator<sup>45</sup> should be consumed in the early stages of polymerization and generate propagating chains. Second, in order to obtain narrow molecular weight distributions, only a small number of monomers should be added during activation. Finally, the contribution of chain-breaking reactions, such as transfer and termination, should be negligible, enabling the synthesis of polymers with high degrees of end functionality.<sup>45</sup> Theoretically, only a low concentration of copper catalyst is

needed, so a decreased amount of copper could not affect the rate of polymerization<sup>43</sup>, providing that a suitable ratio of  $[Cu^I/L]/[Cu^{II}/L]$  is maintained. However, in reality, due to unavoidable and irreversible radical-radical termination events the concentration of  $[Cu^{II}/L]$  increases, as described by the persistent radical effect, and effectively depletes the system of  $[Cu^I/L]$ .<sup>43</sup> Radical concentration is diminished in ATRP due to persistent radical effect (PRE), and the ATRP equilibrium ( $K_{ATRP} = k_a/k_d$ ) is strongly shifted towards dormant species ( $k_a \ll k_d$ ).<sup>45</sup> Due to a low  $Cu^I$  concentration<sup>43</sup>, radical-radical termination events increase, and no further polymerization is possible.

### 2.2.2.2 *ARGET ATRP*

ARGET ATRP (activations regenerated by electron transfer ATRP) is a modification of ATRP which differs from conventional ATRP by the use of reducing agents. The reducing agents<sup>43</sup> such as glucose, hydrazine, ascorbic acid, tin(II) 2-ethylhexanoate ( $Sn(EH)_2$ ), and furthermore, nitrogen-containing agents like  $N,N,N',N'',N''$ -pentamethyldiethylenetriamine (PMDETA) are capable of continuous regeneration of  $Cu^I$  activators. Elemental copper is the most common used reducing agent in ARGET ATRP. The utilization of zerovalent copper ( $Cu^0$ ) should facilitate the reduction of  $Cu^{II}$  to  $Cu^I$ . This was first demonstrated by Matyjaszewski et al. (46) and the rate of polymerization could be increased. The reaction even proceeded in the presence of oxygen and at ambient temperatures with tris(2-(dimethylamino)ethyl)amine ( $Me_6TREN$ ).<sup>43</sup> However, there are also other ways to conduct ARGET ATRP. It can be accomplished by initially adding the oxidatively stable reagents  $Cu^{II}$  and  $Cu^0$  without any air-sensitive  $Cu^I$ .  $Cu^0$  functions as a mild reducing agent<sup>43</sup> in order to produce  $Cu^I$ , but it can also act as a supplemental activator for alkyl halides as well. Another possibility is performing ATRP synthesis with low catalyst concentrations (i.e.,  $[Cu^{II}Br_2] \leq 10$  ppm), but with an excess of reducing agent. Another important aspect is, that the solvation<sup>47</sup> of  $Cu^I$  is better at this oxidation state in the presence of complexing agents which is the reason for the favored dissociation, and an enhanced polymerization rate.  $Cu^0$  and  $Cu^{II}$  are in comparison to  $Cu^I$  relatively stable. To sum up, there are

several advantages for ARGET ATRP such as the simple reaction setup<sup>43</sup>, operation, and withdrawal from resulting polymer.

### **2.2.2.3      *Star polymers by ATRP***

Star polymers can be prepared by ATRP according to two strategies: In the core-first approach, a core molecule is applied as multifunctional initiator and the extension of the arms follows from the core. Correspondingly, the number of initiating sites dedicates the number of arms emanating from the core. The second strategy is called the arm-first method<sup>38,48</sup>, which involves the synthesis of pre-formed linear arms that are coupled to the core. Although normal ATRP was extensively reported to be useful for star polymer synthesis, a great portion of star-star termination products can be obtained. Termination<sup>49</sup> reactions can hinder arm conversion and broaden molecular weight distribution. As a relatively high radical concentration is used during polymerization, these events are likely to occur. To further avoid this, the concentration of radicals has to be lowered, in order to shift the equilibrium towards the dormant species. Another interesting aspect regarding star polymer synthesis implementing the core-first technique, is the incompatibility of certain monomers with the initiating system (e.g., organic halide/copper halide/2,2'-bipyridine) with the monomer (e.g. methacrylic acid).<sup>50</sup>

## 3. Materials and Methods

### 3.1 Chemicals

All chemicals mentioned in the chapter “Dye Synthesis” (4.1.) were purchased from commercial sources (ABCR, Sigma Aldrich, Alfa Aesar, euriso-top, Fluka, Merck, and VWR chemicals) and were used without further purification.  $\text{Pt}(\text{C}_6\text{H}_5\text{CN})\text{Cl}_2$  was obtained according to Hutter<sup>51</sup>. For the preparation of the polymers in chapter “Polymer Synthesis” (4.2),  $\text{Cu}^{\text{I}}\text{Br}$  was purified by washing with glacial acetic acid, diethyl ether, and absolute ethanol. After washing with a solution of 20 mL deionized water and 10 drops concentrated sulphuric acid, a white solid was obtained which was dried at 105 °C in vacuo. 2,2'-Azobisisobutyronitrile (AIBN, 99%, Aldrich) was purified by recrystallization from methanol. The monomers were obtained from Aldrich and purified by passing them through a short basic alumina column to remove radical inhibitors (like hydroquinone and methyl hydroquinone) before use.

### 3.2 Equipment

Reaction progress was checked with thin layer chromatography (TLC). The TLC plates were purchased from Merck (Silica gel 60 F<sub>254</sub> and aluminium oxide 60 F<sub>254</sub>) on aluminium sheets. Detection was done under UV light or by immersion into  $\text{KMnO}_4$  (0.1 wt%). Centrifugation was done with a Heraeus Labofuge 300 with 3000 rpm for 10 minutes. Gel permeation chromatography (GPC) was performed with the following set up: The system operated with THF (WGE Dr. Bures): separating columns from MZ-Gel SD plus, linear 5 $\mu$ , as well as UV and RI detector SEC 3010. Analogously, the system operated with chloroform (Shimadzu): separating columns from columns MZ-Gel SD plus, linear 5 $\mu$ , as well as an UV detector (SPD-20A) and a RI detector (RID 20A). Where possible, differential scanning calorimetry measurements for the determination of the glass transition temperature ( $T_g$ ) were performed with a Perkin Elmer Differential Scanning

Calorimeter (Hyper DSC 8500). The following parameters were acquired: nitrogen flow of 20 mL min<sup>-1</sup>, scanning speed for cooling and heating 20 °C min<sup>-1</sup>. NMR spectroscopy was performed on a Bruker Avance 300 MHz spectrometer. Absorption spectra were traced with a Shimadzu spectrophotometer UV-1800. The emission spectra were recorded on a Hitachi F-7000 fluorescence spectrometer, arranged with a photomultiplier R928 from Hamamatsu. MALDI-TOF mass spectrometry was measured with Micromass ToFSpec 2E time-of flight mass spectrometer. Equipped with a nitrogen laser ( $\lambda = 337$  nm), it was operated at a frequency of 5 Hz) and a time lag focusing unit. Positive ion spectra were recorded in reflection mode with an accelerating voltage of 20 kV. Calibration was done with a polyethylene glycol standard. The data was analyzed with MassLynx-Software V3.5 (Micromass, Waters, Manchester, UK). The best ten shots were averaged to a spectrum. Samples were prepared by dissolution in THF or CH<sub>2</sub>Cl<sub>2</sub> ( $c = 1$  mg mL<sup>-1</sup>). TTA-UC measurements were performed with a Horiba Fluorolog-3 luminescence spectrometer. The polymers were dissolved in 1,4-dioxane and the measurements were taken in a deaerated screw-cap cuvette (Hellma). Excitation was done either with a 635 nm-laser diode (from Roithner Lasertechnik, LDM 635/5LJM, 635 nm, 5 mW) or with a 450 W Xenon lamp at 617 nm. All spectra were recorded in front-face mode.

## 4. Experimental

### 4.1 Dye Synthesis

The preparation of the monomers was essential for the subsequent polymerization, producing defined star polymers via RDRP techniques such as ATRP and RAFT polymerization. Platinum benzoporphyrins were installed as centers of the stars, while statistical copolymers of perylene diester and methyl acrylate emanated from these centers. The synthesis of the monomers is shown in chapter 4.1. In section 4.1.1, the synthesis of the platinum benzoporphyrin dye monomers is depicted. The overall synthetic route for all four monomers consisted of the same reactions. Namely, they were performed in the following order: melting process (1), demetallation (2), platination (3), Suzuki-Miyaura cross-coupling (4) and Steglich esterification (5). From the Suzuki-Miyaura cross-coupling experiments, mono-, di-, tri-, and tetra- (hydroxymethyl)phenyl substituted platinum (II) benzoporphyrin derivatives were obtained. However, the formation of tetra-substituted species was probably hindered due to the sterically demanding *tert*-butyl groups and lead to low yield. The side-products di- and tri- (hydroxymethyl)phenyl substituted platinum (II) benzoporphyrins were submitted to Steglich esterification to attach suited functional groups. Yet for preliminary polymerization experiments, these functionalized chromophores were rather useful as monomers. The overall reaction scheme is given in Figure 11.

#### 4.1.1 Synthetic pathway of the benzoporphyrin dye monomers

In Figure 11, the reaction pathway of the synthesis of the two end compounds, Pt(II) tetra(((2-hexylthio)thioxomethyl)thiopropionatemethylphenyl) *meso*-tetraphenyl tetra(*tert*-butyl)-benzoporphyrin (HTP<sub>4</sub> TPTBTBP Pt) and Pt(II) tetra(2-bromopropanoatemethylphenyl) *meso*-tetraphenyl tetra(*tert*-butyl)-benzoporphyrin (BPMP<sub>4</sub> TPTBTBP Pt) is given. Melting (1) alias template condensation was used for the preparation of the benzoporphyrin ligand, followed by demetallation

(2) of the zinc ligand, platination (3), Suzuki-Miyaura cross-coupling (4) and the Steglich esterification (5) for the preparation of the final monomers. The benefits and drawbacks of these reactions are then discussed in 5.1.1. The isolation of the products was conducted by column chromatography, using dichloromethane (DCM), cyclohexane (CH), and ethyl acetate (EA) as solvents.

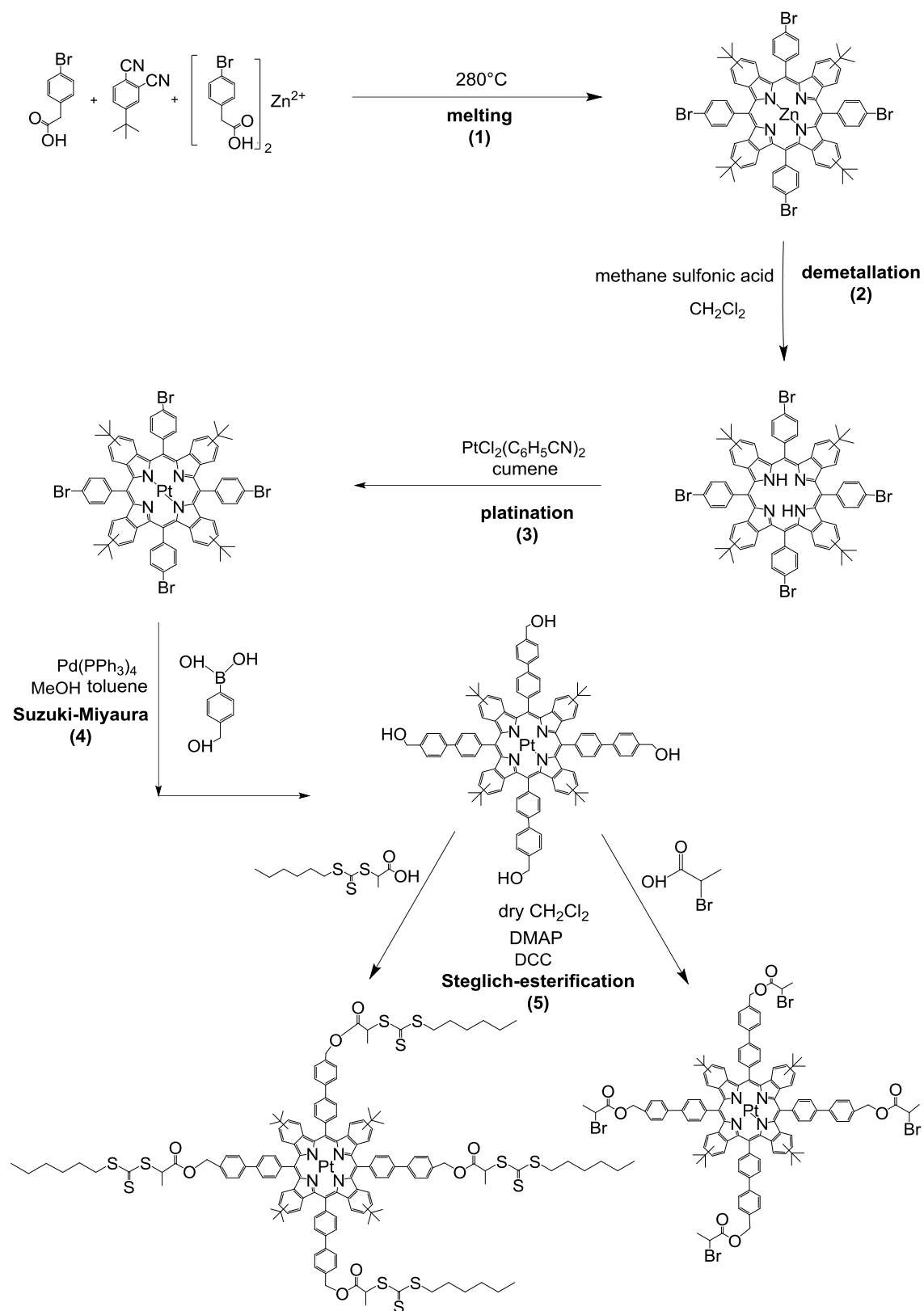


Figure 11. Overall reaction pathway for the synthesis of the benzoporphyrin monomers.

#### 4.1.1.1 Zn(II) tetrabromo meso-tetraphenyl tetra(*tert*-butyl)benzoporphyrin ( $Br_4$ TPTBTBP Zn)

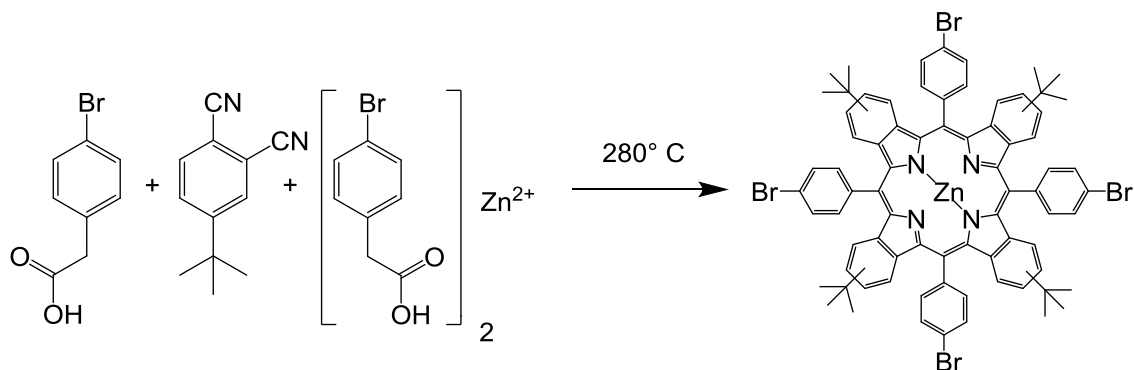


Figure 12. Melting reaction for the synthesis of  $Br_4$  TPTBTBP Zn.

In a mortar, 2-(4-bromophenyl) acetic acid (20.25 g, 94.15 mmol, 5 eq.), Zn-4-bromophenyl acetate (9.282 g, 18.72 mmol, 1 eq.) and 4-(*tert*-butyl) phthalonitrile (13.88 g, 75.32 mmol, 4 eq.) were mixed with a pestle to obtain a white, fine powder. Portions of 0.8 g of this powder were weighted into 4 mL vials, which were equipped with a magnetic stirring bar and a metal screw cap. After placing the vials in a preheated metal block ( $140^\circ C$ ), the temperature was increased to  $280^\circ C$ . After 40 minutes in the metal heating block, the vials were cooled down to room temperature and a dark-green, highly viscose substance was obtained. The vials were smashed with a hammer and the bits of broken glass were dissolved in acetone to collect the product. Acetone was removed under reduced pressure and a green solid mixture containing products and side products was obtained. The green solid was dissolved in ethanol (750 mL) and neutralized with 0.3 M  $NaHCO_3$  solution (200 mL), which was added dropwise to the dissolved product. Green flakes were precipitated and collected. The mother solution was red. Afterwards, the precipitate was dried at  $60^\circ C$  in the drying oven overnight (27 g product). In sum, column chromatography was done three times for purification ( $SiO_2$ , CH: EA, 15:1), ( $SiO_2$ , CH: Ethylacetate, 20:1), ( $SiO_2$ , CH: Ethylacetate, 50:1).

yield: green solid, 2.574 g, 1.803 mmol, 9.6 %

Rf: 0.51 (CH:EE 10:1)

$\lambda_{\max}$  (relative intensity) in acetone: 460 nm (1), 547 nm (0.05), 608 nm (0.09), 654 nm (0.23)

molar absorption coefficient  $\lambda_{\max}/\epsilon$  in acetone: 460 nm, 242 000 M<sup>-1</sup> cm<sup>-1</sup>

<sup>1</sup>H NMR (300 MHz, CDCl<sub>3</sub>)  $\delta$ : 8.21– 7.30 (m, 28H, H<sub>Porphyrin</sub>, H<sub>Ar</sub>), 1.30 (s, 36H, (CH<sub>3</sub>)<sub>3</sub>).

#### 4.1.1.2 *Tetrabromo meso-tetraphenyl tetra(tert-butyl) benzoporphyrin (Br<sub>4</sub> TPTBTBP)*

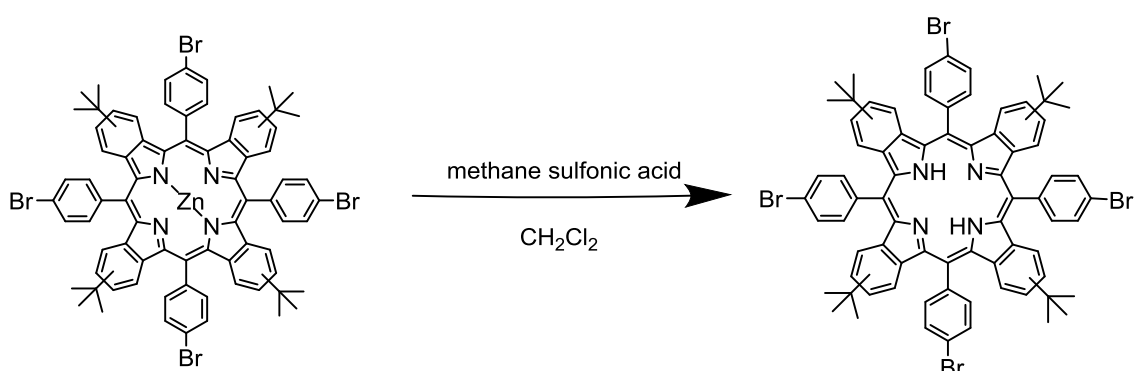


Figure 13. Demetallation reaction of Br<sub>4</sub> TPTBTBP Zn.

Br<sub>4</sub> TPTBTBP Zn (259 mg, 0.181 mmol, 1 eq.) was dissolved in 10 mL acetone. The solution was stirred for 10 minutes. As methanesulfonic acid (850  $\mu$ L, 12.1 mmol, 72.2 eq.) was added, the solution changed after 10 minutes its color from green to brownish. After the reaction, the solution was diluted with CH<sub>2</sub>Cl<sub>2</sub> (60 mL) and neutralized with NaHCO<sub>3</sub> sat. (110 mL). The organic phase was dried with Na<sub>2</sub>SO<sub>4</sub>. Afterwards the solvent was removed and dried in vacuo.

yield: blue crystals, 0.2304 g, 0.1720 mmol, 94 %

$\lambda_{\max}$  (relative intensity) in acetone: 463 nm (1), 591 nm (0.05), 638 nm (0.14), 697 nm (0.05)

$^1\text{H}$  NMR (300 MHz,  $\text{CDCl}_3$ )  $\delta$ : 8.26 – 7.07 (m, 28H,  $\text{H}_{\text{Porphyrin}}$ ,  $\text{H}_{\text{Ar}}$ ), 1.26 (s, 36H,  $(\text{CH}_3)_3$ ), -1.36 (bs, 2H,  $-\text{NH}-$ ).

#### 4.1.1.3 *Pt(II)* tetrabromo meso-tetraphenyl tetra(*tert*-butyl)benzoporphyrin ( $\text{Br}_4$ TPTBTBP Pt)

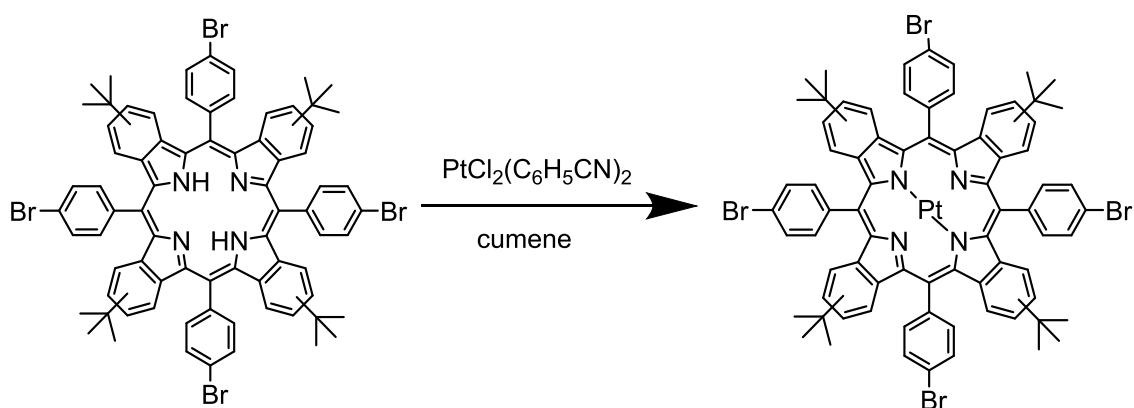


Figure 14. Platinumation reaction yielding  $\text{Br}_4$  TPTBTBP Pt.

In a three-neck round flask, equipped with a dropping funnel and a glass tube to introduce  $\text{N}_2$ , the free ligand  $\text{Br}_4$  TPTBTBP (1.00 g, 0.746 mmol, 1 eq.) was dissolved in cumene (400 mL). In three portions, a suspension of *cis*-dichloro-bis(benzonitrile)platinum (0.847 g, 1.79 mmol, 2.43 eq.) in cumene was slowly added to the solution. During this addition, the solution changed its color from blueish to emerald green. The mixture was heated to reflux to  $150^\circ\text{C}$  and stirred for two days, whereas the nitrogen flow was important to avoid the accumulation of  $\text{HCl}$ , which could protonate the ligand. The solution was decanted and the cumene was removed from the solution ( $90^\circ\text{C}$ , 115 mbar). The product was isolated by column chromatography ( $\text{SiO}_2$ ,  $\text{CH}:\text{CH}_2\text{Cl}_2$ , 3:1).

yield: violet crystals, 0.7033 g, 0.4322 mmol, 60.7%

Rf: 0.6 ( $\text{CH}:\text{CH}_2\text{Cl}_2$ , 3:1)

$\lambda_{\max}$  (relative intensity) in acetone: 426 nm (1), 566 nm (0.075), 618 nm (0.6348)

$^1\text{H NMR}$  (300 MHz,  $\text{CDCl}_3$ )  $\delta$ : 8.19 – 7.22 (m, 28H,  $\text{H}_{\text{Porphyrin}}$ ,  $\text{H}_{\text{Aryl}}$ ), 1.26 (s, 36H,  $(\text{CH}_3)_3$ ).

#### 4.1.1.4 *Pt(II) tetrahydroxymethylphenyl meso-tetraphenyl tetra(tert-butyl)-benzoporphyrin (HMP<sub>4</sub> TPTBTBP Pt)*

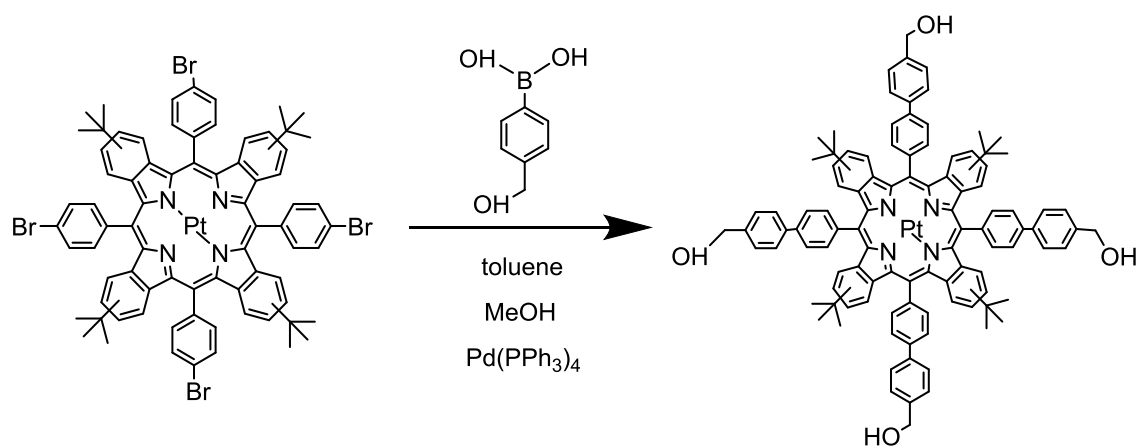


Figure 15. Suzuki-Miyaura cross-coupling reaction yielding HMP<sub>4</sub> TPTBTBP Pt.

A three-neck round flask, filled with Br<sub>4</sub> TPTBTBP Pt (0.699 g, 0.429 mmol, 1 eq.) was evacuated and refilled with N<sub>2</sub> three times. A prepared solvent mixture of toluene/THF/deionized H<sub>2</sub>O (42 mL/42 mL/21 mL) was introduced and the solution was stirred and purged with N<sub>2</sub> for 30 minutes. Afterwards, the 4-(hydroxymethyl) phenyl boronic acid (0.838 g, 5.51 mmol, 12.8 eq.), K<sub>2</sub>CO<sub>3</sub> (2.29 g, 16.5 mmol, 38.5 eq.) and the catalyst Pd(PPh<sub>3</sub>)<sub>4</sub> (0.025 g, 0.022 mmol, 0.049 eq.) were added. Few drops of the phase transfer catalyst Aliquat 336 were added to the solution. The solution was stirred and heated to 70 °C under inert atmosphere for six days. The solution was diluted with CH<sub>2</sub>Cl<sub>2</sub> (100 mL) and NaHCO<sub>3</sub> sat. (35 mL) were added to neutralize the solution. After addition of deionized H<sub>2</sub>O (25 mL), the phases were separated two times and the organic phases were collected

and dried with Na<sub>2</sub>SO<sub>4</sub>. The solvent was removed under reduced pressure and as the green product was not completely dry, it was freeze-dried three times. The product was isolated by column chromatography (SiO<sub>2</sub>) whereas a gradient separation (CH:EA, 5:1; CH:EA, 3:2; CH:EA, 1:1; CH:EA, 2:1; pure EA) was performed to separate the different functionalized products (mono-, di-, tri- and tetrafunctionalized benzoporphyrins).

Yield: green crystals, 0.2023 g, 0.122 mmol, 28.4% (tetra); green crystals, 0.2212 g, 0.134 mmol, 31.2% (tri); green crystals 0.1387 g, 0.086 mmol, 20.0% (di)

R<sub>f</sub>: 0.15 (CH:EA, 1:1, tetra); 0.30 (CH:EA, 1:1, tri); 0.60 (CH:EA, 1:1, di)

<sup>1</sup>H NMR (300 MHz, DMSO) δ: 8.29 - 7.27 (m, 44H, **H**<sub>Porphyrin</sub>, **H**<sub>Aryl</sub>), 5.35 (s, 2H, -OH), 5.15 (s, 2H, -OH), 4.65 (d, 4H, -OCH<sub>2</sub>-), 4.49 (d, J = 5.8 Hz, 4H, -OCH<sub>2</sub>-), 1.14 (s, 36H, -(CH<sub>3</sub>)<sub>3</sub>).

MALDI-TOF MS: m/z: [M<sup>+</sup>] calc. for C<sub>104</sub>H<sub>92</sub>N<sub>4</sub>O<sub>4</sub>Pt: 1656.6793; found, 1656.6797

#### 4.1.1.5 *Pt(II) tetra(2-bromopropanoatemethylphenyl) meso-tetra-phenyl tetra(tert-butyl)-benzoporphyrin (BPMP<sub>4</sub> TPTBTBP Pt)*

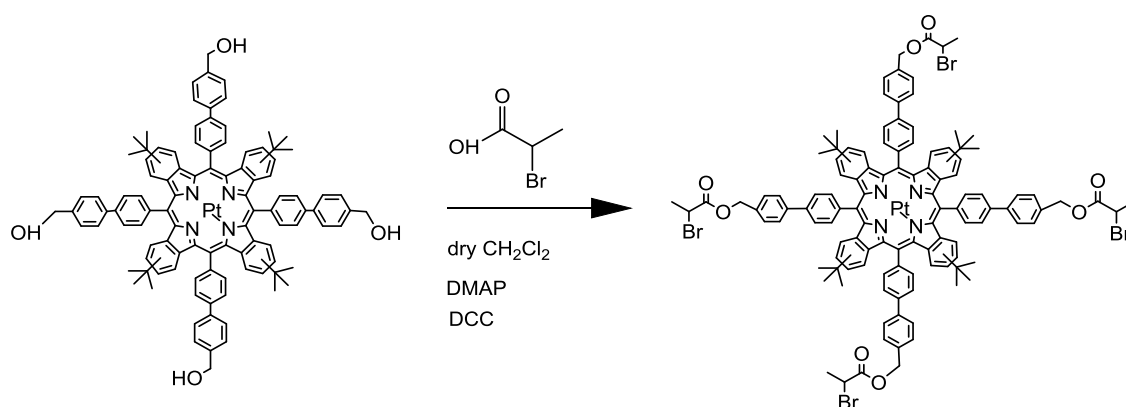


Figure 16. Steglich esterification reaction yielding BPMP<sub>4</sub> TPTBTBP Pt.

A 50 mL Schlenk flask, filled with HMP<sub>4</sub>TPTBTBP Pt (0.247 g, 0.149 mmol, 1 eq.) and 4-(dimethylamino)-pyridin (DMAP) (catalytic amount) was evacuated and purged with nitrogen three times. After deoxygenation, dry CH<sub>2</sub>Cl<sub>2</sub> (15 mL) were added and an ice-bath was placed beneath the flask before 2-bromopropionic acid (283 μL, 3.15 mmol, 21.1 eq.) and dicyclohexylcarbodiimide (DCC) (0.661 g, 3.20 mmol, 21.5 eq.) were added. After the addition of the chemicals and stirring for 15 minutes, the solution was heated to reflux and stirred overnight. The mixture was diluted with CH<sub>2</sub>Cl<sub>2</sub> (15 mL) and NaHCO<sub>3</sub> sat. (4 drops) were added to neutralize the solution. The organic phase was washed with deionized H<sub>2</sub>O (10 mL) and dried over Na<sub>2</sub>SO<sub>4</sub>. The solvent was removed under reduced pressure and as the product was still viscous, it was dried by three freeze-drying cycles. The product was isolated by column chromatography (SiO<sub>2</sub>, CH: EA, 5:1).

yield: small, dark-blue crystals, 96.3 mg, 48.45 μmol, 32.5 %

R<sub>f</sub>: 0.268 (SiO<sub>2</sub>, CH: EA, 5:1)

λ<sub>max</sub> (relative intensity) in acetone: 430 nm (1), 566 nm (0.07), 617 nm (0.56)

molar absorption coefficient λ<sub>max</sub>/ε in acetone: 430 nm, 224 000 M<sup>-1</sup> cm<sup>-1</sup>

MALDI-TOF MS: m/z [M<sup>+</sup>] calc. for C<sub>117</sub>H<sub>107</sub>Br<sub>4</sub>N<sub>4</sub>O<sub>8</sub>Pt: 2211.4465; found, 2213.7354

<sup>1</sup>H NMR (300 MHz, CDCl<sub>3</sub>) δ: 8.40 - 6.87 (m, 44H, H<sub>Porphyrin</sub>, H<sub>Aryl</sub>), 5.38 (s, 8H, -CH<sub>2</sub>-), 4.52 (dt, J = 6.8, 3.8 Hz, 4H, -CHBr-CH<sub>3</sub>), 2.02 – 1.90 (m, 12H, -CH-CH<sub>3</sub>), 1.18 (s, J = 3.5 Hz, 36H, (CH<sub>3</sub>)<sub>3</sub>).

<sup>13</sup>C NMR (76 MHz, CDCl<sub>3</sub>) δ: 141.44 (C<sub>Porphyrin,aryl</sub>), 141.03 (C<sub>Porphyrin</sub>), 140.84 (C<sub>aryl</sub>), 134.93 (C<sub>Porphyrin</sub>), 134.81 (C<sub>Porphyrin,aryl</sub>), 129.19 (CH<sub>Porphyrin,aryl</sub>), 129.08 (CH<sub>Porphyrin,aryl</sub>), 128.55 (CH<sub>Porphyrin,aryl</sub>), 128.16 (CH<sub>aryl</sub>), 128.02 (CH<sub>Porphyrin,aryl</sub>), 127.90 (CH<sub>aryl</sub>), 127.73 (CH<sub>Porphyrin,aryl</sub>), 123.67 (CH<sub>Porphyrin</sub>), 67.55 (CH<sub>2</sub>), 40.16 (CH-Br), 35.13 (C(CH<sub>3</sub>)<sub>3</sub>), 31.51 (CH<sub>3</sub>), 21.85 (CH<sub>3</sub>).

**4.1.1.6 Pt(II) dibromo di(2-bromopropanoatemethylphenyl) meso-tetraphenyl tetra(tert-butyl)-benzoporphyrin (Br<sub>2</sub> BPMP<sub>2</sub> TPTBTBP Pt)**

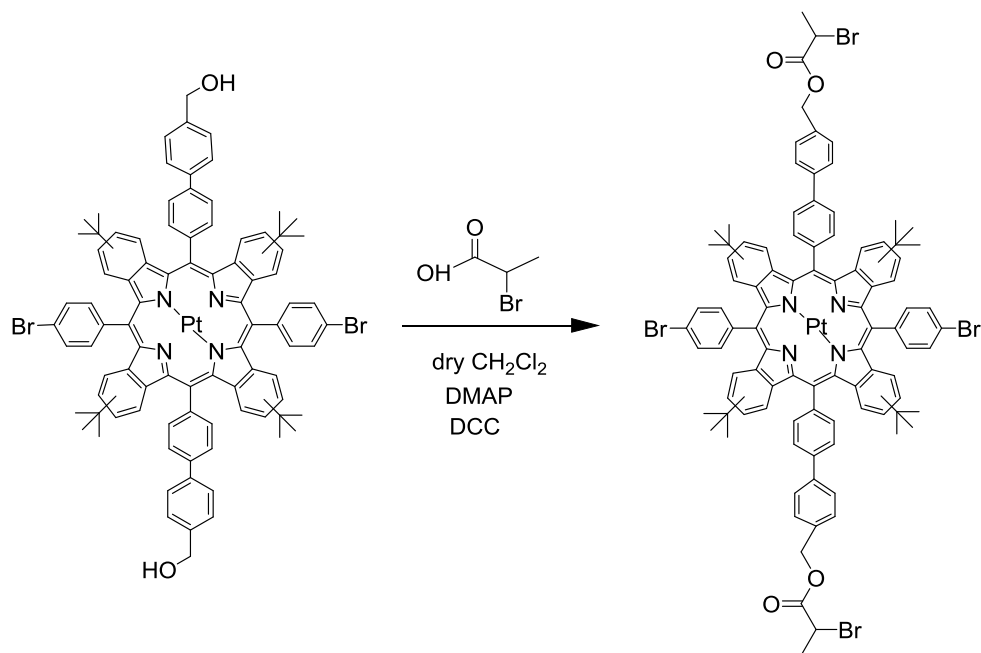


Figure 17. Steglich esterification reaction yielding Br<sub>2</sub> BPMP<sub>2</sub> TPTBTBP Pt.

A 50 mL Schlenk flask, filled with HMP<sub>2</sub> Br<sub>2</sub>TPTBTBP Pt (0.140 g, 0.086 mmol, 1 eq.) and 4-(dimethylamino)-pyridin (DMAP) (catalytic amount) was evacuated and purged with nitrogen three times. After deoxygenation, dry CH<sub>2</sub>Cl<sub>2</sub> (15 mL) were added and an ice-bath was placed beneath the flask before 2-bromopropionic acid (155  $\mu$ L, 1.72 mmol, 19.7 eq.) and dicyclohexylcarbodiimide (DCC) (0.35 g, 1.68 mmol, 19.2 eq.) were added. After the addition of the chemicals and stirring for 15 minutes, the solution was heated to reflux and stirred overnight. The mixture was diluted with CH<sub>2</sub>Cl<sub>2</sub> (15 mL) and NaHCO<sub>3</sub> sat. (4 drops) were added to neutralize the solution. The organic phase was washed with deionized H<sub>2</sub>O (10 mL) and dried over Na<sub>2</sub>SO<sub>4</sub>. The solvent was removed under reduced pressure, freeze-dried three times and dried in vacuo. The product was isolated by column chromatography (SiO<sub>2</sub>, CH: EA, 7:1).

yield: small, dark-green crystals, 124.8 mg, 66.15  $\mu$ mol, 76.5 %

Rf: 0.397 (SiO<sub>2</sub>, CH: EA, 7:1)

$\lambda_{\text{max}}$  (relative intensity) in acetone: 428 nm (1), 566 nm (0.07), 617 nm (0.59)

<sup>1</sup>H NMR (300 MHz, CDCl<sub>3</sub>)  $\delta$  8.60 – 6.79 (m, 36H, H<sub>Porphyrin</sub>, H<sub>Ar</sub>), 4.59 – 4.45 (m, 2H, -CH<sub>2</sub>-), 3.85 (m, 2H, -CH-), 3.44 (s, 2H, -CH<sub>2</sub>-), 2.24 (t,  $J = 37.6$  Hz, 6H, -CH<sub>3</sub>), 1.15 (s, 36H, -(CH<sub>3</sub>)<sub>3</sub>).

<sup>13</sup>C NMR (76 MHz, CDCl<sub>3</sub>)  $\delta$ : 134.86 (C<sub>Porphyrin</sub>), 132.71 (CH<sub>Porphyrin</sub>), 129.19 (CH<sub>aryl</sub>), 129.07 (CH<sub>aryl</sub>), 127.89 (CH<sub>aryl</sub>), 127.72 (CH<sub>aryl</sub>), 123.88 (CH<sub>Porphyrin</sub>), 117.01 (C<sub>Porphyrin</sub>), 67.54 (CH<sub>2</sub>), 40.14 (CH-Br), 35.13 (C(CH<sub>3</sub>)<sub>3</sub>), 34.45 (C(CH<sub>3</sub>)<sub>3</sub>), 34.34 (C(CH<sub>3</sub>)<sub>3</sub>), 31.44 (CH<sub>3</sub>), 21.83 (CH<sub>3</sub>).

#### 4.1.1.7 Pt(II) tetra(((2-hexylthio)thioxomethyl)thiopropionatemethylphenyl) meso-tetraphenyl tetra(tert-butyl)-benzoporphyrin (HTP<sub>4</sub> TPTBTBP Pt)

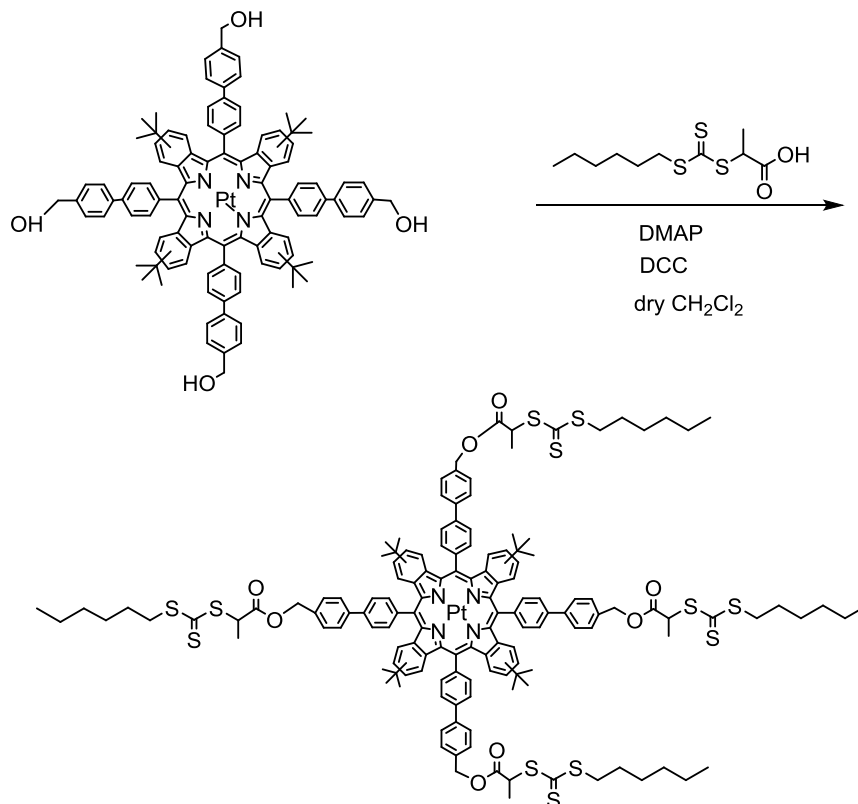


Figure 18. Steglich esterification reaction of HMP<sub>4</sub> TPTBTBP Pt.

A 100 mL Schlenk flask, filled with HMP<sub>4</sub> TPTBTBP Pt (0.047 g, 0.028 mmol, 1 eq.) and 4-(dimethylamino)-pyridin (DMAP) (catalytic amount), was evacuated and purged with nitrogen three times. After deoxygenation, dry CH<sub>2</sub>Cl<sub>2</sub> (15 mL) was added and an ice-bath was placed beneath the flask before 2-((hexylthio)thioxomethyl)thiopropionic acid (0.091 g, 0.343 mmol, 12 eq.) and dicyclohexylcarbodiimide (DCC) (0.070 g, 0.340 mmol, 12 eq.) were added. After the addition of the chemicals and stirring for 15 minutes, the solution was heated to reflux and stirred overnight. As the reaction progressed, the solution got a dark blue color. The mixture was diluted with CH<sub>2</sub>Cl<sub>2</sub> (25 mL) and NaHCO<sub>3</sub> sat. (4 mL) was added to neutralize the solution. The organic phase was washed with deionized H<sub>2</sub>O (10 mL) and dried over Na<sub>2</sub>SO<sub>4</sub>. The solvent was removed under reduced pressure. The product was isolated by column chromatography (SiO<sub>2</sub>, CH: EA, 7:1).

yield: green crystals, 30.1 mg, 11.3 mmol, 40%

R<sub>f</sub>: 0.24 (SiO<sub>2</sub>, CH: EA, 10:1)

$\lambda_{\max}$  (relative intensity) in DCM: 1432 (0.616), 569 (0.041), 619 (0.55)

molar absorption coefficient  $\lambda_{\max}/\epsilon$  in DCM: 432 nm, 221 800 M<sup>-1</sup> cm<sup>-1</sup>

<sup>1</sup>H NMR (300 MHz, CDCl<sub>3</sub>)  $\delta$ : 8.42 – 7.14 (m, 44H, H<sub>Porphyrin</sub>, H<sub>Aryl</sub>), 5.34 (m, 8H, -OCH<sub>2</sub>-), 4.99 (m, 4H, -CH-CH<sub>3</sub>), 3.48 – 3.32 (m, 8H, -S-CH<sub>2</sub>-), 1.73 – 1.70 (m, 8H, -CH<sub>2</sub>-), 1.45 (s, 12H, -CH-CH<sub>3</sub>), 1.33 (m, 24H, -CH<sub>2</sub>-), 1.21 (s, *J* = 3.5 Hz, 36H, -C(CH<sub>3</sub>)<sub>3</sub>), 0.91 (s, 12H, -CH<sub>2</sub>-CH<sub>3</sub>).

<sup>13</sup>C NMR (76 MHz, CDCl<sub>3</sub>)  $\delta$  129.05 (CH<sub>Porphyrin,aryl</sub>), 127.87 (CH<sub>Porphyrin,aryl</sub>), 96.10 (C<sub>Porphyrin</sub>), 67.46 (CH<sub>2</sub>), 48.18 (CH), 37.49 (CH<sub>2</sub>), 31.50 (CH<sub>3</sub>), 31.39 (CH<sub>2</sub>), 30.94 (CH<sub>2</sub>), 28.05 (CH<sub>2</sub>), 22.63 (CH<sub>2</sub>), 17.09 (CH<sub>3</sub>), 14.14 (CH<sub>3</sub>).

MALDI-TOF MS: m/z: [M<sup>+</sup>] calc. for C<sub>144</sub>H<sub>156</sub>N<sub>4</sub>O<sub>8</sub>PtS<sub>12</sub>: 2649.8704; found, 2649.8250

**4.1.1.8 Pt(II) monobromo tris(((2-hexylthio)thioxomethyl)thiopropionate methylphenyl) meso-tetraphenyl tetra(tert-butyl)-benzoporphyrin (Br HTP<sub>3</sub> TPTBTBP Pt)**

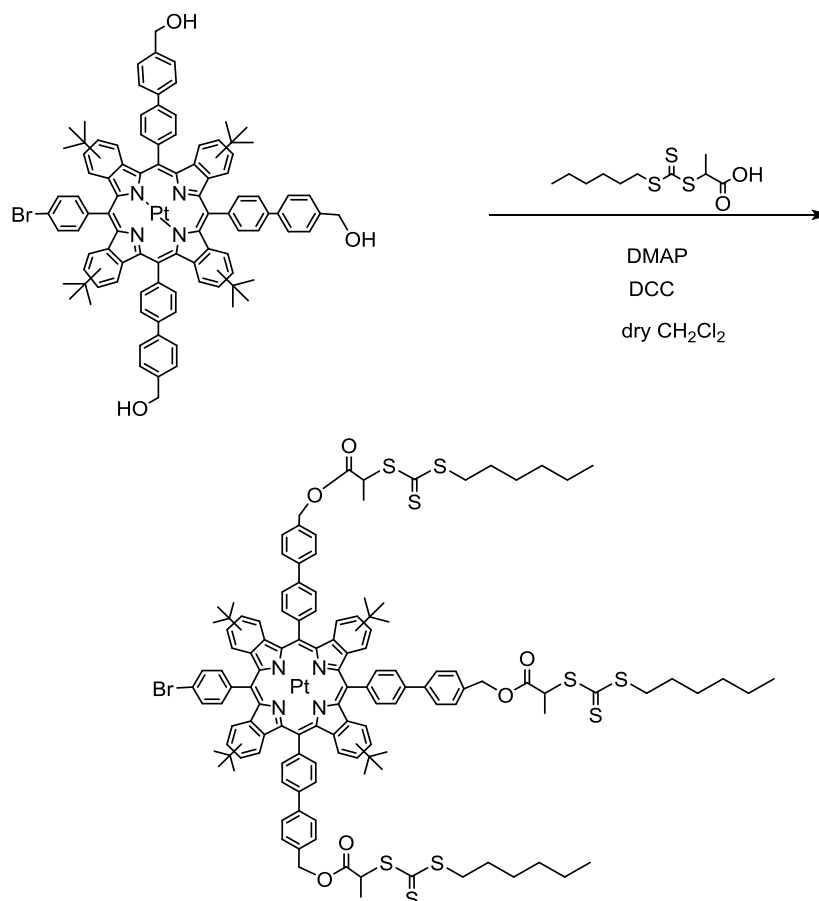


Figure 19. Steglich esterification reaction of Br HMP<sub>3</sub> TPTBTBP Pt.

A 100 mL Schlenk flask, filled with Br HMP<sub>3</sub> TPTBTBP Pt (0.126 g, 0.076 mmol, 1 eq.) and 4-(dimethylamino)-pyridin (DMAP) (catalytic amount), was evacuated and purged with nitrogen three times. After deoxygenation, dry CH<sub>2</sub>Cl<sub>2</sub> (15 mL) were added and an ice-bath was placed beneath the flask before 2-((hexylthio)thioxomethyl)thiopropionic acid (0.187 g, 0.700 mmol, 9.16 eq.) and dicyclohexylcarbodiimide (DCC) (0.154 g, 0.744 mmol, 9.72 eq.) were added. After the addition of the chemicals and stirring for 15 minutes, the solution was heated to reflux and stirred overnight. As the reaction progressed, the solution got a dark blue color. The mixture was diluted with CH<sub>2</sub>Cl<sub>2</sub> (40 mL) and NaHCO<sub>3</sub> sat. (15 drops)

was added to neutralize the solution. The organic phase was washed with deionized H<sub>2</sub>O (25 mL) and dried over Na<sub>2</sub>SO<sub>4</sub>. The solvent was removed under reduced pressure. The product was isolated by column chromatography (SiO<sub>2</sub>, CH: EA, 5:1).

yield: green crystals, 67 mg, 28.2 mmol, 37%

R<sub>f</sub>: 0.26 (SiO<sub>2</sub>, CH: EA, 12:1)

<sup>1</sup>H NMR (300 MHz, CDCl<sub>3</sub>) δ 8.38 – 7.02 (m, 40H, H<sub>Porphyrin</sub>, H<sub>ar</sub>), 5.35 (s, 6H, -OCH<sub>2</sub>-), 5.05 – 4.91 (m, 3H, -CH-CH<sub>3</sub>), 3.41 (t, *J* = 7.4 Hz, 6H, -S-CH<sub>2</sub>-), 1.72 (m, 6H, -CH<sub>2</sub>-), 1.60 (d, *J* = 7.0 Hz, 9H, -CH-CH<sub>3</sub>), 1.32 (s, 6H, -CH<sub>2</sub>-), 1.26 (m, 12H, -CH<sub>2</sub>-), 1.18 (s, 36H, -(CH<sub>3</sub>)<sub>3</sub>), 0.90 (s, 9H, -CH<sub>2</sub>-CH<sub>3</sub>).

<sup>13</sup>C NMR (76 MHz, CDCl<sub>3</sub>) δ: 129.05(CH<sub>Porphyrin,aryl</sub>), 127.97(CH<sub>aryl</sub>), 127.86 (CH<sub>Porphyrin</sub>), 127.69 (CH<sub>aryl</sub>), 124.07 (CH<sub>Porphyrin,aryl</sub>), 96.78 (C<sub>Porphyrin</sub>), 93.37 (C<sub>Porphyrin</sub>), 67.45 (CH<sub>2</sub>), 48.17 (CH), 37.49 (CH<sub>2</sub>), 31.51 (CH<sub>3</sub>), 31.39 (CH<sub>2</sub>), 28.04 (CH<sub>2</sub>), 22.63 (CH<sub>2</sub>), 17.08 (CH<sub>3</sub>), 14.14 (CH<sub>3</sub>).

MALDI-TOF MS: *m/z*: [M<sup>+</sup>] calc. for C<sub>127</sub>H<sub>133</sub>BrN<sub>4</sub>O<sub>6</sub>PtS<sub>9</sub>: 2374.6558; found, 2375.4158

## 4.1.2 Synthetic pathway of PDE<sub>mon</sub>

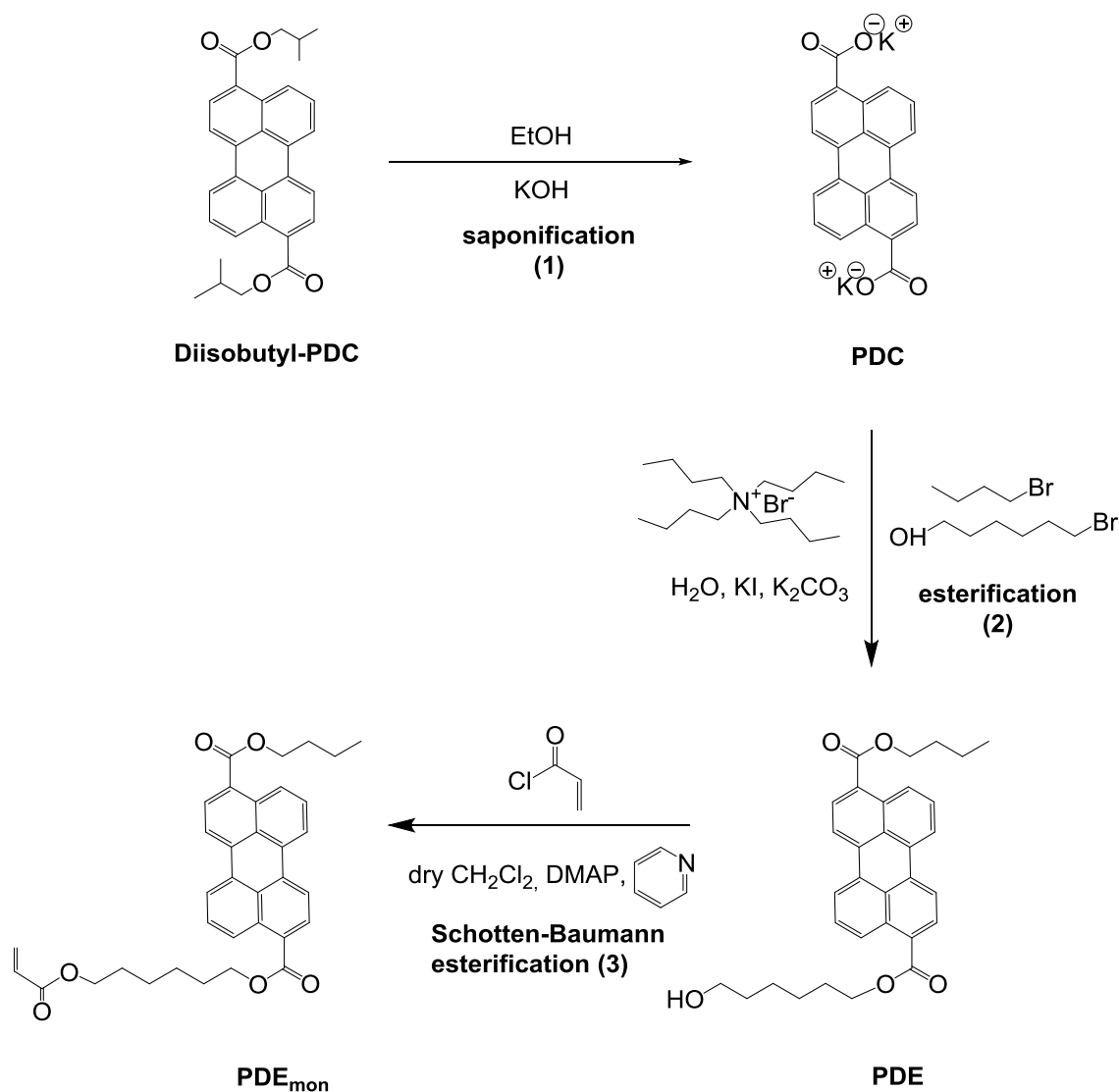


Figure 20. Overall reaction scheme of the synthesis of the PDE monomer.

The synthesis of the emitter molecule was comparably simple, regarding the synthesis of the sensitizer molecule. The reaction pathway, which is shown in Figure 20, consisted of three steps only: 3-(6-(acryloyloxy)hexyl) 9-butyl perylene-3,9-dicarboxylate (PDE<sub>mon</sub>) was synthesized by saponification (1), further esterification (2) and finally by Schotten-Baumann esterification (3).

#### 4.1.2.1 Potassium perylene 3,9-dicarboxylate (PDC)

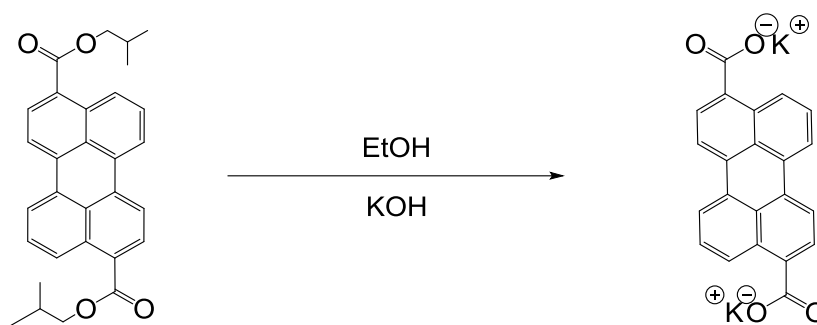


Figure 21. Saponification reaction for the synthesis of PDC.

A 250 mL 3-neck flask equipped with a stirring bar was filled with diisobutyl-*perylen*e-3,9-dicarboxylate (2.99 g, 6.61 mmol, 1 eq.). After the addition of ethanol (100 mL) and KOH (1.49 g, 26.6 mmol, 4 eq.), the solution was heated to reflux and stirred vigorously for 72 h. The color of the solution changed from yellow to orange, whereas precipitate was formed at the bottom of the flask. The yellow solution was filtered, washed with a bulk of DCM and dried in vacuo.

yield: yellow solid, 2.379 g, 5.684 mmol, 86 %

$\lambda_{\max}$  (relative intensity) in deionized H<sub>2</sub>O: 420 nm (0.87), 446 nm (1)

<sup>1</sup>H NMR (300 MHz, D<sub>2</sub>O)  $\delta$ : 8.25 – 8.13 (m, 4H, H<sub>Perylene</sub>), 8.04 (d,  $J$  = 8.3 Hz, 2H, H<sub>Perylene</sub>), 7.54 (dd,  $J$  = 19.1, 7.8 Hz, 4H, H<sub>Perylene</sub>).

#### 4.1.2.2 3-butyl 9-(6-hydroxyhexyl) perylene-3,9-dicarboxylate (PDE)

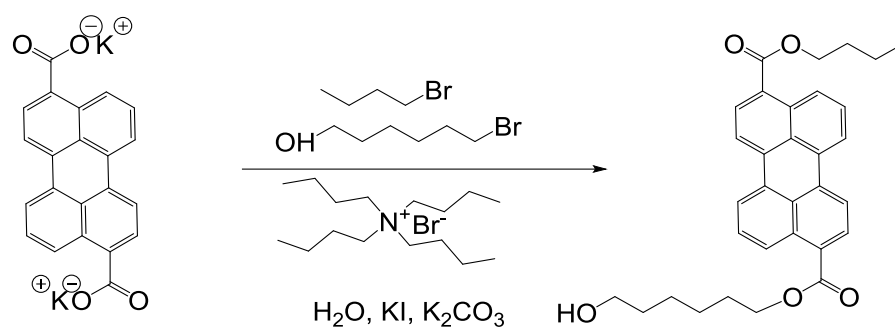


Figure 22. Esterification reaction yielding PDE.

A two-neck flask was filled with PDC (2.37 g, 5.67 mmol, 1 eq.), K<sub>2</sub>CO<sub>3</sub> (3.33 g, 24.1 mmol, 4.25 eq.), KI (spatula tip) and tetra-*n*-butylammonium bromide (1.66 g, 5.16 mmol, 0.910 eq.). H<sub>2</sub>O (86 mL) was added and the solution was heated to reflux. As 1-bromobutane (614  $\mu$ L, 5.73 mmol, 1.01 eq.) and 6-bromo-1-hexanol (750  $\mu$ L, 5.73 mmol, 1.01 eq.) were added, the color of the solution turned from orange to red orange. The solution was heated at 60°C overnight, whereas red-orange precipitate was formed. The precipitate was filtered off by suction-filtration. The product was isolated by column chromatography (SiO<sub>2</sub>, CH<sub>2</sub>Cl<sub>2</sub>: MeOH, 20:1).

yield: orange solid, 0.5261 g, 18.7 %

R<sub>f</sub>: 0.439 (CH<sub>2</sub>Cl<sub>2</sub>: MeOH, 20:1)

<sup>1</sup>H NMR (300 MHz, CDCl<sub>3</sub>)  $\delta$ : 8.92 (d,  $J$  = 8.8 Hz, 1H, H<sub>Perylene</sub>), 8.83 (d,  $J$  = 8.7 Hz, 1H, H<sub>Perylene</sub>), 8.24 (m,  $J$  = 17.4, 7.3, 4.2 Hz, 6H, H<sub>Perylene</sub>), 7.63 (t,  $J$  = 7.9 Hz, 2H, H<sub>Perylene</sub>), 4.46 (t,  $J$  = 12.2, 6.7 Hz, 4H, -COO-CH<sub>2</sub>-), 3.72 – 3.32 (m, 2H, -CH<sub>2</sub>-OH), 1.82 (m, 2H, H<sub>Alkyl</sub>), 1.66 – 1.44 (m, 10H, H<sub>Alkyl</sub>), 1.03 (t,  $J$  = 7.3 Hz, 3H, -CH<sub>2</sub>-CH<sub>3</sub>).

#### 4.1.2.3 3-(6-(acryloyloxy)hexyl)9-butyl perylene-3,9-dicarboxylate ( $PDE_{mon}$ )

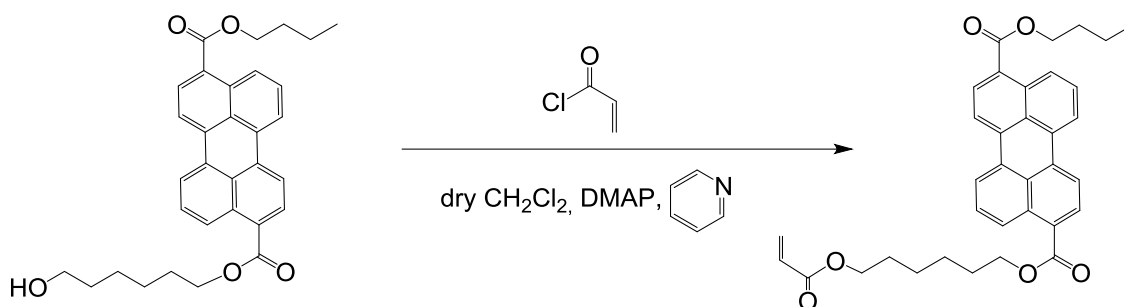


Figure 23. Schotten-Baumann reaction for the synthesis of  $PDE_{mon}$ .

A 100 mL Schlenk flask, filled with PDE (0.48 g, 0.87 mmol, 1 eq.) and equipped with a magnetic stirring bar, was evacuated and refilled with N<sub>2</sub> three times. After addition of dry CH<sub>2</sub>Cl<sub>2</sub> (20 mL), an ice-bath was placed beneath the flask and acryloyl chloride (106  $\mu$ L, 1.31 mmol, 1.49 eq.) was introduced dropwise. Pyridine (70  $\mu$ L, 0.87 mmol, 1 eq.) and DMAP (catalytic amount) were added and the color of the solution turned deep orange. The mixture was stirred overnight at room temperature. The reaction was quenched by the addition of H<sub>2</sub>O (1 mL) and the solution turned cloudy. The solution was diluted with CH<sub>2</sub>Cl<sub>2</sub> and neutralized with NaHCO<sub>3</sub> sat. The organic phase was extracted two times. The combined organic phases were dried over Na<sub>2</sub>SO<sub>4</sub>. The solvent was removed under reduced pressure. The product was isolated by column chromatography which was performed two times (SiO<sub>2</sub>, CH : EA, 5:1; pure DCM).

yield: orange solid, 0.1608 g, 0.2848 mmol, 32.7%

R<sub>f</sub>: 0.367 (CH.EA, 5:1); 0.452 (pure DCM)

$\lambda_{max}$  (relative intensity) in DCM: 440 (0.85), 465 (1)

molar absorption coefficient  $\lambda_{max}/\epsilon$  in DCM: 465 nm, 29 200 M<sup>-1</sup> cm<sup>-1</sup>

$^1\text{H}$  NMR (300 MHz,  $\text{CDCl}_3$ )  $\delta$ : 8.94 (d,  $J = 8.0$  Hz, 1H,  $\text{H}_{\text{Perylene}}$ ), 8.85 (d,  $J = 8.5$  Hz, 1H,  $\text{H}_{\text{Perylene}}$ ), 8.35 – 8.18 (m, 6H,  $\text{H}_{\text{Perylene}}$ ), 7.65 (t,  $J = 8.1$  Hz, 2H,  $\text{H}_{\text{Perylene}}$ ), 6.40 (d,  $J = 17.7$  Hz, 1H,  $-\text{CH}=\text{CH}_2$ ), 6.12 (dd,  $J = 17.3, 10.4$  Hz, 1H,  $\text{CH}=\text{CH}_2$ ), 5.81 (d,  $J = 10.2$  Hz, 1H,  $-\text{CH}=\text{CH}_2$ ), 4.43 (t,  $J = 6.5$  Hz, 4H,  $-\text{COO}-\text{CH}_2-$ ), 4.19 (t,  $J = 6.6$  Hz, 2H,  $-\text{O}-\text{CH}_2-$ ), 1.86 (m,  $J = 7.5$  Hz, 4H,  $-\text{CH}_2-$ ), 1.78 – 1.70 (m, 2H,  $-\text{CH}_2-$ ), 1.54 (s, 6H,  $-\text{CH}_2-$ ), 1.03 (t,  $J = 7.4$  Hz, 3H,  $-\text{CH}_2-\text{CH}_3$ ).

MALDI-TOF MS:  $m/z$ :  $[\text{M}^+]$  calc. for  $\text{C}_{35}\text{H}_{34}\text{O}_6$ : 550.2355; found, 550.2343

$^{13}\text{C}$  NMR (76 MHz,  $\text{CDCl}_3$ )  $\delta$ : 167.36 ( $\text{C}=\text{O}$ ), 132.75 ( $\text{CH}_2$ , Perylene), 131.12 ( $\text{CH}_{\text{Perylene}}$ ), 131.08 ( $\text{CH}_{\text{Perylene}}$ ), 130.91 ( $\text{C}_{\text{Perylene}}$ ), 130.70 ( $\text{C}_{\text{Perylene}}$ ), 130.52 ( $\text{CH}_{\text{Perylene}}$ ), 128.71 ( $\text{CH}_2$ , Perylene), 128.27 ( $\text{CH}_{\text{Perylene}}$ ), 128.08 ( $\text{CH}_{\text{Perylene}}$ ), 126.01 ( $\text{CH}_{\text{Perylene}}$ ), 122.48 ( $\text{C}_{\text{Perylene}}$ ), 122.14 ( $\text{CH}_{\text{Perylene}}$ ), 121.36 ( $\text{CH}_{\text{Perylene}}$ ), 120.45 ( $\text{CH}_{\text{Perylene}}$ ), 119.76 ( $\text{CH}_{\text{Perylene}}$ ), 65.23 ( $\text{O}-\text{CH}_2$ ), 64.62 ( $\text{O}-\text{CH}_2$ ), 61.30 ( $\text{O}-\text{CH}_2$ ), 31.00 ( $\text{CH}_2$ ), 28.84 ( $\text{CH}_2$ ), 28.72 ( $\text{CH}_2$ ), 26.02 ( $\text{CH}_2$ ), 25.87 ( $\text{CH}_2$ ), 19.56 ( $\text{CH}_2$ ), 13.97 ( $\text{CH}_3$ ).

## 4.2 Polymer Synthesis

### 4.2.1 Preliminary studies and strategic considerations for RAFT polymerization

The synthesis of star polymers by RAFT polymerization was approached with a series of preliminary experiments, which are displayed in this chapter 4.2.1. The main aim was to test the RAFT polymerization procedure, and to establish the optimal reaction conditions. As already described in the section above (4.1), the side products of Suzuki-Miyaura cross-coupling were applied to Steglich esterification to link functional groups to the platinum (II) benzoporphyrin, to obtain monomers for preliminary experiments. Resulting from the Steglich esterification with the precursor platinum (II) monobromo tris-(2-bromopropanoatemethylphenyl) meso-tetraphenyl tetra(tert-butyl)-benzoporphyrin (Br BPMP<sub>3</sub> TPTBTBP Pt) with 2-(((hexylthio)carbonothioyl)thio)propanoic acid, the monomer Br HTP<sub>3</sub> TPTBTBP Pt was obtained. Br HTP<sub>3</sub> TPTBTBP Pt was established in the preliminary experiments as a center of star polymers with emanating chains. In the first experiments, the R-group approach by RAFT polymerization was investigated by using the platinated benzoporphyrin as the core, with emanating chains of methyl methacrylate respectively methyl acrylate. Synthesis by R-approach means, that the core is the fragmenting species and 2-(((hexylthio)carbonothioyl)thio) the stabilizing group. Therefore, methyl methacrylate and methyl acrylate were tested towards molecular weights and molecular weight distributions. In order, these experiments were abbreviated as Br HTP<sub>3</sub> TPTBTBP Pt - (matrix)<sub>100</sub>, indicating an intended polymerization degree of 100 per arm. However, the polymerization yielded low molecular weights. The AIBN concentration was varied to perform a controlled polymerization. The AIBN concentration was decreased from initially six equivalents per RAFT-agent to 0.2 per RAFT-agent attached to the benzoporphyrin. By further decreasing AIBN concentration (0.1 eq. per RAFT-agent), polymerization was unsuccessful. Then, the reaction conditions were modified. As working under dry conditions with Schlenk flasks as polymerization tubes was rather unwieldy, it was operated with 4 mL vials, sealed with a septum. The working procedure was further modified by purification of the reagents, AIBN was recrystallized in methanol and methyl acrylate was purified. Stock solutions of the

reagents were prepared to facilitate precise operation. In order to test RAFT polymerization with the perylene diester monomer, statistical copolymers entitled as  $\text{PDE}_{\text{mon}} - (\text{matrix})_{100}$  were produced, whereas 2-((hexylthio)thiooxomethyl)thio)propionic acid was used as a RAFT-agent. As matrices, methyl methacrylate and methyl acrylate were applied. However, only small product amounts were available, so that characterization was only performed with NMR – spectroscopy. Star polymers bearing only the platinum (II) benzoporphyrin and the matrix monomer, were synthesized. Afterwards, star polymers consisting of sensitizer and emitter were synthesized, by copolymerization of platinum (II) benzoporphyrin as a center and copolymers of the matrix (either methyl methacrylate or methyl acrylate) and perylene diester monomer as emanating chains were established. Finally, by having asserted the optimal reaction conditions, the three star polymers bearing four arms per center, were synthesized.

#### 4.2.1.1 Statistical perylene-MA-copolymer

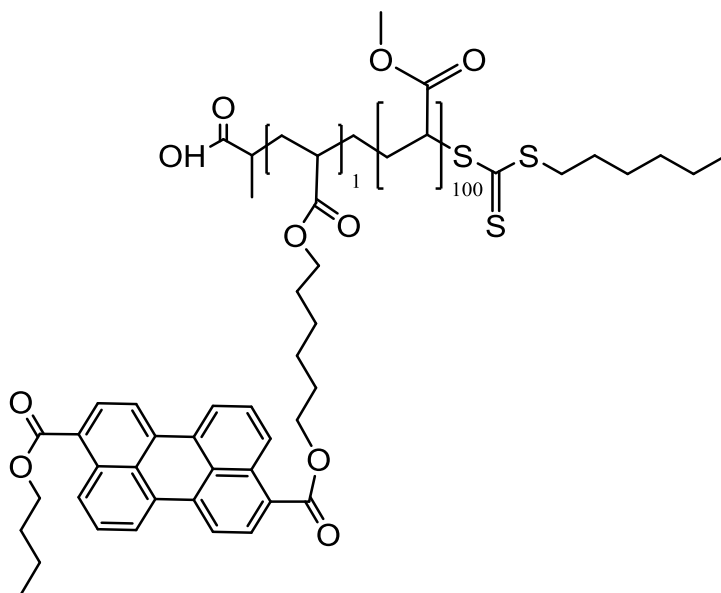


Figure 24. Statistical perylene-MA-copolymer.

A 10 mL Schlenk flask was evacuated and refilled with nitrogen three times. Then AIBN (1.79 mg, 10.9  $\mu\text{mol}$ , 5.29 eq.) together with 2-((hexylthio)thioxomethyl)thiopropionic acid (0.550 mg, 2.06  $\mu\text{mol}$ , 1 eq.) was introduced and dissolved in dry toluene (1 mL). PDE<sub>mon</sub> (3.00 mg, 2.57 mmol, 1 eq.) which was diluted in dry toluene was transferred to the reaction flask and then the mixture was heated up to 60° C. After stirring for 15 minutes, the monomer methyl acrylate (45.5  $\mu\text{L}$ , 502  $\mu\text{mol}$ , 244 eq.) was introduced. The reaction was terminated after 16 hours by cooling down the mixture, which was precipitated in an excess of glacial *n*-pentane.

$^1\text{H}$  NMR (300 MHz,  $\text{CDCl}_3$ )  $\delta$ : 8.85 (m, 2H, H<sub>peryl</sub>), 8.22 (m, 6H, H<sub>peryl</sub>), 7.67 (m, 2H, H<sub>peryl</sub>), 4.44 (m, 6H, -COO-CH<sub>2,perylene</sub>-), 3.61 (s, -OCH<sub>3,PMA</sub>-), 2.33 (bs, -CH<sub>2,PMA</sub>-), 1.36 (bs, -CH<sub>3,PMA</sub>-).

yield: orange, soft polymer, 2.1 mg

M<sub>n,exp</sub>: not determined (low yield)

M<sub>n,theor</sub>: 15 500 g mol<sup>-1</sup>

#### 4.2.1.2 Statistical perylene-MMA-copolymer

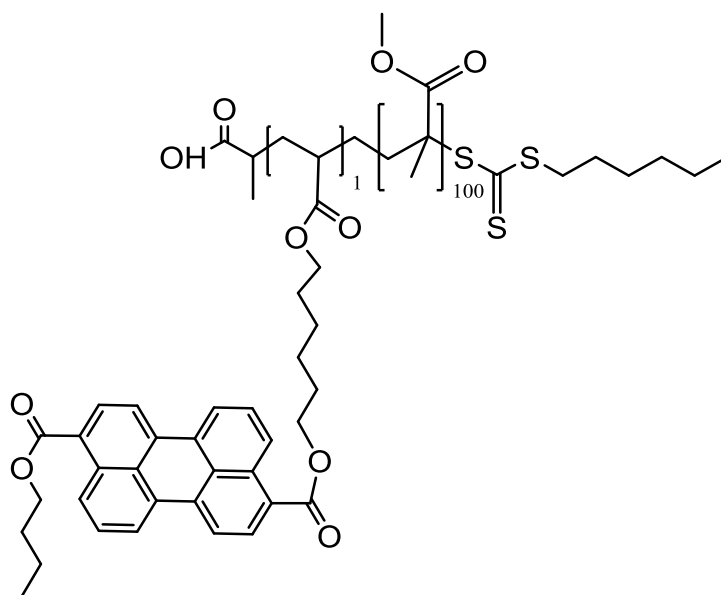


Figure 25. Statistical perylene-MMA-copolymer.

A Schlenk flask was evacuated and refilled with nitrogen three times. Then AIBN (3.28 mg, 0.019 mmol, 2.53 eq.) together with 2-((hexylthio)thiooxomethyl)thio)propionic acid (2.50 mg, 0.008 mmol, 1 eq.) was introduced and dissolved in dry toluene (1 mL). PDE<sub>mon</sub> (4.53 mg, 0.008 mmol, 1 eq.) which was diluted in dry toluene was transferred to the reaction flask and then the mixture was heated up to 60°C. After stirring for 15 minutes, the monomer methyl methacrylate (84  $\mu$ L, 0.79 mmol, 99 eq.) was introduced. The reaction was terminated after 16 hours by cooling down the mixture in an ice-bath and precipitation in an excess of *n*-pentane.

$^1\text{H NMR}$  (300 MHz,  $\text{CDCl}_3$ )  $\delta$  8.99 – 8.77 (m, 2H;  $\text{H}_{\text{perylene}}$ ), 8.38 – 8.09 (m, 6H,  $\text{H}_{\text{perylene}}$ ), 7.71 – 7.62 (m, 2H,  $\text{H}_{\text{perylene}}$ ), 4.43 (s, 6H,  $-\text{COO}-\text{CH}_2,_{\text{perylene}}$ ), 3.61 (s,  $-\text{O}-\text{CH}_3,_{\text{PMMA}}$ ), 2.24 (bs,  $-\text{CH}_2,_{\text{PMMA}}$ ), 1.35 (bs,  $-\text{CH}_3,_{\text{PMMA}}$ ).

yield: orange, solid polymer, 3.2 mg

$M_{n,\text{exp}}$ : not determined (low yield)

$M_{n,\text{theor}}$ : 7 700  $\text{g mol}^{-1}$

### 4.2.1.3 Benzoporphyrin-MA star polymer

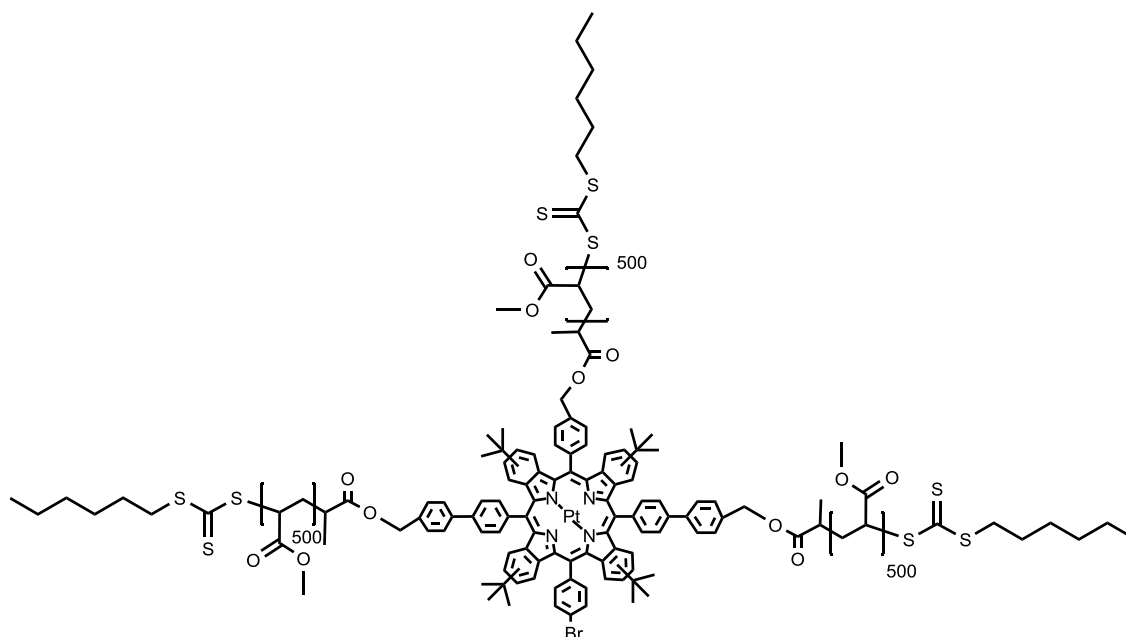


Figure 26. Benzoporphyrin-MA star polymer.

In a 4 mL vial equipped with a stirring bar and a septum, AIBN (0.18 mg, 1.1  $\mu\text{mol}$  0.64 eq.) was introduced and dissolved in dry toluene (1 mL). The vial was degassed for half an hour. Br HTP<sub>3</sub> TPTBTBP Pt (4.1 mg, 1.7  $\mu\text{mol}$ , 1 eq.) which was diluted in dry toluene was transferred to the reaction flask by a needle and syringe and then the mixture was heated up to 60°C. After stirring for 15 minutes, the monomer methyl acrylate (227.5  $\mu\text{L}$ , 2.51 mmol, 1476 eq.) was introduced. The reaction was terminated after 16 hours by cooling down the mixture in an ice-bath and precipitation in an excess of *n*-pentane.

<sup>1</sup>H NMR (300 MHz, CDCl<sub>3</sub>)  $\delta$  8.04 – 6.86 (m, 40H, H<sub>porph</sub>), 4.94 – 4.10 (m, -COO-CH<sub>2</sub>-), 3.90 – 3.11 (m, -OCH<sub>3,PMA</sub>-), 2.30 (bs, -CH<sub>2,PMA</sub>-), 1.95 – 1.33 (m, -CH<sub>2,PMA</sub>-), 1.24 (s, 36H, -C(CH<sub>3</sub>)<sub>3</sub>-), 0.92 (bs, -CH<sub>2,porph</sub>-).

yield: green, soft polymer, 38.2 mg

M<sub>n,exp</sub>: 7 686 g mol<sup>-1</sup>

PDI: 1.52

$M_{n,theor}$ : 46 000 g mol<sup>-1</sup>

#### 4.2.1.4 Benzoporphyrin-MMA star polymer

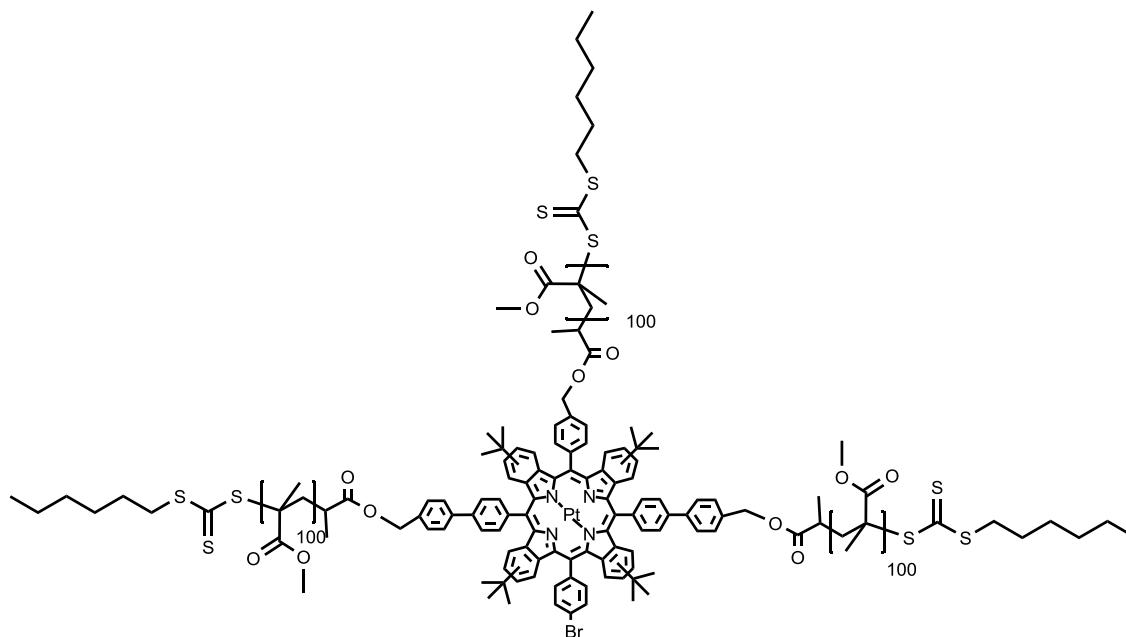


Figure 27. Benzoporphyrin-MMA star polymer.

A Schlenk flask was evacuated and refilled with nitrogen three times. Then, AIBN (2.00 mg, 12.2  $\mu$ mol, 5.77 eq.) was introduced and dissolved in dry toluene (1 mL). Br HTP<sub>3</sub> TPTBTBP Pt (5.00 mg, 2.11  $\mu$ mol, 1 eq.) which was diluted in dry toluene was transferred to the reaction flask and then the mixture was heated up to 60° C. After stirring for 15 minutes, the monomer methyl methacrylate (66.8  $\mu$ L, 628  $\mu$ mol, 300 eq.) was introduced. The reaction was terminated after 16 hours by cooling down the mixture in an ice-bath and precipitation in an excess of *n*-pentane.

$^1\text{H}$  NMR (300 MHz,  $\text{CDCl}_3$ )  $\delta$  7.40 – 7.06 (m, 30H,  $\text{H}_{\text{Porphyrin}}$ ,  $\text{H}_{\text{aryl}}$ ), 3.48 (s,  $-\text{O}-\text{CH}_3, \text{PMMA}$ ), 2.36 (s, 12H,  $-\text{OCH}_2, \text{Porphyrin}^-$ ), 1.18 (bs,  $-\text{CH}_2, \text{PMMA}$ ), 1.33 (bs,  $-\text{CH}_3, \text{PMMA}$ ).

yield: green, solid polymer, 52.4 mg

$M_{n, \text{theor}}$ : 12 600  $\text{g mol}^{-1}$

PDI: 1.35

$M_{n, \text{exp}}$ : 16 270  $\text{g mol}^{-1}$

#### 4.2.1.5 Statistical benzoporphyrin-MA-perylene star polymer

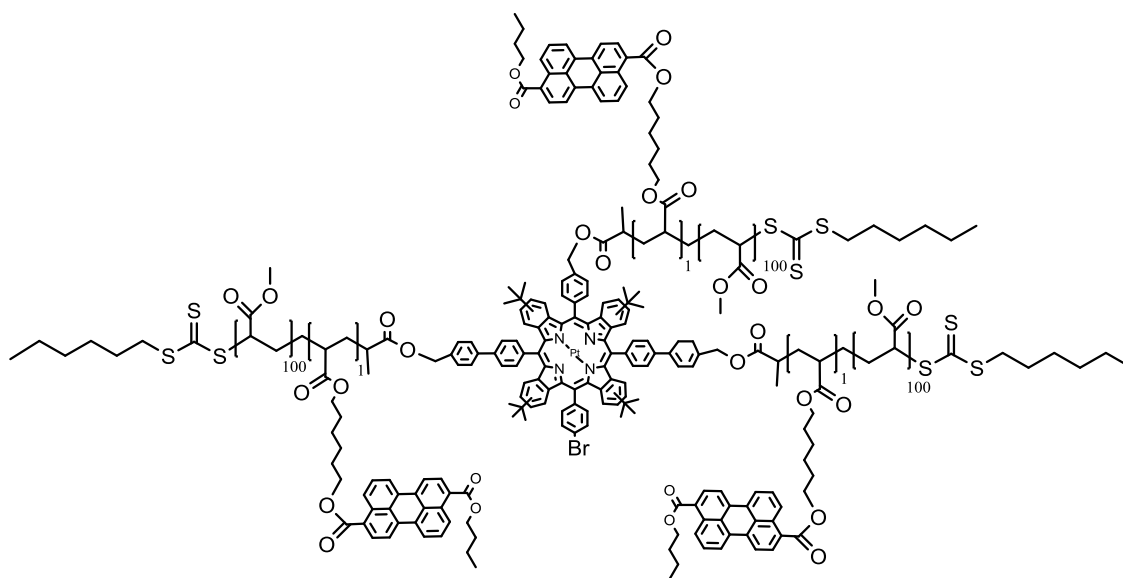


Figure 28. Statistical benzoporphyrin-MA-perylene star polymer.

A Schlenk flask was evacuated and refilled with nitrogen three times. Then, AIBN (1.72 mg, 10.4  $\mu\text{mol}$ , 6.16 eq.) was introduced and dissolved in dry toluene (1 mL). Br HTP<sub>3</sub> TPTBTBP Pt (4.07 mg, 1.71  $\mu\text{mol}$ , 1 eq.) which was diluted in dry toluene was transferred to the reaction flask and then the mixture was heated up to 60°C. After stirring for 15 minutes, a mixture of the monomer methyl acrylate (45.5  $\mu\text{L}$ , 0.502 mmol, 295 eq.) and PDE<sub>mon</sub> (3 mg, 5.45  $\mu\text{mol}$  g, 3.18 eq) was

introduced. The reaction was terminated after 16 hours by cooling down the mixture in an ice-bath and precipitation in an excess of *n*-pentane.

$^1\text{H NMR}$  (300 MHz,  $\text{CDCl}_3$ )  $\delta$ : 7.79 (m, 48H,  $\text{H}_{\text{porph}}$ ,  $\text{H}_{\text{perylene}}$ ), 4.94 – 4.13 (m, 3H,  $-\text{COO}-\text{CH}_2-$ ,  $-\text{CH}-\text{CH}_3$ ), 3.66 (s,  $-\text{OCH}_3, \text{PMA}-$ ), 2.24 (bs,  $-\text{CH}_2, \text{PMA}-$ ), 1.60 (m,  $-\text{CH}_2, \text{porph}-$ ), 0.88 (s, 44H,  $-\text{CH}_3, \text{PMA}-$ ,  $-\text{CH}_3, \text{porph}$ ).

yield: grass-green, soft polymer, 7.6 mg

$M_{n, \text{exp}}$ : 3 200  $\text{g mol}^{-1}$

PDI: 1.98

$M_{n, \text{theor}}$ : 12 700  $\text{g mol}^{-1}$

#### 4.2.1.6 Statistical benzoporphyrin-MMA-perylene star polymer

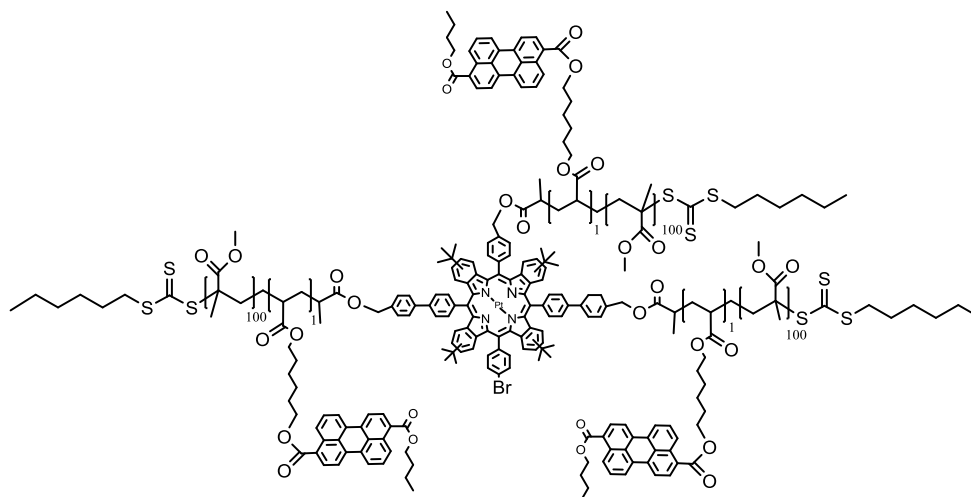


Figure 29. Statistical benzoporphyrin-MMA-perylene star polymer.

A Schlenk flask was evacuated and refilled with nitrogen three times. Then, AIBN (1.67 mg, 10.2  $\mu\text{mol}$ , 6 eq.) was introduced and dissolved in dry toluene (1 mL).

Br HTP<sub>3</sub> TPTBTBP Pt (4.07 mg, 1.7 μmol, 1 eq.) which was diluted in dry toluene was transferred to the reaction flask and then the mixture was heated up to 60°C. After stirring for 15 minutes, a mixture of the monomer methyl methacrylate (53.5 μL, 0.502 mmol, 295 eq.) and PDE<sub>mon</sub> (3 mg, 5.45 μmol, 3.18 eq.) was introduced. The reaction was terminated after 16 hours by cooling down the mixture in an ice-bath and precipitation in an excess of *n*-pentane.

<sup>1</sup>H NMR (300 MHz, CDCl<sub>3</sub>) δ: 9.03 – 8.81 (m, 2H; H<sub>perylene</sub>), 8.56 – 7.32 (m, 48H, H<sub>perylene</sub>, H<sub>porph</sub>), 5.26 – 4.81 (m, 3H, -CH-CH<sub>3</sub>), 4.43 (m, 12H, -COO-CH<sub>2</sub>,<sub>perylene</sub>-), 3.60 (s, 3H, -O-CH<sub>3</sub>,<sub>PMMA</sub>-), 1.85 (bs, -CH<sub>2</sub>,<sub>PMMA</sub>-), 1.51 – 0.63 (bs, -CH<sub>3</sub>,<sub>PMMA</sub>).

yield: grass-green, solid polymer, 17.1 mg

M<sub>n,exp</sub>: 13 800 g mol<sup>-1</sup>

PDI: 4.68

M<sub>n,theor</sub>: 14 200 g mol<sup>-1</sup>

## 4.2.2 Preparation of star polymers

### 4.2.2.1 Polymer I

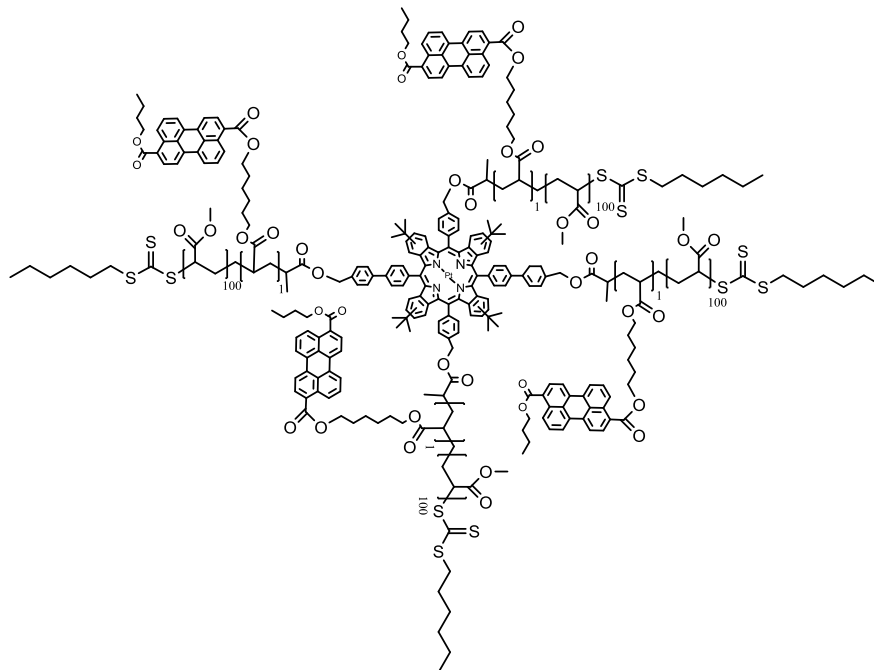


Figure 30. Structure of polymer I.

To a 4 mL vial equipped with a septum, dry toluene (1 mL) was introduced and deaerated by bubbling nitrogen through the solution for half an hour. Afterwards, AIBN (0.79 mg, 4.8  $\mu\text{mol}$ , 0.8 eq.) was added from a prepared stock-solution. HTP<sub>4</sub> TPTBTBP Pt (16 mg, 6.0  $\mu\text{mol}$ , 1 eq.) which was diluted in dry toluene was transferred to the reaction flask by a needle and syringe and then the mixture was heated up to 60°C. After stirring for 15 minutes, a mixture of the monomer methyl acrylate (219  $\mu\text{L}$ , 2.41 mmol, 402 eq.) and PDE<sub>mon</sub> (13.63 mg, 24.14  $\mu\text{mol}$ , 4 eq.) was introduced. The reaction process was controlled by TLC. After 16 hours, the reaction was terminated by cooling down the mixture and precipitation in an excess of glacial *n*-pentane.

<sup>1</sup>H NMR (300 MHz, CDCl<sub>3</sub>)  $\delta$ : 8.89 (d,  $J$  = 8.6 Hz, 2H, H<sub>perylene</sub>), 8.80 (d,  $J$  = 8.5 Hz, 2H, H<sub>perylene</sub>), 8.61 – 7.87 (m, 42H, H<sub>perylene</sub>, H<sub>porph</sub>), 7.61 (s, 10H, H<sub>perylene</sub>,

$H_{\text{porph}}$ ), 6.39 (d,  $J = 17.2$  Hz, 1H,  $H_{\text{perylene}}$ ), 6.10 (dd,  $J = 17.3, 10.4$  Hz, 1H,  $H_{\text{perylene}}$ ), 5.80 (d,  $J = 10.4$  Hz, 1H,  $H_{\text{perylene}}$ ), 5.30 (d,  $J = 16.5$  Hz, 12H, , - $\text{OCH}_2$ ,<sub>porph</sub>-), 4.70 – 4.02 (m, 145H, - $\text{COO-CH}_2$ -,  $H_{\text{perylene}}$ ), 3.91 – 3.51 (s, 3H, -- $\text{O-CH}_3$ ,  $H_{\text{PMA}}$ ), 2.05 – 1.70 (bs, - $\text{CH}_2$ -,  $H_{\text{PMA}}$ ), 1.71 (d,  $J = 6.5$  Hz, 14H, - $\text{CH}_2$ -,  $H_{\text{perylene}}$ ), 1.54 – 1.46 (m, 12H, - $\text{CH}_2$ -,  $H_{\text{porph}}$ ), 1.21 (d,  $J = 20.5$  Hz, 52H,  $H_{\text{porph}}$ , - $\text{CH}_2$ -), 1.04 – 0.99 (m, 3H, - $\text{CH}_3$ ,  $H_{\text{perylene}}$ ), 0.86 (s, 15H, - $\text{CH}_3$ ,  $H_{\text{porph}}$ ).

yield: grass-green, soft polymer, 34.0 mg

$M_{n,\text{exp}}$ : 5 100 g mol<sup>-1</sup>

PDI: 1.33

$M_{n,\text{theor}}$ : 11 000 g mol<sup>-1</sup>

#### 4.2.2.2 Polymer II

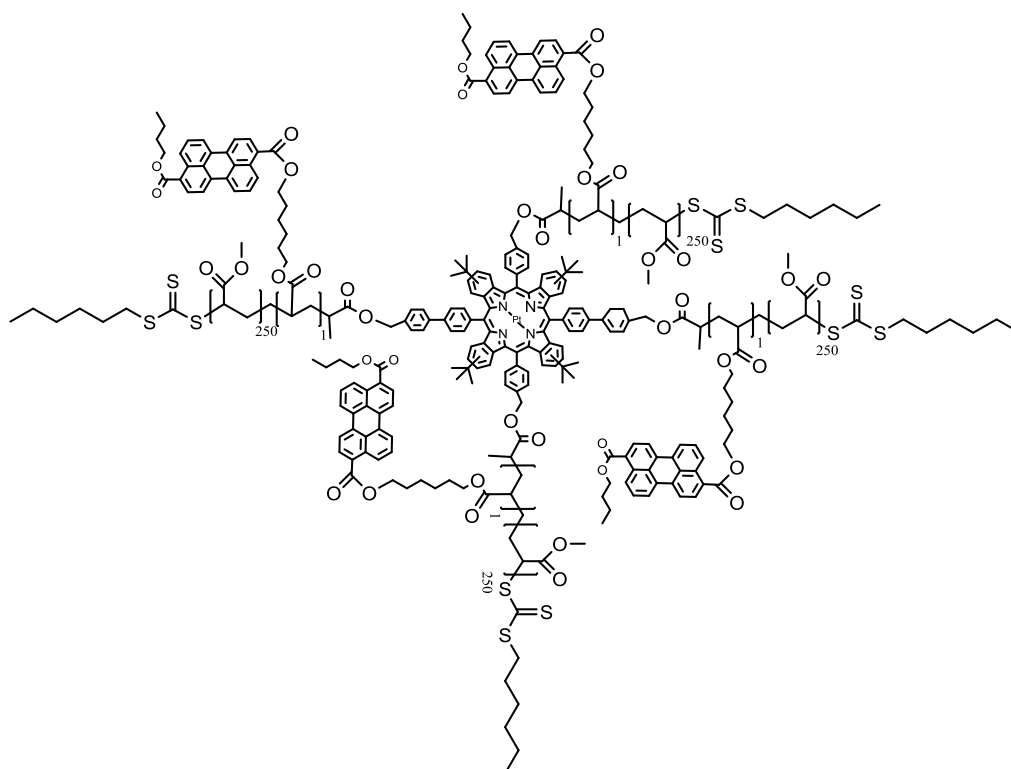


Figure 31. Structure of polymer II.

To a 4 mL vial equipped with a septum, dry toluene (1 mL) was introduced and deaerated by bubbling nitrogen for half an hour. Afterwards, AIBN (0.40 mg, 2.4  $\mu\text{mol}$ , 0.8 eq.) was added from a prepared stock-solution. HTP<sub>4</sub> TPTBTBP Pt (8 mg, 3  $\mu\text{mol}$ , 1 eq.) which was diluted in dry toluene was transferred to the reaction flask by a needle and syringe and then the mixture was heated up to 60°C. After stirring for 15 minutes, a mixture of the monomer methyl acrylate (274  $\mu\text{L}$ , 3.02 mmol, 1000 eq.) and PDE<sub>mon</sub> (6.8 mg, 1.2  $\mu\text{mol}$ , 4 eq.) was introduced. The reaction process was controlled by TLC. After 16 hours, the reaction was terminated by cooling down the mixture and precipitation in excess of glacial *n*-pentane.

<sup>1</sup>H NMR (300 MHz, CDCl<sub>3</sub>)  $\delta$ : 8.44 – 7.44 (m, 48H, H<sub>perylene</sub>, H<sub>porph</sub>), 5.03 – 4.00 (m, -COO-CH<sub>2,porph</sub>-, -COO-CH<sub>2,perylene</sub>-), 3.98 – 3.37 (m, -COO-CH<sub>2</sub>-, H<sub>perylene</sub>), 2.58 – 2.07 (bs, -CH<sub>2</sub>-, H<sub>PMA</sub>), 1.55 (m, -CH<sub>2</sub>-, H<sub>porph</sub>), 0.87 (s, 36H, H<sub>porph</sub>).

yield: grass-green, soft polymer, 14.9 mg

M<sub>n,exp</sub>: 6 800 g mol<sup>-1</sup>

PDI: 1.59

M<sub>n,theor</sub>: 23 500 g mol<sup>-1</sup>

### 4.2.2.3 Polymer III

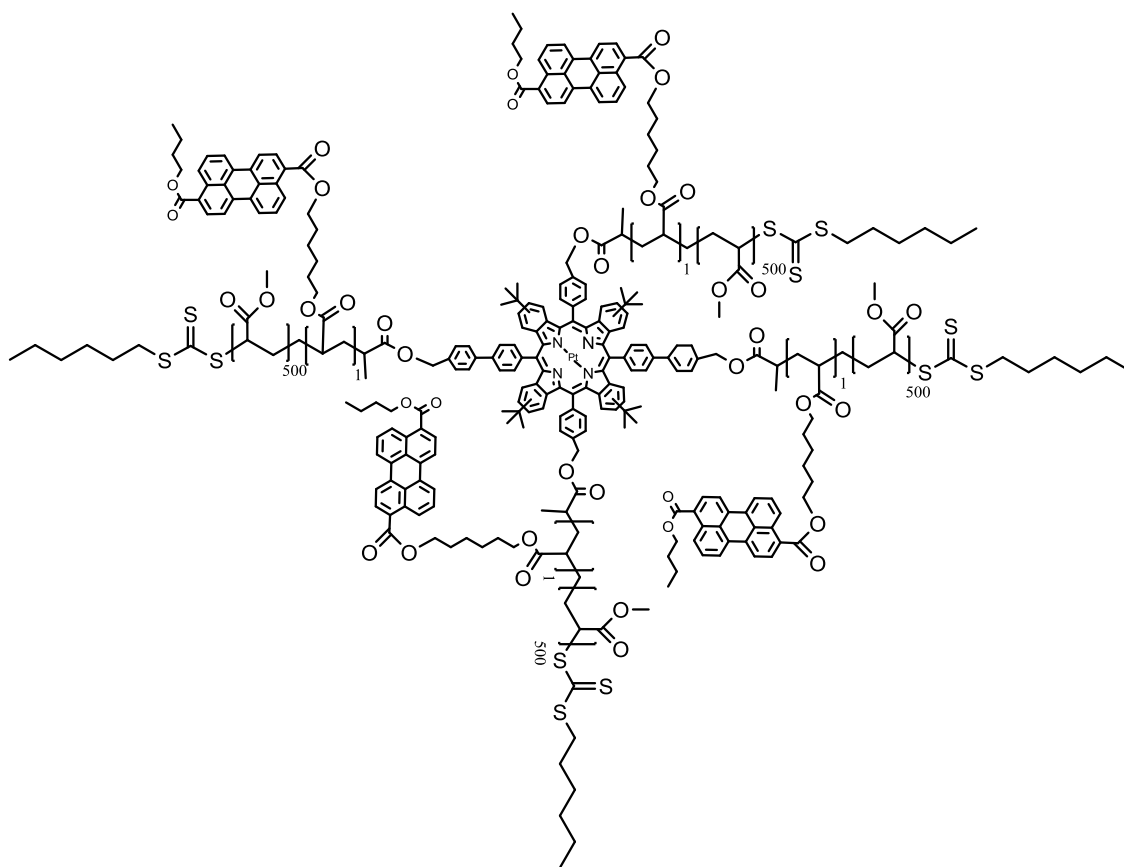


Figure 32. Structure of polymer III.

To a 4 mL vial equipped with a septum, dry toluene (1 mL) was introduced and deaerated by bubbling nitrogen through the solution for half an hour. Afterwards, AIBN (0.20 mg, 1.2  $\mu\text{mol}$ , 0.8 eq.) was added from a prepared stock-solution. HTP<sub>4</sub> TPTBTBP Pt (4.0 mg, 1.5  $\mu\text{mol}$ , 1 eq.) which was diluted in dry toluene was transferred to the reaction flask by a needle and syringe and then the mixture was heated up to 60°C. After stirring for 15 minutes, a mixture of the monomer methyl acrylate (274  $\mu\text{L}$ , 3.02 mmol, 2000 eq.) and PDE<sub>mon</sub> (3.41 mg, 4 eq., 6.0  $\mu\text{mol}$ ,) was introduced. The reaction process was controlled by TLC. After 16 hours, the reaction was terminated by cooling down the mixture in an ice-bath and precipitation in an excess of *n*-pentane.

$^1\text{H}$  NMR (300 MHz,  $\text{CDCl}_3$ )  $\delta$ : 8.43 – 7.62 (m, 48H,  $\text{H}_{\text{perylene}}$ ,  $\text{H}_{\text{porph}}$ ), 5.30 (d,  $J = 16.2$  Hz, 12H,  $-\text{OCH}_2_{\text{porph-}}$ ), 4.37 – 3.49 (m, 4H,  $-\text{COO}-\text{CH}_2_{\text{perylene-}}$ ), 2.98 – 2.19 (m, bs,  $-\text{CH}_2_{\text{PMA-}}$ ), 1.52 (m, 12H,  $-\text{CH}_2_{\text{porph-}}$ ), 0.87 (s, 36H,  $-\text{CH}_3_{\text{porph-}}$ ).

yield: grass-green, soft polymer, 16.5 mg

$M_{n,\text{exp}}$ : 5 100 g mol $^{-1}$

PDI: 1.30

$M_{n,\text{theor}}$ : 44 300 g mol $^{-1}$

### 4.2.3 Strategic considerations for ATR polymerization

In order to obtain star polymers by ATRP polymerization, several steps to accomplish the polymerization were undertaken. In the first step, PMMA was synthesized as a model substance. By doing this, it was observed, that the purification of Cu<sup>I</sup>Br was essential to obtain a clean product in a high yield. This polymerization procedure, which was expected to be successful for a variety of monomers was applied also to the initiator star molecule Br<sub>2</sub> BPMP<sub>2</sub> TBPTBTBP Pt.

First, the polymerization was tested with Cu<sup>I</sup>Br, which was not purified. Not only the yield was low (41%), but also the product was impure (green color derived from impurities). However, after purification of Cu<sup>I</sup>Br, the product was white and the yield was significantly higher (90%). The reaction progress was optically traceable as the solution turned from brownish to greenish as more Cu<sup>I</sup> was converted to the Cu<sup>II</sup> ligand complex. The greenish color could be removed by filtering over Celite. The final reaction conversion was obtained after 20 hours conversion.

The general reaction procedure, described in section 4.2.3.2, was applied to other matrices like styrene and ethyl acrylate. The outcome was the same as for methyl methacrylate as a matrix. Additionally, this reaction procedure was tested also with an excess of Cu<sup>I</sup>Br (27.7 eq.) and as ARGET ATRP polymerization by the addition of Cu<sup>0</sup>. The findings are explained below (5.3).

#### 4.2.3.1 PMMA as a model substance

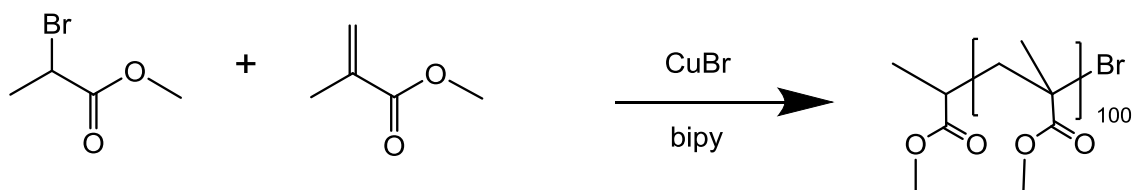


Figure 33. ATRP of PMMA.

A Schlenk flask, filled with copper (I) bromide (35.8 mg, 0.243 mmol, 2.58 eq.) was evacuated and refilled with nitrogen three times. Afterwards toluene (3 mL) was added and methyl methacrylate (1 mL, 9.38 mmol, 100 eq.) was added to the solution. As the ligand 2,2'-bipyridine (47.3 mg, 0.303 mmol, 3.23 eq.) was added, the solution turned brownish. After heating the flask to 90°C, the initiator methyl-2-bromopropionate (10.5  $\mu$ L, 93.8  $\mu$ mol, 1 eq.) was added. The solution was stirred overnight at 90°C. The solution was diluted in toluene and filtered over Celite and precipitated in 15 mL *n*-pentane. The precipitate was filtered and dried in vacuo.

$^1\text{H NMR}$  (300 MHz,  $\text{CDCl}_3$ )  $\delta$  3.60 (s, 3H;  $-\text{OCH}_3$ ), 2.12 – 1.67 (m, 2H; C- $\text{CH}_2$ ), 1.50 – 0.68 (m, 3H; C- $\text{CH}_3$ ).

yield: white, solid polymer, 0.94 g

$M_{n,\text{theor}}$ : 10 200  $\text{g mol}^{-1}$

PDI: 1.27

$M_{n,\text{exp}}$ : 9 200  $\text{g mol}^{-1}$

$T_g$ : 81.41 °C

### 4.2.3.2 Copolymer of Br<sub>2</sub> BPMP<sub>2</sub> TBPTBTBP Pt and MMA as matrix monomer

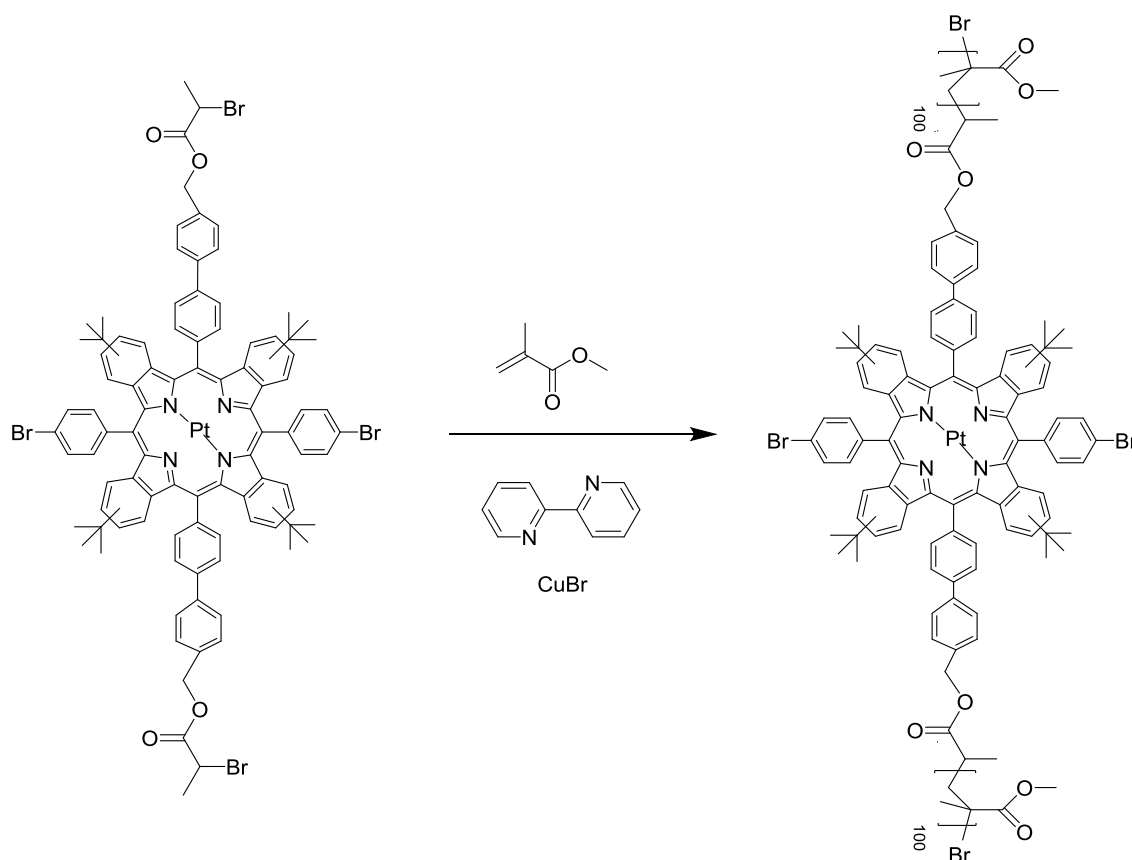


Figure 34. ATRP of Br<sub>2</sub> BPMP<sub>2</sub> TPTBTBP Pt with MMA.

Stock solutions of Br<sub>2</sub> BPMP<sub>2</sub> TPTBTBP Pt (21.9 g L<sup>-1</sup>) and 2,2'-bipyridine (14.3 g L<sup>-1</sup>) have been prepared with dry toluene as solvent (see appendix, Table A 1). For methyl methacrylate, no stock solution was prepared because it was already liquid. Cu<sup>I</sup>Br was not soluble in toluene.

Copper (I) bromide (0.608 mg, 4.20 μmol, 2 eq.) was weighted into a Schlenk flask which was evacuated and refilled with nitrogen three times. Afterwards toluene (0.5 mL) was added and methyl methacrylate (45.1 μL, 424 μmol, 200 eq.) were added to the solution. As the ligand 2,2'-bipyridine (92.9 μL of the stock solution, 8.50 μmol, 4 eq.) was added, the solution turned brownish. After heating the flask to 90°C, the initiator Br<sub>2</sub> BPMP<sub>2</sub> TBPTBTBP Pt (183 μL of the stock solution, 2.10 μmol, 1 eq.) was added. The solution was stirred for five days at 90°C. The solution was diluted in toluene, filtered over Celite which was washed first with toluene and second with acetone. The solution was slowly precipitated

in cold pentane (15 mL). The green precipitate (about 0.5 mg) was filtered and dried in vacuo. Because of the low yield (0.1 mg), no reasonable analysis could be done.

## 5. Results and Discussion

### 5.1 Dye Characterization

#### 5.1.1 Benzoporphyrin synthesis and characterization

For the synthesis of the sensitizer monomer, the template method<sup>12,51</sup> was used in the first step. This reaction was based on the condensation of phthalimide and phenylacetic acid. The template method was chosen due to its simplicity as it can be performed in only one step. To obtain tetra-bromo-substituted benzoporphyrins, phenyl acetic acid, zinc 4-bromophenylacetate, and 4-(*tert*-butyl)phthalonitrile were melted with a 5:1:4 ratio in a pre-heated metal block. The yield was expectedly low due to the occurrence of many side-products.

The UV-VIS spectrum was used for primary characterization (Figure 35). The molecule exhibited a strong absorption at 460 nm which is characteristic for a porphyrin (Soret-Band) and three Q-bands at 547 nm, 608 nm and 654 nm. The Soret band was attributed to the singlet state, whereas the Q band originates from the spin-triplet excited state.<sup>52</sup> Furthermore, the product was characterized by <sup>1</sup>H - NMR spectroscopy.

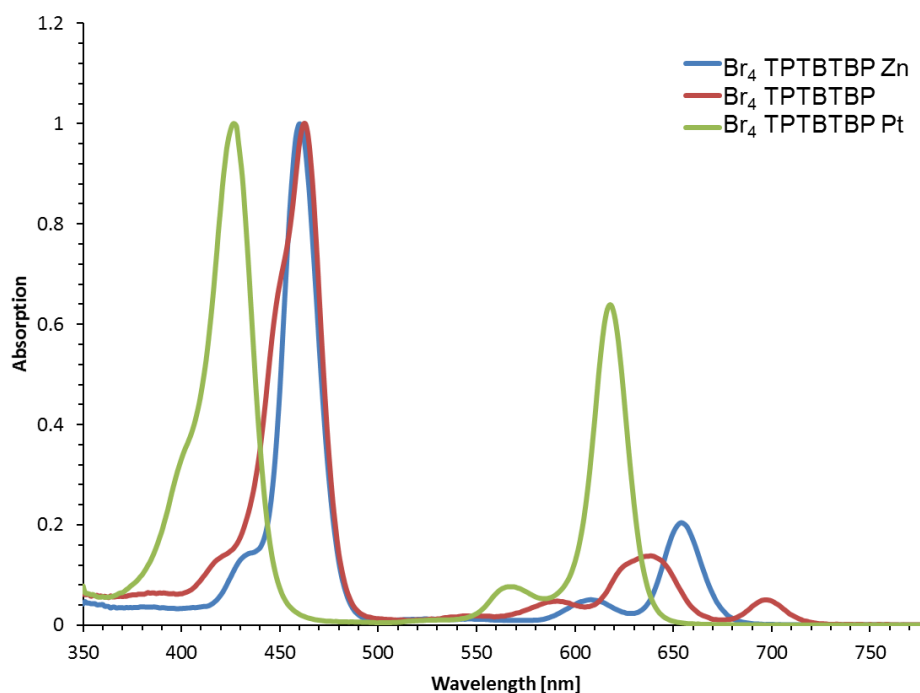


Figure 35. UV-VIS absorption spectra for the identification of Br<sub>4</sub> TPTBTBP Zn, Br<sub>4</sub> TPTBTBP and Br<sub>4</sub> TPTBTBP Pt.

The Zn<sup>II</sup> complex was later on demetallated and then platinated. The demetallation was performed with methane sulfonic acid, a strong acid (pK<sub>a</sub> -1.9).<sup>53</sup> This reaction was performed within 15 minutes and a red-brown free ligand was isolated. As depicted in Figure 35, the UV-VIS characterization yielded a Soret-band which showed a slight bathochromic shift compared to Br<sub>4</sub> TPTBTBP Zn for the Soret-band at 463 nm (3 nm) and Q-bands at 591 nm, 639 nm and 697 nm. The absorption bands correspond to values<sup>12</sup> present in the literature at large. In <sup>1</sup>H - NMR spectroscopy, the protons of the free ligand were detectable at -1.36 ppm.

The next step, the platination was comparably more laborious. Therefore, the demetallated complex (free ligand) was dissolved in cumene, which was heated up to 150° C and the platinum salt, Pt(C<sub>6</sub>H<sub>5</sub>CN)Cl<sub>2</sub> was added carefully dropwise. As HCl gas evolved during this reaction, the side product H<sub>4</sub>TPTBTBPBr<sub>4</sub><sup>2+</sup> can be formed. Hutter et al. investigated this reaction in 2014.<sup>51</sup> They showed that for H<sub>4</sub>TPTBTBPBr<sub>4</sub><sup>2+</sup> there was a characteristic absorption band at 504 nm. To avoid this reaction product, the evolving HCl gas which could protonate the free ligand was removed by constant nitrogen gas flow. In the UV-VIS spectrum, three characteristic bands could be shown, one at 426 nm (Soret-band), and two Q-bands,

whereas the Q-band at 566 nm had a much lower intensity than the one at 618 nm (Figure 35).

By Suzuki cross-coupling, four hydroxymethylphenyl-substituents were attached to the core, which were later on the precursors for the four-armed star monomer. This reaction is exceptional not only due to the convenient formation of carbon-carbon  $sp^2$ - $sp^2$  bonds, but also because of its mild reaction conditions. Therefore, 4-(hydroxymethyl)phenylboronic acid was used together with the highly active palladium catalyst  $Pd(PPh_3)_4$  in a basic environment, forming mono-, di-, tri-, and tetra- (hydroxymethyl)phenyl substituted  $Pt^{II}$  complexes. However, the yield for desired product was rather low (28.4%), considering that the catalyst was constantly added to the mixture and a 3-fold excess of educts (4-hydroxymethyl phenyl boronic acid and potassium carbonate) was used. This effect can be caused by the steric hindrance of the *tert*-butyl groups, which increase the solubility on the one hand, but lower the accessibility to the hydroxyl-groups on the other hand. The mono-, di- and tri- (hydroxymethyl)phenyl substituted  $Pt^{II}$  complexes were also isolated and used for preliminary studies.

As already mentioned in the sections above (4.1; 4.2), the side products of Suzuki-Miyaura cross-coupling were applied to Steglich esterification to link functional groups to the platinum (II) benzoporphyrin, to obtain monomers for preliminary experiments. Resulting from the Steglich esterification with the precursor platinum (II) monobromo tris-(2-bromopropanoatemethylphenyl) meso-tetra-phenyl tetra(*tert*-butyl)-benzoporphyrin (Br BPMP<sub>3</sub> TPTBTBP Pt) with 2-(((hexylthio)carbonothioyl)thio)propanoic acid, the monomer Br HTP<sub>3</sub> TPTBTBP Pt was obtained. The esterification is exceptional not only by its easy feasibility, but also by its fast reaction time. The addition of the reagents was essential, which was DDC (dicyclohexylcarbodiimide), which was capable for the formation of amides and DMAP (4-dimethylaminopyridine), which acted as an acyl transfer agent. The Steglich esterification was the key step to produce the different benzoporphyrin monomers, either for ATRP or for RAFT polymerization. For Br HTP<sub>3</sub> TPTBTBP Pt and HTP<sub>4</sub> BrTPTBTBP Pt, the yields obtained were 37% and 40% respectively. As a couple of side products were formed, which were visible by thin layer chromatography under UV-lamp irradiation, they were separated by column chromatography. Br HTP<sub>3</sub> TPTBTBP Pt was established in the preliminary RAFT

polymerization experiments as a center of star polymers with three emanating arms. HTP<sub>4</sub> Br TPTBTBP Pt was used as the star polymer center with four emanating arms, having different polymerization degrees (*polymer I, polymer II, polymer III*).

The absorption spectra of the benzoporphyrin monomer end-products do not change from the absorption spectrum after the platination (Figure 35 and Figure 36). Zhao reported that the absorption wavelength cannot be readily changed by chemical modification.<sup>54</sup> This was also determined by Hutter, who reported that the substitution has a very minor effect on the spectral properties of the dyes.<sup>51</sup>

#### **5.1.1.1 Identification of HTP<sub>4</sub> TPTBTBP Pt and Br HTP<sub>3</sub> TPTBTBP Pt**

The monomers for preliminary RAFT experiments, Br HTP<sub>3</sub> TPTBTBP Pt and final star polymer synthesis, HTP<sub>4</sub> TPTBTBP Pt respectively were analyzed via UV-VIS, <sup>1</sup>H-NMR spectroscopy, <sup>13</sup>C - NMR spectroscopy and MALDI-TOF MS. These monomers were well soluble in dichloromethane, therefore dichloromethane was used for analysis (UV-VIS spectroscopy and MALDI-TOF MS respectively) deuterated chloroform for NMR experiments. However, they were not soluble in acetone.

In UV-VIS spectroscopy, HTP<sub>4</sub> TPTBTBP Pt monomer (used later on for RAFT polymerization) showed a Soret-band at 432.5 nm and two Q-bands at 569 nm and at 619 nm. The Q band at 619 nm has a relatively high intensity, which is reasoned by the increased conjugation between the four fused benzo groups<sup>23</sup> and the macrocycle of the compounds. The emission spectrum (Figure 36) showed a broad phosphorescence signal with the peak maximum at 781 nm (excitation at 432 nm). The bathochromic shifts can be explained by the heavy atom effect of halogen atoms. The bathochromic shift is less significant if there is a larger distance from the  $\pi$ -conjugated core of the chromophore.<sup>51,54</sup> The molar extinction coefficient ( $222\,000\text{ M}^{-1}\text{ cm}^{-1}$ ), which was obtained at the Soret band at 432 nm correlated well to literature values.<sup>51</sup>

The monomer for preliminary RAFT experiments (Br HTP<sub>3</sub> TPTBTBP Pt) was analyzed via <sup>1</sup>H - NMR spectroscopy, <sup>13</sup>C - NMR spectroscopy and MALDI-TOF MS. <sup>1</sup>H - NMR spectroscopy showed the secondary and tertiary carbons as well as the methylene compound attached to the sulfur atom. However, the other signals deriving from the hexyl- chain, occurring between 1.31 ppm and 1.87 ppm overlapped. The analysis by <sup>13</sup>C - NMR spectroscopy showed clear signals for the aliphatic carbon atoms (between 14.14 ppm and 67.45 ppm), which revealed that the 2- ((hexylthio)thioxomethyl)thio)propionic acid had been attached to the benzoporphyrin precursor. Due to overlapping signals, the aromatic carbon atoms and quaternary atoms could not be exactly determined. The signals of the carboxyl- and thiocarbonyl- carbon atoms disappeared in the noise. The compound was finally identified with MALDI-TOF MS (m/z (calculated) 2374.6558; m/z 2375.4158 (found)).

Almost the same was true for HTP<sub>4</sub> TPTBTBP Pt monomer. Using <sup>1</sup>H - NMR spectroscopy, the aromatic moieties could be clearly shown due to the symmetrical structure. In <sup>13</sup>C - NMR spectroscopy, the aliphatic signals were resolved well, in contrast to the aromatic structure. Signals expected for quaternary carbons from the porphyrin and from the aryl groups appeared at the same chemical shifts as the signals of the CH atoms or disappeared in the noise. Likewise mentioned above for Br HTP<sub>3</sub> TPTBTBP Pt, also with HTP<sub>4</sub> TPTBTBP Pt, the carbonyl – carbon atoms and thiocarbonyl – carbon atoms respectively could not be obtained from the <sup>13</sup>C – NMR spectrum. The identity of the structure was confirmed by MALDI-TOF MS, whereas the calculated m/z was 2649.8704; whereas the determined m/z was 2649.8250.

#### **5.1.1.2 Identification of BPMP<sub>4</sub> TPTBTBP Pt and Br<sub>2</sub> BPMP<sub>2</sub> TPTBTBP Pt**

The initiators for ATRP experiments were analyzed via <sup>1</sup>H – NMR spectroscopy, <sup>13</sup>C – NMR spectroscopy, UV-VIS spectroscopy and MALDI-TOF mass spectrometry. BPMP<sub>4</sub> TPTBTBP Pt characterized by UV-VIS spectroscopy, showed a Soret-band at 430 nm. The Q-bands were detected at 566 nm and at 617 nm.

The peaks of the  $^1\text{H}$  - NMR spectrum were well resolved, especially the peak at 5.27 ppm for the methyl-protons and the proton attached at the carbon near the bromine at 4.44 ppm. This result could be confirmed by  $^{13}\text{C}$  - NMR spectroscopy, obtaining the corresponding carbon - atoms. The mass obtained from the MALDI-TOF MS analysis was  $m/z$  2213.7354, which was higher than the calculated  $m/z$  2210.4429. As mass accuracy is linked to the resolution, this can be explained by the low resolution (see appendix, Figure A 7).

As precursor of  $\text{BPMP}_4$  TPTBTBP Pt the clean, symmetrical  $\text{HTP}_4$  TPTBTBP Pt was used. However, for the synthesis of  $\text{Br}_2$   $\text{BPMP}_2$  TPTBTBP Pt the asymmetrical  $\text{Br}_2$   $\text{HTP}_2$  TPTBTBP Pt was utilized. The precursor was a product mixture of the 1,2- and 1,3- substituted  $\text{Br}_2$   $\text{HTP}_2$  TPTBTBP Pt and contained impurities which were visible at the TLC plate under the UV lamp. The protons of the obtained  $^1\text{H}$  - NMR spectrum were attributable. However, as it was a well-known for asymmetrical porphyrins, the spectra were not resolved well. The Steglich esterification worked out as the carbons of the  $^{13}\text{C}$  - NMR spectrum were identified at the positions 40.14 ppm (CH-Br) and 67.54 ppm ( $\text{CH}_2$ ). Though, signals occurring between 24-84 ppm and 28.52 ppm as well as 74.72 ppm were attributed to the impurities. In the MALDI-TOF MS spectrum, there is a mass difference between the calculated molecular ion and the determined one of 93.1523 (see appendix, Figure A 6). However, this mass difference could not be further explained.

### 5.1.2 Perylene diester synthesis and characterization

In Figure 20, the synthesis scheme of  $\text{PDE}_{\text{mon}}$  is depicted. The synthesis was started from diisobutyl-perylene-3,9-dicarboxylate (diisobutyl-PDC), which was converted to potassium perylene 3,9-dicarboxylate (PDC) by saponification. Due to different solubility (PDC i.e. potassium salt soluble in water), the separation was easily maintained. In the second step (esterification), the spacers (1-bromobutane and 6-bromo-1-hexanol) were attached to the ester backbone. After the alcohol (1-hexanol) was attached to the perylene backbone, further esterification could be facilitated. However, also the symmetrical byproduct, diisobutyl perylene-3,9-dicarboxylate was generated, which was separated from the main

product by column chromatography. The main product and the side product were detectable by thin layer chromatography. The asymmetrical target molecule, 3-butyl 9-(6-hydroxyhexyl) perylene-3,9-dicarboxylate (PDE) occurred at a different  $R_f$  value than the side product. The products were characterized by  $^1\text{H}$  - NMR spectroscopy and UV-VIS spectroscopy. The results from these analysis matched well with the values present in the literature<sup>12</sup>. However, the low yield of PDE (18.7%) can be reasoned by multiple separation steps. In the last step, the Einhorn variation of the Schotten-Baumann esterification was applied to synthesize 3-(6-(acryloyloxy)hexyl)9-butyl perylene-3,9-dicarboxylate ( $\text{PDE}_{\text{mon}}$ ). Acryloyl chloride was attached to the alcohol (1-hexanol) in order to obtain a double bond for the final monomer. The methyl acrylate group of  $\text{PDE}_{\text{mon}}$  was suited as polymerizable group and resembled the polymerization matrix, methyl acrylate (MA) used for ATRP and RAFT polymerizations respectively. Analysis was done with  $^1\text{H}$  - NMR spectroscopy,  $^{13}\text{C}$  - NMR spectroscopy, UV-VIS spectroscopy, and MALDI-TOF MS.

The results of UV-VIS spectroscopy are shown in Figure 36. The absorption spectrum of the  $\text{PDE}_{\text{mon}}$  showed two strong absorption bands at 464.5 nm and at 439.5 nm. Furthermore, a small shoulder at 413 nm was detected. The emission spectrum was excited at 440 nm and showed a small shoulder at 481 nm, a maximum at 510 nm, and a broad shoulder at 546 nm (Figure 36). The molar extinction coefficient  $\epsilon$  was determined as  $29\,200\ \text{M}^{-1}\ \text{cm}^{-1}$  at 465 nm, in dichloromethane, which is in accordance with what has been suggested by the literature<sup>12</sup> at hand.

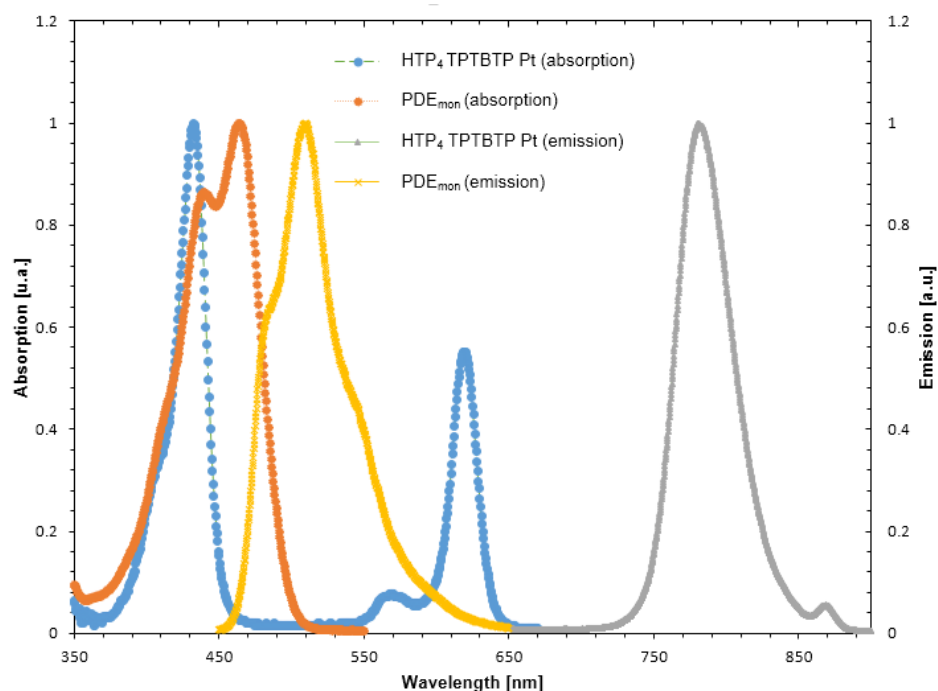


Figure 36. Absorption and emission spectra for HTP<sub>4</sub>TPTBTP Pt and PDE<sub>mon</sub>.

The chemical shifts detected by <sup>1</sup>H - NMR spectroscopy matched well those expected, and the methyl acrylate group with characteristic peaks at 6.40 ppm, 6.12 ppm and 5.81 ppm could be identified. In <sup>13</sup>C - NMR spectroscopy, the signals of the aliphatic carbon atoms and carbonyl atoms were detected. However, the signals of the quaternary carbon atoms of perylene overlapped with signals of the CH-groups of perylene respectively and had a low intensity. With MALDI-TOF MS, the PDE<sub>mon</sub> was shown to correlate well with the experimental data m/z 550.2343 (m/z 550.2355 calculated).

## 5.2 Polymer Characterization

### 5.2.1 Preliminary studies

RAFT copolymerizations of PDE<sub>mon</sub> and benzoporphyrin were performed in order to evaluate the reaction conditions, the feasibility with the monomers, and subsequent the yields. Thereby, AIBN was chosen as an initiator. As a CTA, trithiocarbonate was implemented. The resulting polymers were analyzed by size exclusion chromatography and <sup>1</sup>H – NMR spectroscopy. The control of the polymerization depended on the ratio between RAFT agent and initiator and the type of monomer used. The goal was to synthesize star polymers implementing both PDE<sub>mon</sub> and benzoporphyrin (Br HTP<sub>3</sub> TPTBTBP Pt) via R group approach (see 4.2.2 and 5.2.2). In the <sup>1</sup>H - NMR spectra, it could be shown, that polymers were produced. However, the benzo-moieties were not detected as clear signals. This can be explained by the molecular weight of the polymer, which was higher than the amount of benzoporphyrin. Therefore, the signals of the benzoporphyrin moieties were smaller, in relation to what would have been expected. The SEC data delivered various results, which implied high molecular weights and low PDIs (see 5.2.1.1). However, due to limited amounts of samples, no further methods of characterization were utilized. Another preliminary experiment, the copolymerization of a matrix monomer (either MMA or MA) with the perylene diester monomer produced interesting results. As RAFT reagent, 2-((hexylthio)thioxomethyl)thio)propionic acid was used. One can claim, that RAFT polymerization of the matrix monomers with the RAFT agents definitely proceeded. However, it is not completely clear if the perylene diester monomer was covalently tied to the chain as the perylene diester monomer precipitated in *n*-pentane. There is the indication in the <sup>1</sup>H - NMR-spectra that it may have succeeded, as the protons of the vinyl group were not visible.

#### 5.2.1.1 Selection of the matrix

In the experimental section, it was shown that the RAFT polymerization via R-group approach was tested with two different matrices. The choice of the matrix

was essential, as it determined the reaction mechanism and subsequently, the composition of the end product. Accordingly, material characteristics like the glass transition temperature ( $T_g$ ) are inherently connected to the matrix. Furthermore, this plays an important role for the TTA-UC measurements in order to facilitate the energy transfer steps. The polymer composition influences the preparation of thin films and it is thus essential that the matrix does not absorb the irradiance so that TTA-UC can be properly observed. In the preliminary experiments, methyl methacrylate and methyl acrylate were tested as matrices and were compared to each other. Typically for poly(methyl methacrylate) (PMMA), the obtained star polymers including methyl methacrylate as a matrix, were transparent and thermoplastic ( $T_g \sim 100^\circ\text{C}$ ). Contrastingly, star polymers with methyl acrylate were soft due to the low glass transition temperature ( $T_g \sim 10^\circ\text{C}$ ). Apart from the material properties, the reaction mechanism of RAFT polymerization is different. In the literature, the hybrid behavior of MMA in RAFT polymerization is a well-known fact. Hybrid behavior<sup>55</sup> describes the occurrence of a combination of conventional chain-transfer and free radical polymerization during the RAFT polymerization of MMA. Although the same reaction conditions were installed for the star polymer synthesis, very different molecular weights for the methyl acrylate and methyl methacrylate respectively star polymers were obtained. Therefore, it was observable that the molecular weight of the star polymer depended on the matrix. Exemplary, the results of the three-armed star polymers are shown. The three-armed star polymers consisted of platinumated benzoporphyrins as the centers and copolymers of a perylene diester acrylate and either MMA or MA as matrix monomer. For the three-armed star polymer installing methyl methacrylate as a matrix (benzoporphyrin-(MMA)<sub>100</sub> – perylene), the  $M_n$  was 13 809 g mol<sup>-1</sup>, while having a broad molecular weight distribution of 4.68 (Figure 37). In contrast to that, the three-armed star polymer which also consisted of the perylene diester monomer, but methyl acrylate as a matrix monomer, had a derived  $M_n$  of 3200 g mol<sup>-1</sup>, the polydispersity index being 1.98 (Figure 38). Comparing the molecular weight distribution curves (Figure 37 and Figure 38), a high-molecular shoulder was obtained for the MMA star polymer (benzoporphyrin-(MMA)<sub>100</sub> – perylene), whereas this could not be detected for the corresponding MA star polymer (benzoporphyrin-(MA)<sub>100</sub> – perylene). A higher molar mass frac-

tion was also reported by Paulus et al. (55), who researched the RAFT polymerization with MMA in the microwave reactor and observed hybrid behavior. Paulus interpreted the high-molecular mass fraction from the SEC traces as chain coupling. Accordingly, star-star coupling may have occurred in the preparation of (benzoporphyrin-(MMA)<sub>100</sub> – perylene). It was shown, that the  $M_n$  and PDI were higher for this MMA star polymer compared to the corresponding MA star polymer. The high  $M_n$  as well as the broad polydispersity of MMA compared to MA, can be an indication for hybrid behavior, which has been reported in several previous studies<sup>55–57</sup>. Hybrid behavior is caused by a slow transfer constant<sup>57</sup> ( $k_{tr}$ ), which decreases the rate of addition ( $k_p$ ). For methyl methacrylate (MMA), only tertiary leaving groups which efficiently reinitiate the polymerization process, are suitable as RAFT-agents in order to obtain a narrow polydispersity. Therefore, the RAFT agent utilized for MMA polymerization was not appropriate. Finding the optimal reaction conditions is important to ensure that the pre-equilibrium of the RAFT process is completed fast on the time scale of the polymerization. Considering these aspects, methyl acrylate (MA) was selected as an appropriate matrix for *polymers I-III*.

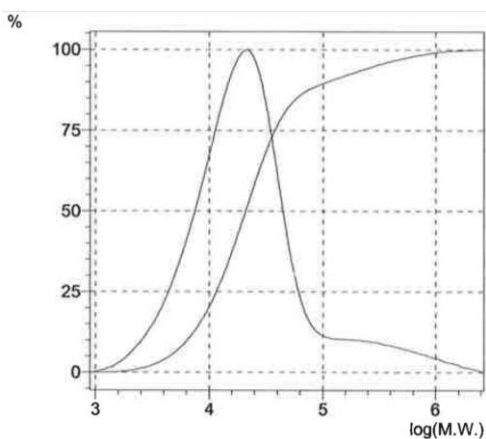


Figure 37. Molecular weight distribution curve of preliminary experiments yielding the three-armed (benzoporphyrin-(MMA)<sub>100</sub> – perylene) star polymer (GPC, solvent: chloroform).

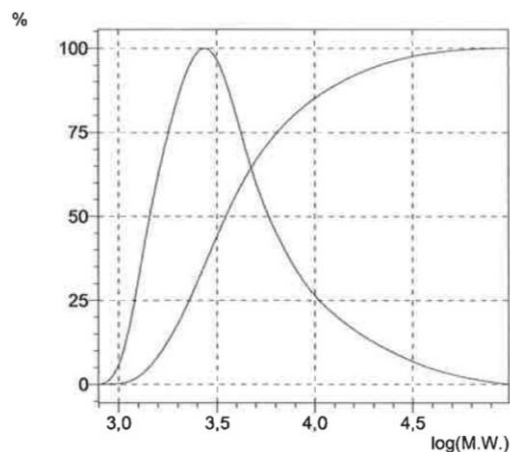


Figure 38. Molecular weight distribution curve of preliminary experiments yielding the three-armed (benzoporphyrin-(MA)<sub>100</sub> – perylene) star polymer (GPC, solvent: chloroform).

## 5.2.2 Star polymers

Following the R-group approach via RAFT, three star polymers were synthesized with different theoretical chain lengths for each arm (100, 250 and 500). The procedure was also performed with a planned chain length of 1000 per arm, however, no polymer could be isolated. Using HTP<sub>4</sub> TPTBTBP Pt as a chain transfer agent, methyl acrylate was used as a matrix monomer. Methyl acrylate was suited as matrix monomer because of the lower polydispersity indices, and the absent hybrid behavior in contrast to methyl methacrylate (3.2.1.1). Furthermore, methyl acrylate does not exhibit any UV-absorbance above 300 nm.<sup>38</sup> PDE<sub>mon</sub> was intended to be incorporated into the polymer chain. The results depicted in chapter 4.2.2 are discussed in the following section. As characterization methods, size exclusion chromatography, DSC, MALDI-TOF MS and <sup>1</sup>H - NMR spectroscopy were applied.

Table 1. Determined number average molecular weights and polydispersity indices for *polymer I*, *polymer II* and *polymer III*.

<b><i>Polymer</i></b>	<b>Chain length per arm</b>	<b>M<sub>n</sub> high-molecular weight peak [g mol<sup>-1</sup>]</b>	<b>M<sub>n</sub> low-molecular peak [g mol<sup>-1</sup>]</b>	<b>M<sub>n</sub> peak sum determined [g mol<sup>-1</sup>]</b>	<b>M<sub>n</sub> peak sum theoretical [g mol<sup>-1</sup>]</b>	<b>PDI sum</b>
<i>Polymer I</i>	100	10,600	4,100	5,100	13,100	1.33
<i>Polymer II</i>	250	11,000	3,300	6,800	25,700	1.59
<i>Polymer III</i>	500	12,800	4,500	5,100	46,400	1.30

The theoretical number average molecular weights given in Table 1 were calculated by assuming an overall conversion of 24%. As the average monomer conversion ( $x$ ) for one RAFT-agent chain was expected to be 70% after 16 hours due to literature values<sup>38,50</sup>, the overall conversion of a four-fold substituted substrate or four arms emanating was assumed to be about 24%.

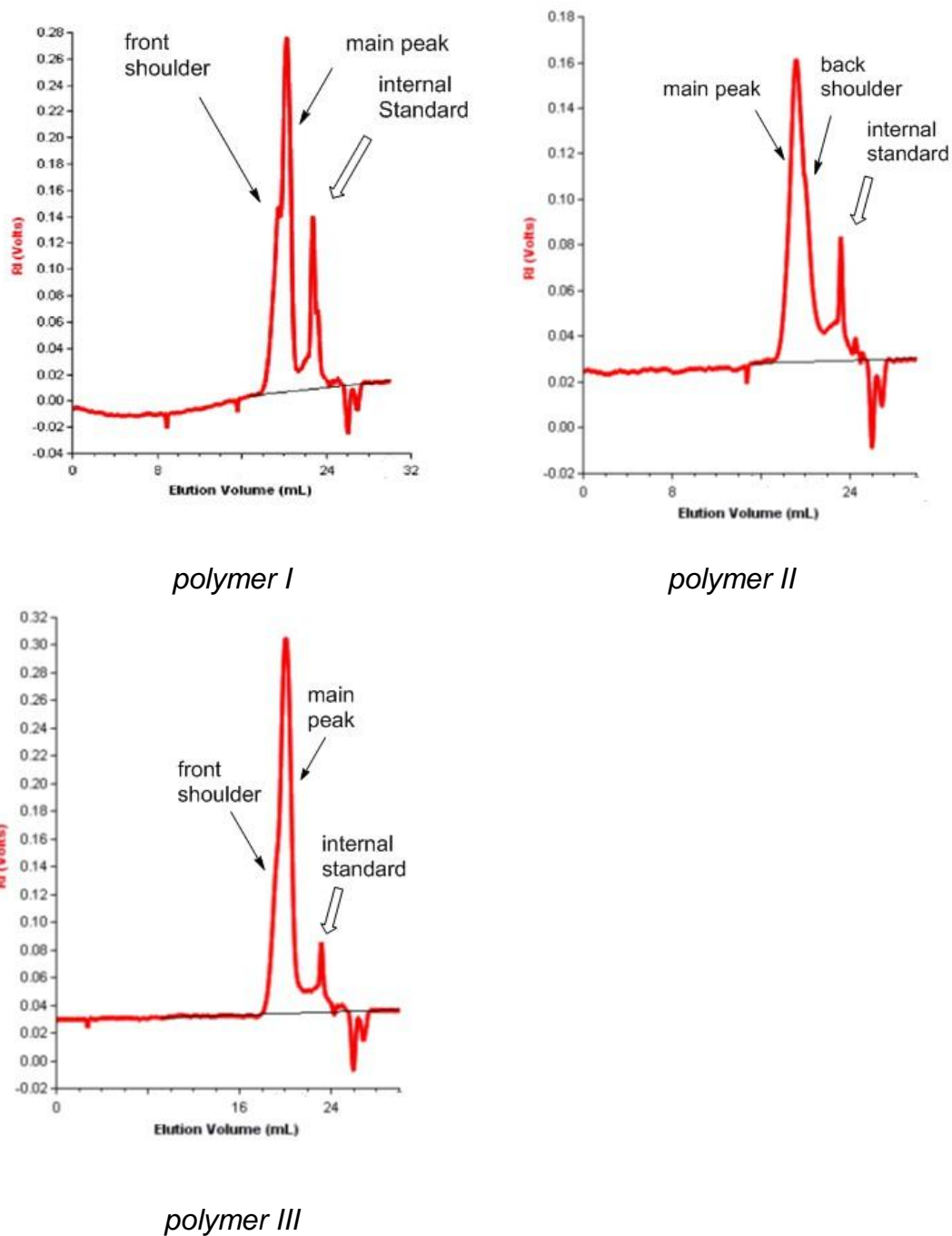


Figure 39. Peak shapes obtained from the GPC analysis.

In Table 1 and Figure 39, the results from GPC (gel phase chromatography) are depicted. The molecular weight distribution was evaluated via RI - detection, which was sensitive to the overall mass fraction of the polymer<sup>38</sup> (Figure 39). It was a fact that the obtained number average molecular weights were much lower

than the calculated number average molecular weights. Furthermore, the GPC traces showed bimodal molecular weight distributions. Additionally, a high-molecular peak and a low-molecular peak were detected.

For *polymer I*, a number average molecular weight of 5,100 g mol<sup>-1</sup> was obtained by integration of the bimodal molecular weight distribution. It is a well-known fact that GPC often underestimates the molecular weights of star polymers due to smaller hydrodynamic volumes.<sup>4</sup> This results in longer retention times<sup>4,58</sup> and, therefore, a lower apparent molecular weight than for linear polymers. By separate integration of the peaks, a high-molecular peak could be obtained with a number average molecular weight of 11,000 g mol<sup>-1</sup>. This was close to the theoretical number average molecular weight of *polymer I* (13,100 g mol<sup>-1</sup>). Furthermore, a yield of 34.0 mg was obtained, which was higher than for *polymer II* and *polymer III*. However, it was not clear if the perylene diester monomer was incorporated in the star. The <sup>1</sup>H - NMR spectrum of *polymer I* (Figure 40) showed that the protons of the methyl acrylate were still detectable (6.10 ppm (dd), 6.39 ppm (d), 5.80 ppm (d)). The aromatic proton peaks of perylene were detectable at 8.89 ppm (d) and at 8.80 ppm (d). However, for *polymer II* and *polymer III*, the methyl acrylate protons of the perylene diester monomer were not observed.

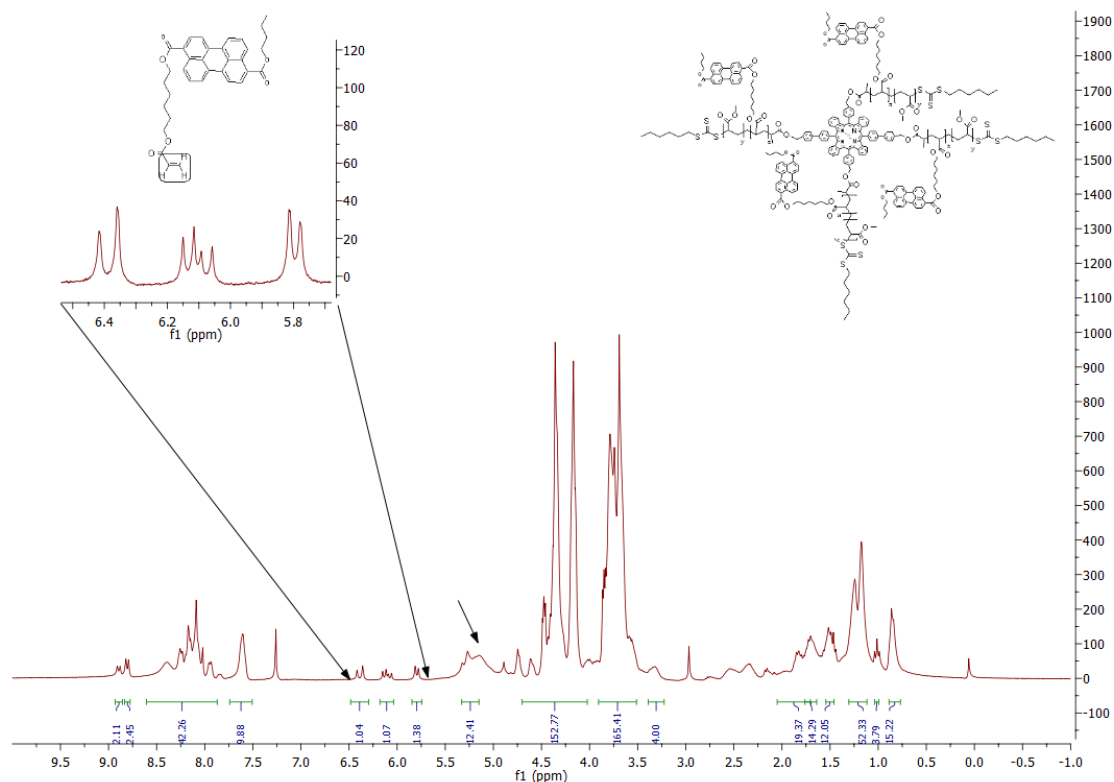


Figure 40. <sup>1</sup>H NMR spectrum of *polymer I* (benzoporphyrin - (MA)<sub>100</sub> – perylene star polymer).

As shown in Figure 39, *polymer II* exhibited a high content of high-molecular species (11,000 g mol<sup>-1</sup>) compared to *polymer I* and *polymer III*. Thus, this value was rather low, regarding the theoretical number average molecular weight (25,700 g mol<sup>-1</sup>). The yield obtained was 14.9 mg, which was lower than calculated. In the <sup>1</sup>H - NMR spectrum, the methyl acrylate protons of the perylene diester monomer were not detectable, which can be attributed to the low concentration.

For *polymer III*, it was expected that the molecular weight of the star polymer with an expected polymerization degree of 500 per arm was far higher compared to *polymer I* and *polymer III*. However, the high-molecular peak was only 12,800 g mol<sup>-1</sup>. It was assumed, that the polymerization was not finished after 16 hours, or termination events occurred due to this long reaction time. The long reaction time was chosen, as the chain transfer agent was not dissipated after six hours reaction time. However, the reaction time was not optimized. It is therefore unclear if a longer reaction time of more than 16 hours could have yielded higher molecular weights. This might be an interesting aspect to consider in further investigations.

As mentioned above, the methyl acrylate protons of the perylene diester monomer were not observed in the  $^1\text{H}$  - NMR spectrum and a yield of 16.5 mg was obtained.

Above all, the RAFT mechanism itself can be responsible for the low conversions, as it consists of an equilibrium between living and dormant species. Boschmann reported that the R-group approach for star polymerization is restricted to the low monomer conversion regime and therefore hampers the formation of long chains and high molecular masses.<sup>38</sup> The production of dead chains is likely to be a termination event and in order to avoid this, it is important to keep the radical concentration<sup>41</sup> (in respect to the RAFT agent) as low as possible since side reactions can be the consequence. As mentioned above, termination events occur due to long reaction times, but can also be caused by the presence of oxygen. In the presence of oxygen, it can be assumed that every radical introduced will eventually terminate or react with oxygen, producing a dead chain devoid<sup>59</sup> of the RAFT end group. Thus, the absence of oxygen is particularly important to achieve highly controlled polymerizations and to preserve livingness.<sup>59</sup> As the reaction vessels and the reactants were degassed for half an hour, termination by oxygen is not favorable, but cannot be completely obviated.

As shown in the  $^1\text{H}$  - NMR spectrum for *polymer I* (Figure 40) and for the other polymers, peaks between 4.0 ppm and 5.0 ppm were obtained. The signals were interpreted to derive from side reactions, such as the intermediate radical propagation. As it was discussed in the previous and following sections, impurities can be produced by side reactions.<sup>50</sup> Having a trithiocarbonate species as a CTA, side products and by-products such as star polymers with dead arms<sup>41</sup>, linear dead polymers and linear polymer capped with the trithiocarbonate moiety can evolve. In other words, copolymerization of a macromonomer RAFT agent with monosubstituted monomers such as acrylates and styrene is a major issue. (Linear) Macro-RAFT agent<sup>41</sup> could have formed, which would have increased the molecular weight linearly with conversion.

It was disputed if the perylene diester monomer was covalently linked to the star. From the preliminary experiments, covalent linkage was not proven, but assumed to be favorable, however to a limited extent. In theory, the propyl spacer should

diminish  $\pi$ - $\pi$  stacking<sup>16</sup> of the perylene molecules. Furthermore, the spacer maintained some flexibility while promoting efficient energy transfer between emitters and sensitizers. The spacer was implied to limit steric hindrance around the vinyl group. However, independent confirmation of these results was requested. One approach could be the end group analysis of the star polymers using  $^1\text{H}$  - NMR spectroscopy. But as the end group signals were not clearly resolved in the  $^1\text{H}$  NMR spectroscopy, this would not allow for calculations of molecular weights.<sup>5</sup> In Figure 41, the MALDI-TOF MS spectrum of *polymer I* is given. However, only the matrix could be obtained. The experiment was performed with a range of matrices (DCTB, alpha, dithranol with and without sodium), however, the molecular ions as well as the molecular weight distribution were not detectable. The molecular ions are usually well resolved in the range between  $m/z$  1000 and  $m/z$  2000.

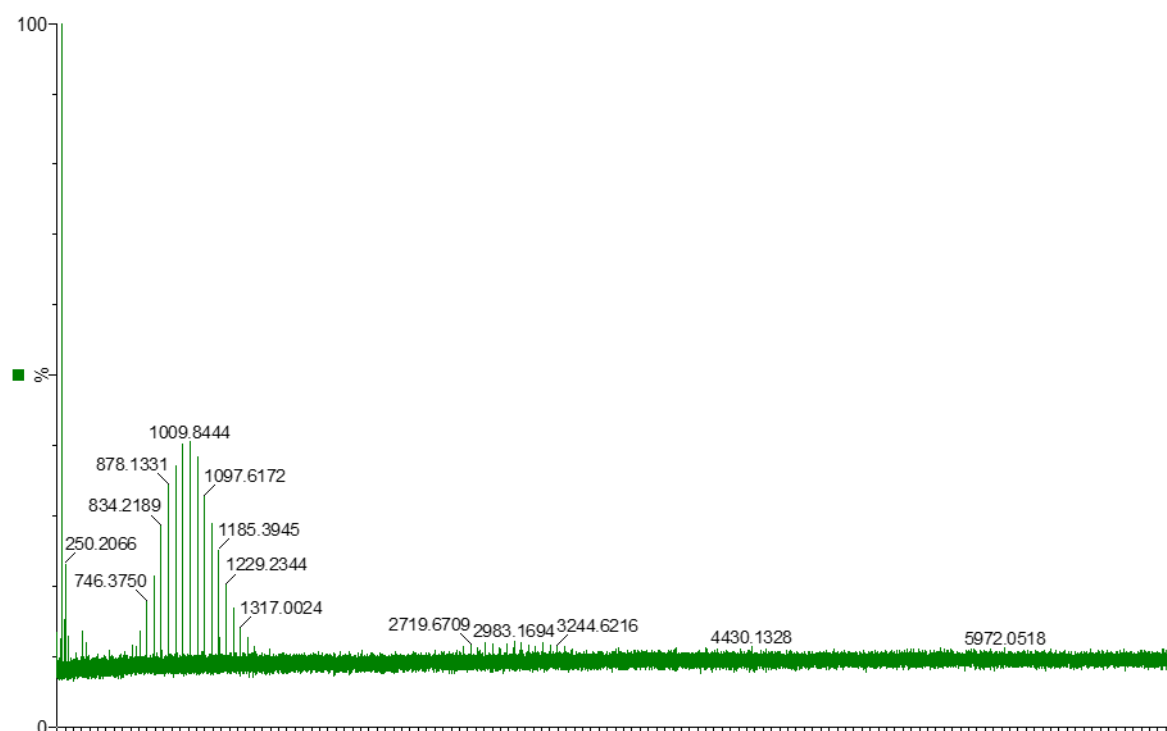


Figure 41. MALDI-TOF MS spectrum of *polymer I* utilizing sodium dithranol as a matrix.

### 5.3 ATRP experiments

The intention was to polymerize a matrix monomer (BPMP<sub>4</sub> TPTBTBP Pt) and the perylene moiety (PDE<sub>mon</sub>) by atom transfer radical polymerization. From the minimal amounts obtained from these experiments, no meaningful characterization experiments could be performed. In the following chapter, the reasons for the unsuccessful ATRP reaction are discussed.

The procedure was tested by synthesizing a model substance (PMMA). The synthesis is given in section 4.2.3.1. The background literature was derived from various sources<sup>60,61</sup>. The polymer was verified by <sup>1</sup>H - NMR spectroscopy, DSC (see appendix, Figure A1) and GPC measurements. By using <sup>1</sup>H – NMR spectroscopy (Figure 42), it could be successfully shown that PMMA was synthesized. An atactic microstructure was obtained, which was given by the triads (rr, mr, mm).<sup>62</sup> With the DSC (T<sub>g</sub> of 81.41°C) and GPC (M<sub>n</sub> of 9160 g mol<sup>-1</sup>) results, a polymer could be identified.

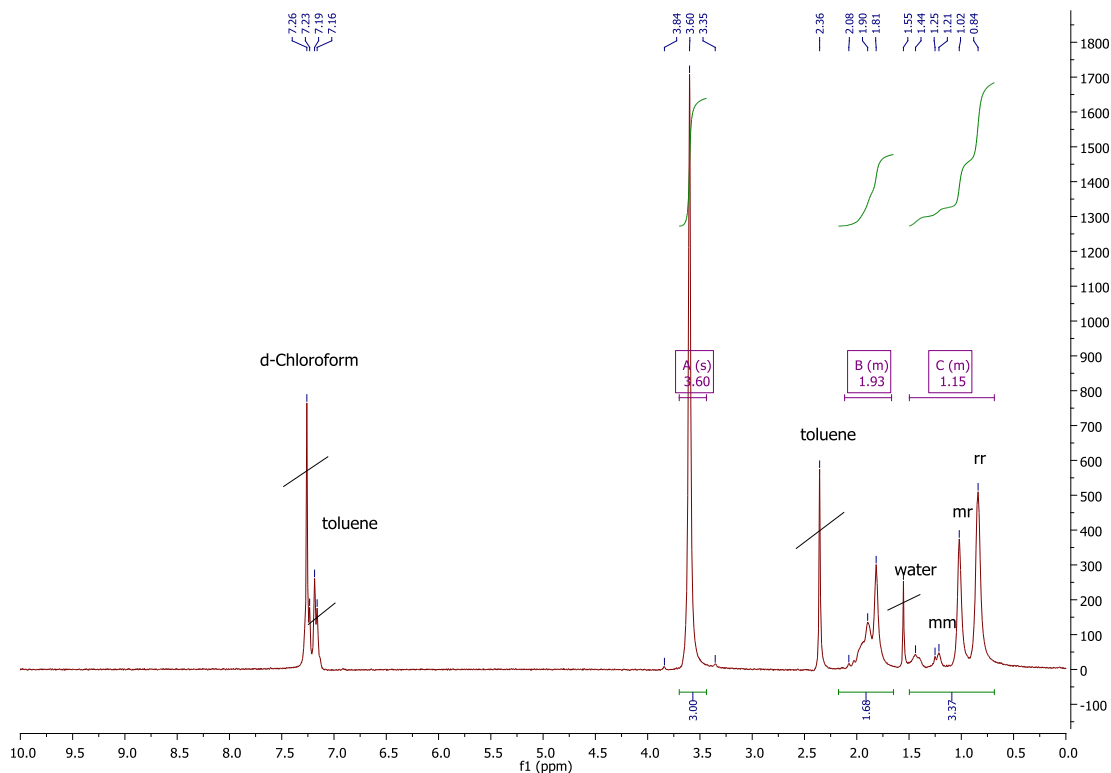


Figure 42. <sup>1</sup>H-NMR spectrum of PMMA synthesized by ATRP.



polymerization, there were several factors to consider. The porphyrin we synthesized should be installed as the center of the star polymer. However, the initiator we synthesized was a sterically very demanding one due to the aromatic rings and the Pt<sup>II</sup> as the central atom. The central atom Pt<sup>II</sup> could have altered the quadratic planar structure, typically for porphyrin to a more convoluted structure. Having a more convoluted structure, substitution reactions are more likely to occur. However, the substitution of Pt<sup>II</sup> by Cu<sup>II</sup> was not confirmed in our studies, as there were no changes in the UV-VIS spectra observable. Other authors, who reported the substitution, observed changes<sup>5,63</sup> in the UV-VIS spectra. High<sup>5</sup> reported that all polymers clearly displayed two Q bands with maxima above 450 nm that were attributable to the free-base porphyrin and a Cu<sup>II</sup> porphyrin complex respectively.

Regarding the publication by High, the possibility to install Pd<sup>II</sup> as a central atom in order to obtain appropriate TTA-UC sensitizers was considered. High and others managed to obtain a Pd<sup>II</sup> porphyrin molecule by polymerising the free ligand and later on introduce Pd<sup>II</sup> as a salt. However, they reported that using MMA, the polymerization proceeded slowly, and the product was only obtained after five days. Thereby, they assumed the degradation of the end groups. However, they also did not preclude star-star termination to have taken place.<sup>5</sup>

As reported in the experimental part (4.2.3), an excess of Cu<sup>I</sup>Br was used in order to enhance the polymerization rate. However, a very small quantity of product was obtained after five days. High<sup>63</sup> and coworkers reported that an excess of copper may split the ester bond between the porphyrin and the growing polymer chain. Another possible explanation is that the increase of the Cu<sup>I</sup> concentration results in an increased radical<sup>63</sup> concentration at the start of the polymerization. Hence, this was subsequently followed by an increase in termination reactions.

We tested ARGET ATRP polymerization and used Cu<sup>0</sup> as a reducing agent. Indeed, the reaction time could be decreased. The conversion to the first polymeric species on the thin layer chromatography plate could be obtained after 30 minutes (ARGET ATRP) and 3 hours (ATRP) respectively. Though the yield was not higher than with the other experiments surveyed.

Another interesting aspect which was reported by Matyjaszewski<sup>64</sup> was that negative results (e.g., no polymerization) may suggest not only that the chosen catalytic system is not active enough, but also that it is too active. Hence, an excess of radicals is formed and the polymerization is terminated at a very early stage. The nature of the ligand is another important point, because the ligand has to manage to easily fit to the sleeping species to form the metal-ligand species. 2,2'-bipyridine is deemed as a moderate ligand molecule and slow conversions are reported. The ligand molecule and the matrix have to combine well to one another. MMA and 2,2'-bipyridine was reported as an appropriate system, further styrene, MA and BA are also suited for ATRP polymerization with this ligand. High also reported poor initiation efficiency (the rate of propagation exceeds the rate of initiation in the early part of the polymerization) of the porphyrin in the bulk mixture.<sup>5</sup> Low solubility of the porphyrin initiator hampered the initiation, though this was not apparent from simple inspection.<sup>5</sup> ATR polymerization was reported with various solvents such as toluene, anisole, acetonitrile, whereas toluene was most commonly used.

As it was clear after a while, that the ATR polymerization did not work out, new solutions of the occurring problems were conceived such as ATRP from extended chains or the combination of ATRP and Click chemistry. However, as reported in the previous sections, the RAFT polymerization was selected as the appropriate method (see chapter 5.2.).

## 5.4 TTA-UC measurements

The star polymers titled as *polymer I-III* were tested for TTA-UC in solution at room temperature. The polymer solutions were excited by a 450 W Xe lamp ( $244 \mu\text{mol s}^{-1} \text{m}^{-2}$ ) at 618 nm and a monochromatic 635 nm LED ( $36\ 195 \mu\text{mol s}^{-1} \text{m}^{-2}$ ) respectively.

The polymers were diluted with 1,4-dioxane so that each polymer had a concentration of  $10.5 \text{ g L}^{-1}$ .<sup>1,12</sup> Afterwards, the solutions were sealed with a screw-cap and deoxygenated by bubbling argon for 10 minutes. The excitation wavelength

was determined by UV-VIS spectroscopy at 618 nm. The settings for the Fluorolog Horiba spectrometer were adjusted (14 nm maximum slit width) in order to fall below 2 000 000 CPS for the corrected emission. The spectra were recorded in front-face mode.

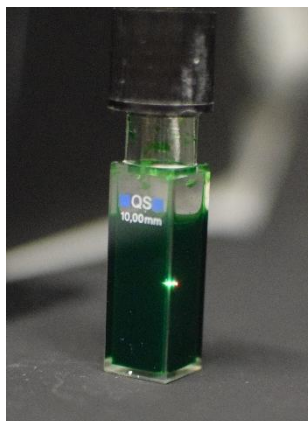


Figure 44. Green fluorescence determined by excitation with a laser diode at 635 nm (*polymer I*, 1,4-dioxane).

Figure 44 shows the cuvette of *polymer I* diluted in 1,4-dioxane. The up-converted green fluorescence was shown for the polymer with the highest quantum yield. It was excited with a laser 635 nm LED. The TTA – UC signal occurs approximately at similar intensity as the phosphorescence signal, which indicates a high quantum yield. Although, this implies that the energy transfer from the sensitizer to the emitter is less effective.<sup>12</sup>

In the TTA-UC measurements, a broad phosphorescence signal was observed with a maximum at 781 nm. The smaller TTA-UC signal occurred between 480 nm and 550 nm, whereas the peak maximum was at 503 nm (Figure 45).

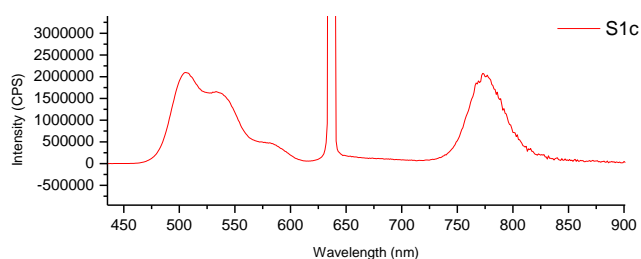


Figure 45. TTA emission spectrum of *polymer I*.

### 5.4.1 Quantum yields

The quantum yields of the anti-Stokes fluorescence were calculated by using the software Origin. Therefore, the area below the emission band of the annihilator<sup>65</sup> was integrated and compared to respective area below the emission band of the sensitizer without the annihilator. Following from this approach, the determined values were only estimated. In Figure 45, the TTA emission spectrum of the *polymer I* with the highest quantum yields is shown (Table 2,  $\phi(\text{lamp}) = 0.22$ ,  $\phi(\text{laser}) = 1.75$ ). It was found out that *polymer I*, which was implemented as the polymer with the lowest chain length (100) per arm had the highest quantum efficiency and accordingly to that, the most promising TTA-UC spectra.

Table 2. Quantum efficiencies by excitation with the lamp resp. laser source. Measurements were performed in 1,4-dioxane solution.  $M_n$  and  $M_w/M_n$  were determined by gel phase chromatography.

<i>Polymer</i>	Chain length per arm	$M_n$ peak sum determined [g mol <sup>-1</sup> ]	$M_w/M_n$	Quant. Eff. lamp [%]	Quant. Eff. laser [%]
<i>I</i>	100	5,100	1.33	0.22	1.75
<i>II</i>	250	6,800	1.59	0.06	0.88
<i>III</i>	500	5,100	1.30	0.11	0.45

The quantum yields displayed in Table 1 have to be accepted with reservation, as the determined molecular weights were lower and  $PDE_{\text{mon}}$  was probably not tethered to the star polymer as intended. As  $PDE_{\text{mon}}$  precipitated incompletely in *n*-pentane, there is the option that the perylene was diluted. Therefore, the perylene moiety had translational and rotational mobility in solution which makes TTA-UC better feasible and increases the quantum yield. In the literature, it was reported that the perylene moieties tend to aggregation and  $\pi$ - $\pi$ -stacking. The ratio of emitter molecules to sensitizer molecules has to be considered, especially when they are compared with the values present in the literature. In our polymerizations, the ratio of emitter to sensitizer was chosen to be 4:1, due to the consensus established by previous studies<sup>12</sup>. It has to be noticed, that the ratio between sensitizer and emitter changes by increasing the molecular weight of the

polymer. In this regard, the concentration of the annihilator has to be adapted to the number average molecular weight of the polymer. In order to study this correlation, concentration series would have to be measured.

The quantum efficiencies for a very similar system implementing unbound dyes, examined by Hollauf<sup>12</sup>, with a ratio of emitter to sensitizer (5:1) exhibited a value of 8.7% (PDE<sub>mon</sub> : TPTBTBP Pt<sub>mon</sub>). However, covalent attachment of the dyes to a polymer matrix showed a lower value for the quantum yield (3%<sup>12</sup>). However, to the best of our knowledge, distance measurements have not been reported with TTA-UC systems. Short distances between chromophores, however can lead to aggregation and self-quenching effects.<sup>12</sup> The statistical distribution of emitter molecules in a polymeric chain was reported as highly effective in TTA-UC systems by Hollauf.<sup>12</sup>

## 5.4.2 Light irradiance dependent measurements

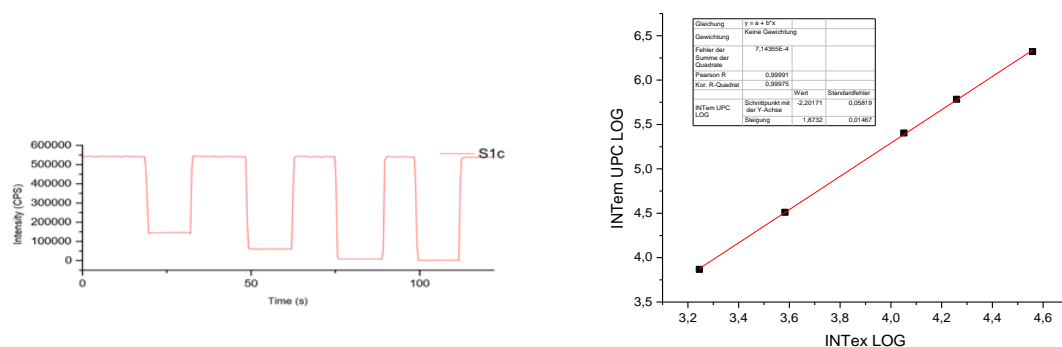


Figure 46. Quadratic dependence on excitation intensity of *polymer III* (left) and logarithmic plot of the TTA emission spectrum (right).

Light irradiance dependent measurements were performed using different transmission filter such as 50%, 30%, 10% and 5% to decrease the excitation light. By doing that, a non-linear process such as TTA-UC was identified and a quadratic

dependence on excitation intensity (Figure 46, left) was shown. Non-linear processes like TTA-UC exhibit a slope of around 2, which means that the process is below saturation (Figure 46, right).<sup>65</sup> This value of saturation also implies, that higher values of the TTA-UC can be obtained with at a higher excitation energy. The correlation coefficients ( $R^2=0.99$ ) suggested well linear fits (see appendix, Figure A 8 - Figure A 13). The results indicated that the triplet decay pathway was (quasi) first order (phosphorescence, quenching, and intersystem crossing).<sup>12,66</sup> Due to a constant baseline, the polymer solutions were assumed to be photostable. Photostability is an excellent feature, as this property is of particular interest for practical applications such as in up-conversion.<sup>65</sup> The benzoporphyrin derivatives may become unstable against oxidation and reduction by destabilization of the third LUMO and the first HOMO of the porphyrin due to  $\pi$ -ring expansion.<sup>65</sup> Photostability<sup>51</sup> is an important aspect, especially in practical applications, such as in high light density applications or long-term measurements.

## 6. Outlook and Conclusions

The goal of the master thesis was the investigation of the sensitizer-emitter distance in star polymers and the dependence on the triplet-triplet annihilation photon up-conversion (TTA-UC) quantum yields. In TTA-UC, two dyes a so-called sensitizer and an emitter were used to interact with each other. By the excitation of the sensitizer at a low excitation energy, the first singlet excited state of the sensitizer was produced. Multiple energy transfer steps followed, such as intersystem crossing, formation of the triplet excited state of the sensitizer, triplet-triplet energy transfer from the sensitizer to the emitter, and, the most important, triplet-triplet annihilation. The annihilation of two excited emitter triplet states leads to an excited singlet state of higher energy, which decays radiatively. Photons of higher energy are produced, which relax to the ground state. The radiative decay is observable as anti-Stokes fluorescence. The sensitizer and emitter dyes were synthesized before they were applied as monomers for the star polymers. Platinum (II) benzoporphyrin monomers which act as sensitizers in TTA-UC were synthesized in a five-step reaction pathway (melting process, demetallation, platination, Suzuki-Miyaura cross-coupling, and Steglich esterification). The perylene diester monomers, which acted as emitters in TTA-UC were also synthesized by three steps (saponification, esterification and Schotten-Baumann esterification) and characterized. In order to produce polymers with low polydispersity indices and equal chain lengths, reversible deactivation radical polymerization techniques were tested with the monomers. After low yields were obtained with ATR polymerization, which was reasoned by the interaction of the metals and the sterically demanding nature, RAFT polymerization was the method of choice. The RAFT process has several advantages as a synthetic method because it does not require a metal additive<sup>39</sup> and it is applicable to a wide range of monomers. Preliminary experiments were performed in order to establish the optimal reaction conditions, which were the exclusion of oxygen, the purity of the initiator AIBN and the removal of inhibitors from the monomers. Furthermore, due preliminary experiments, the matrix monomer was selected according to several criteria. The results of MMA and MA were compared due to several factors such as material characteristics, reaction mechanism and application for TTA-UC experiments.

Due to the possible hybrid behavior of MMA, which is a combination of conventional chain-transfer and free radical polymerization during the RAFT polymerization of MMA, MA was instead chosen as a matrix. After the preliminary experiments, three final star polymers were synthesized. The star polymers contained a platinum (II) benzoporphyrin as a center with four polymeric arms emanating. The arms consisted of a statistical copolymer of perylene diester and methyl acrylate as a matrix. From the GPC measurements, bimodal molecular weight distributions were obtained indicating a low-molecular and a high-molecular fraction. The molecular weights determined by GPC were, however, far below the calculated ones. The calculated values of the number average molecular weights ( $M_n$ ), without separate integration of the peaks are given in the following: 5 100 g mol<sup>-1</sup> *polymer I*, 6 800 g mol<sup>-1</sup> *polymer II* and 5 100 g mol<sup>-1</sup> *polymer III*. The theoretical number average molecular weights ( $M_n$ ) were much higher as shown in the following: 13 100 g mol<sup>-1</sup> *polymer I*, 25 700 g mol<sup>-1</sup> *polymer II* and 46 200 g mol<sup>-1</sup> *polymer III*. The low molecular weights detected were caused with the reaction mechanism of the RAFT star polymerization following the R-group approach<sup>38</sup>, which limits monomer conversion and impedes the formation of long chains and high molecular masses. The reaction time was chosen to be 16 hours. It was not investigated, if a longer reaction time would have yielded polymers with longer chain lengths. However, long reaction times in RAFT polymerization can also have a negative impact, as termination events are more likely to occur. The formation of dead chains is linked to RAFT polymerization and the formation of dead chains is especially observed at prolonged reaction times and at the presence of oxygen. However, as the reaction vessels were degassed, termination by oxygen was not favorable but could not be completely excluded. The covalent linkage of perylene diester monomer, which was used as an emitter molecule in TTA-UC, was also disputed, as the perylene diester monomer precipitated in n-pentane due to low solubility. It was assumed that the perylene diester monomer was covalently attached, however to a limited extend. This could be an interesting aspect to investigate in further studies. Therefore, the results obtained for TTA-UC, which were carried out in solution, have to be regarded with some precaution. We did not conduct concentration studies, which could be performed in further studies after adaption of the strategy. To sum up, in this master thesis, preliminary

experiments for the synthesis of star polymers by RAFT polymerization were performed, which only few authors reported in the context of TTA-UC before.

## 7. References

- 1 S. M. Borisov, C. Larndorfer and I. Klimant, *Adv. Funct. Mater.*, 2012, **22**, 4360–4368.
- 2 S. M. Borisov, G. Zenkl and I. Klimant, *ACS Appl. Mater. Interfaces*, 2010, **2**, 366–374.
- 3 M. Quaranta, S. M. Borisov and I. Klimant, *Bioanal. Rev.*, 2012, **4**, 115–157.
- 4 L. Wu, R. McHale, G. Feng and X. Wang, *Int. J. Polym. Sci.*, , DOI:10.1155/2011/109693.
- 5 L. R. H. High, S. J. Holder and H. V. Penfold, *Macromolecules*, 2007, **40**, 7157–7165.
- 6 N. Qiu, Y. Li, S. Han, G. Cui, T. Satoh, T. Kakuchi and Q. Duan, *J. Photochem. Photobiol. A Chem.*, 2014, **283**, 38–44.
- 7 J. B. Beil and S. C. Zimmerman, *Macromolecules*, 2004, **37**, 778–787.
- 8 G. I. Dzhardimalieva and I. E. Uflyand, *Dalt. Trans.*, 2017, **46**, 10139–10176.
- 9 M. Jaymand, M. Hatamzadeh and Y. Omid, *Prog. Polym. Sci.*, 2015, **47**, 26–69.
- 10 Z. Zhang, P. Zhang, Y. Wang and W. Zhang, *Polym. Chem.*, 2016, **7**, 3950–3976.
- 11 Z. Yang, Y. Yuan, R. Jiang, N. Fu, X. Lu, C. Tian, W. Hu, Q. Fan and W. Huang, *Polym. Chem.*, 2014, **5**, 1372–1380.
- 12 M. Hollauf, P. W. Zach, S. M. Borisov, B. J. Müller, D. Beichel, M. Tscherner, S. Köstler, P. Hartmann, A.-C. Knall and G. Trimmel, *J. Mater. Chem. C*, 2017, **5**, 7535–7545.
- 13 J. Zhao, S. Ji and H. Guo, *RSC Adv.*, 2011, **1**, 937.

- 14 T. N. Singh-Rachford and F. N. Castellano, *Coord. Chem. Rev.*, 2010, **254**, 2560–2573.
- 15 C. A. Parker and C. G. Hatchard, *J. Phys. Chem.*, 1962, **66**, 2506–2511.
- 16 S. H. Lee, M. A. Ayer, R. Vadrucci, C. Weder and Y. C. Simon, *Polym. Chem.*, 2014, **5**, 6898–6904.
- 17 J. H. Kim and J. H. Kim, *J. Am. Chem. Soc.*, 2012, **134**, 17478–17481.
- 18 R. Vadrucci, C. Weder and Y. C. Simon, *Mater. Horiz.*, 2015, **2**, 120–124.
- 19 Y. C. Simon and C. Weder, *J. Mater. Chem.*, 2012, **22**, 20817–20830.
- 20 A. Monguzzi, J. Mézyk, F. Scotognella, R. Tubino and F. Meinardi, *Phys. Rev. B - Condens. Matter Mater. Phys.*, 2008, **78**, 2–6.
- 21 X. Jiang, X. Guo, J. Peng, D. Zhao and Y. Ma, *ACS Appl. Mater. Interfaces*, 2016, **8**, 11441–11449.
- 22 T. Rudolph, S. Crotty, U. S. Schubert and F. H. Schacher, *E-Polymers*, 2015, **15**, 227–235.
- 23 L. Ye, Z. Ou, Y. Fang, S. Xue, Y. Song, L. Wang, M. Wang and K. M. Kadish, *RSC Adv.*, 2015, **5**, 77088–77096.
- 24 G. Seybold and G. Wagenblast, 1989, **11**, 303–317.
- 25 X. Cui, A. Charaf-Eddin, J. Wang, B. Le Guennic, J. Zhao and D. Jacquemin, *J. Org. Chem.*, 2014, **79**, 2038–2048.
- 26 Y. Sun and Z. Li, *Polym. Chem.*, 2017, **8**, 4422–4427.
- 27 S. H. Lee, D. C. Thévenaz, C. Weder and Y. C. Simon, *J. Polym. Sci. Part A Polym. Chem.*, 2015, **53**, 1629–1639.
- 28 R. Vadrucci, C. Weder and Y. C. Simon, *J. Mater. Chem. C*, 2014, **2**, 2837–2841.
- 29 P. C. Boutin, K. P. Ghiggino, T. L. Kelly and R. P. Steer, *J. Phys. Chem.*

- Lett.*, 2013, **4**, 4113–4118.
- 30 A. J. Tilley, M. J. Kim, M. Chen and K. P. Ghiggino, *Polym. (United Kingdom)*, 2013, **54**, 2865–2872.
- 31 G. Moad, E. Rizzardo and S. H. Thang, *Aust. J. Chem.*, 2009, **62**, 1402–1472.
- 32 J. Chiefari, Y. K. Chong, F. Ercole, J. Krstina, J. Jeffery, T. P. T. Le, R. T. A. Mayadunne, G. F. Meijs, C. L. Moad, G. Moad, E. Rizzardo and S. H. Thang, *Macromolecules*, 1998, **31**, 5559–5562.
- 33 S. Perrier, C. Barner-Kowollik, J. F. Quinn, P. Vana and T. P. Davis, *Macromolecules*, 2002, **35**, 8300–8306.
- 34 A. Favier and M. T. Charreyre, *Macromol. Rapid Commun.*, 2006, **27**, 653–692.
- 35 W. A. Braunecker and K. Matyjaszewski, *Prog. Polym. Sci.*, 2007, **32**, 93–146.
- 36 A. Filippov, E. Chernikova, V. Golubev, G. Gryn'ova, C. Yeh Lin and M. L. Coote, *InTech*, 2012, 407–136.
- 37 T. G. McKenzie, Q. Fu, M. Uchiyama, K. Satoh, J. Xu, C. Boyer, M. Kamigaito and G. G. Qiao, *Adv. Sci.*, 2016, **3**, 1–9.
- 38 D. Boschmann and P. Vana, *Macromolecules*, 2007, **40**, 2683–2693.
- 39 M. H. Stenzel and T. P. Davis, *J. Polym. Sci. Part A Polym. Chem.*, 2002, **40**, 4498–4512.
- 40 C. Rossner, Q. Tang, O. Glatter, M. Müller and P. Vana, *Langmuir*, 2017, **33**, 2017–2026.
- 41 M. H. Stenzel, in *Handbook of RAFT Polymerization*, ed. C. Barner-Kowollik, Wiley-VCH, Weinheim, 2008, pp. 343–349.
- 42 H. Mori and H. Ookuma, *Macromolecules*, 2008, 6925–6934.

- 43 Y. Kwak, A. J. D. Magenau and K. Matyjaszewski, *Macromolecules*, 2011, **44**, 811–819.
- 44 K. Matyjaszewski, P. J. Miller, J. Pyun, G. Kickelbick and S. Diamanti, *Macromolecules*, 1999, **32**, 6526–6535.
- 45 T. Pintauer and K. Matyjaszewski, *Chem. Soc. Rev.*, 2008, **37**, 1087.
- 46 K. Matyjaszewski, S. Coca, S. G. Gaynor, M. Wei and B. E. Woodworth, *Macromolecules*, 1997, **30**, 7348–7350.
- 47 G. Lligadas, B. M. Rosen, M. J. Monteiro and V. Percec, *Macromolecules*, 2008, **41**, 8360–8364.
- 48 H. Gao and K. Matyjaszewski, *Macromolecules*, 2006, **39**, 3154–3160.
- 49 J. Burdyńska, H. Y. Cho, L. Mueller and K. Matyjaszewski, *Macromolecules*, 2010, **43**, 9227–9229.
- 50 R. T. A. Mayadunne, J. Jeffery, G. Moad and E. Rizzardo, *Macromolecules*, 2003, **36**, 1505–1513.
- 51 L. H. Hutter, B. J. Müller, K. Koren, S. M. Borisov and I. Klimant, *J. Mater. Chem. C*, 2014, **2**, 7589–7598.
- 52 Y. Tao, Q. Xu, N. Li, J. Lu, L. Wang and X. Xia, *Polymer (Guildf.)*, 2011, **52**, 4261–4267.
- 53 J. Clayden, N. Greeves, S. Warren and P. Wothers, *Organic Chemistry*, Oxford University Press, New York, 2nd edn., 2001.
- 54 J. Zhao, *Chem. Soc. Rev.*, 2013, **42**, 5323–5351.
- 55 R. M. Paulus, C. R. Becer, R. Hoogenboom and U. S. Schubert, *Aust. J. Chem.*, 2009, **62**, 254–259.
- 56 G. Johnston-Hall, A. Theis, M. J. Monteiro, T. P. Davis, M. H. Stenzel and C. Barner-Kowollik, *Macromol. Chem. Phys.*, 2005, **206**, 2047–2053.
- 57 G. Moad and C. Barner-Kowollik, in *Handbook of RAFT Polymerization*,

- ed. C. Barner-Kowollik, Wiley-VCH, Weinheim, 2008, p. 58 and 89.
- 58 P. Moschogianni, S. Pispas and N. Hadjichristidis, *J. Polym. Sci. Part A Polym. Chem.*, 2001, **39**, 650–655.
- 59 M. R. Hill, R. N. Carmean and B. S. Sumerlin, *Macromolecules*, 2015, **48**, 5459–5469.
- 60 D. M. Haddleton, A. J. Clark, D. J. Duncalf, A. M. Heming, D. Kukulj and A. J. Shooter, 1998, **2**, 381–385.
- 61 D. M. Haddleton, D. J. Duncalf, D. Kukulj, A. M. Heming, A. J. Shooter and A. J. Clark, *J. Mater. Chem.*, 1998, **8**, 1525–1532.
- 62 Horst Friebolin, *Ein- und zweidimensionale NMR-Spektroskopie*, Wiley-VCH, Weinheim, 5th edn., 2013.
- 63 F. de Loos, I. C. Reynhout, J. J. L. M. Cornelissen, A. E. Rowan and R. J. M. Nolte, *Chem. Commun.*, 2005, 60–62.
- 64 K. Matyjaszewski and J. Xia, *Chem. Rev.*, 2001, **101**, 2921–2990.
- 65 P. W. Zach, S. A. Freunberger, I. Klimant and S. M. Borisov, *ACS Appl. Mater. Interfaces*, 2017, **9**, 38008–38023.
- 66 Y. Y. Cheng, T. Khoury, R. G. C. R. Clady, M. J. Y. Tayebjee, N. J. Ekins-Daukes, M. J. Crossley and T. W. Schmidt, *Phys. Chem. Chem. Phys.*, 2010, **12**, 66–71.

## 8. List of Tables

Table 1. Determined number average molecular weights and polydispersity indices for <i>polymer I</i> , <i>polymer II</i> and <i>polymer III</i> .....	79
Table 2. Quantum efficiencies by excitation with the lamp resp. laser source. Measurements were performed in 1,4-dioxane solution. $M_n$ and $M_w/M_n$ were determined by gel phase chromatography. ....	90

## 9. List of Figures

Figure 1. Scheme of the steps involved in the TTA-UC. <sup>12</sup> .....	14
Figure 2. General structure of porphyrin. ....	16
Figure 3. Structure of diisobutyl perylene-3,9-dicarboxylate (Solvent Green 5). .....	17
Figure 4. Polymers prepared by RAFT polymerization, carrying Ru(bpy) <sub>3</sub> and DPA units. <sup>29</sup> Copyright (2013) Elsevier. ....	19
Figure 5. Covalent attachment of PdmPH3PMA, MMA and DPAMA. <sup>27</sup> Copyright (2015) John Wiley and Sons. ....	20
Figure 6. Covalent attachment of PDE, TPTBTBP Pt and DME by Hollauf and Zach. <sup>12</sup> .....	20
Figure 7. Mechanism of RAFT polymerization. <sup>33</sup> .....	22
Figure 8. Structure of a thiocarbonylthio RAFT agent. ....	23
Figure 9. Star polymer synthesis following Z group approach (above) and R group approach (below) respectively.....	24
Figure 10. General ATRP mechanism of copper/2,2'-bipyridine. <sup>45</sup> Copyright (2008) Royal Society of Chemistry.....	26
Figure 11. Overall reaction pathway for the synthesis of the benzoporphyrin monomers. ....	33
Figure 12. Melting reaction for the synthesis of Br <sub>4</sub> TPTBTBP Zn.....	34
Figure 13. Demetallation reaction of Br <sub>4</sub> TPTBTBP Zn. ....	35
Figure 14. Platination reaction yielding Br <sub>4</sub> TPTBTBP Pt. ....	36
Figure 15. Suzuki-Miyaura cross-coupling reaction yielding HMP <sub>4</sub> TPTBTBP Pt. .....	37
Figure 16. Steglich esterification reaction yielding BPMP <sub>4</sub> TPTBTBP Pt.....	38
Figure 17. Steglich esterification reaction yielding Br <sub>2</sub> BPMP <sub>2</sub> TPTBTBP Pt....	40
Figure 18. Steglich esterification reaction of HMP <sub>4</sub> TPTBTBP Pt.....	41
Figure 19. Steglich esterification reaction of Br HMP <sub>3</sub> TPTBTBP Pt. ....	43
Figure 20. Overall reaction scheme of the synthesis of the PDE monomer. ....	45
Figure 21. Saponification reaction for the synthesis of PDC. ....	46
Figure 22. Esterification reaction yielding PDE. ....	47
Figure 23. Schotten-Baumann reaction for the synthesis of PDE <sub>mon</sub> .....	48
Figure 24. Statistical perylene-MA-copolymer.....	51
Figure 25. Statistical perylene-MMA-copolymer.....	53
Figure 26. Benzoporphyrin-MA star polymer.....	54
Figure 27. Benzoporphyrin-MMA star polymer.....	55
Figure 28. Statistical benzoporphyrin-MA-perylene star polymer. ....	56
Figure 29. Statistical benzoporphyrin-MMA-perylene star polymer. ....	57
Figure 30. Structure of polymer I.....	59
Figure 31. Structure of polymer II.....	60
Figure 32. Structure of polymer III.....	62
Figure 33. ATRP of PMMA.....	65
Figure 34. ATRP of Br <sub>2</sub> BPMP <sub>2</sub> TPTBTBP Pt with MMA. ....	66
Figure 35. UV-VIS absorption spectra for the identification of Br <sub>4</sub> TPTBTBP Zn, Br <sub>4</sub> TPTBTBP and Br <sub>4</sub> TPTBTBP Pt. ....	69

Figure 36. Absorption and emission spectra for HTP <sub>4</sub> TPTBTP Pt and PDE <sub>mon</sub> .	75
Figure 37. Molecular weight distribution curve of preliminary experiments yielding the three-armed (benzoporphyrin-(MMA) <sub>100</sub> – perylene) star polymer (GPC, solvent: chloroform).....	78
Figure 38. Molecular weight distribution curve of preliminary experiments yielding the three-armed (benzoporphyrin-(MA) <sub>100</sub> – perylene) star polymer (GPC, solvent: chloroform).....	78
Figure 39. Peak shapes obtained from the GPC analysis. ....	80
Figure 40. <sup>1</sup> H NMR spectrum of <i>polymer I</i> (benzoporphyrin - (MA) <sub>100</sub> – perylene star polymer). ....	82
Figure 41. MALDI-TOF MS spectrum of <i>polymer I</i> utilizing sodium dithranol as a matrix. ....	84
Figure 42. <sup>1</sup> H-NMR spectrum of PMMA synthesized by ATRP.....	85
Figure 43. ATRP synthesis of a porphyrin-core star molecule, applying MMA as a matrix. <sup>5</sup> Copyright (2007) American Chemical Society.....	86
Figure 44. Green fluorescence determined by excitation with a laser diode at 635 nm ( <i>polymer I</i> , 1,4-dioxane). ....	89
Figure 45. TTA emission spectrum of <i>polymer I</i> .....	89
Figure 46. Quadratic dependence on excitation intensity of <i>polymer III</i> (left) and logarithmic plot of the TTA emission spectrum (right). ....	91

## 10. Appendix

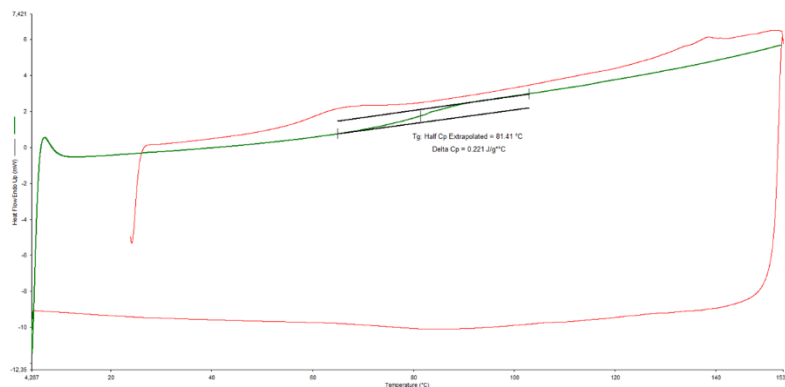


Figure A 1. DSC of PMMA synthesized by ATRP.

Table A 1. Preparation of the stock solutions for ATRP experiments (4.2.3.2).

	<b>M [g mol<sup>-1</sup>]</b>	<b>m [g]</b>	<b>n [mmol]</b>	<b>Solvent[mL]</b>	<b>Stock solution [g L<sup>-1</sup>]</b>
<i>2,2'-Bipyridine</i>	156.19	0.00285	0.0182	0.2	14.25
<i>Br2 BPMP2 TBPTBTBP Pt</i>	1887.30	0.00547	0.0029	0.25	21.88

Table A 2. Average molecular weights and polymer indices of polymers I, II and III.

<b>Polymer</b>	<b>Theoretical chain lengths per arm</b>	<b>M<sub>n</sub> [g mol<sup>-1</sup>]</b>	<b>M<sub>w</sub> [g mol<sup>-1</sup>]</b>	<b>M<sub>z</sub> [g mol<sup>-1</sup>]</b>	<b>PDI</b>
<i>I</i>	100	5120	6808	9482	1.33
<i>II</i>	250	6829	10910	15550	1.59
<i>III</i>	500	5057	6587	8644	1.30

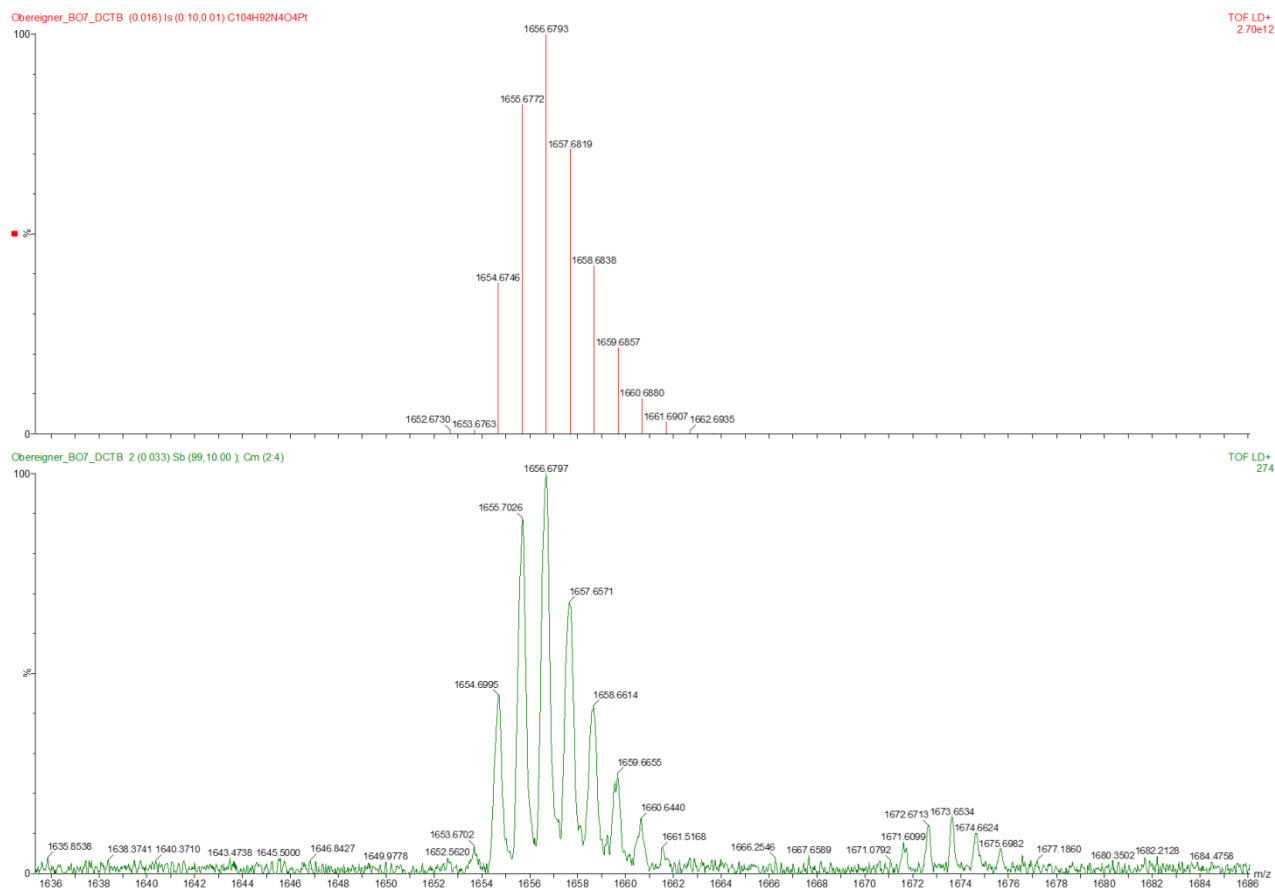


Figure A 2. MALDI-TOF MS of Pt(II) tetrahydroxymethylphenyl *meso*-tetraphenyl tetra(*tert*-butyl)-benzoporphyrin (HMP<sub>4</sub> TPTBTBP Pt). Calculated m/z [M<sup>+</sup>] calc. for C<sub>104</sub>H<sub>92</sub>N<sub>4</sub>O<sub>4</sub>Pt: 1656.6793; found, 1656.6797.

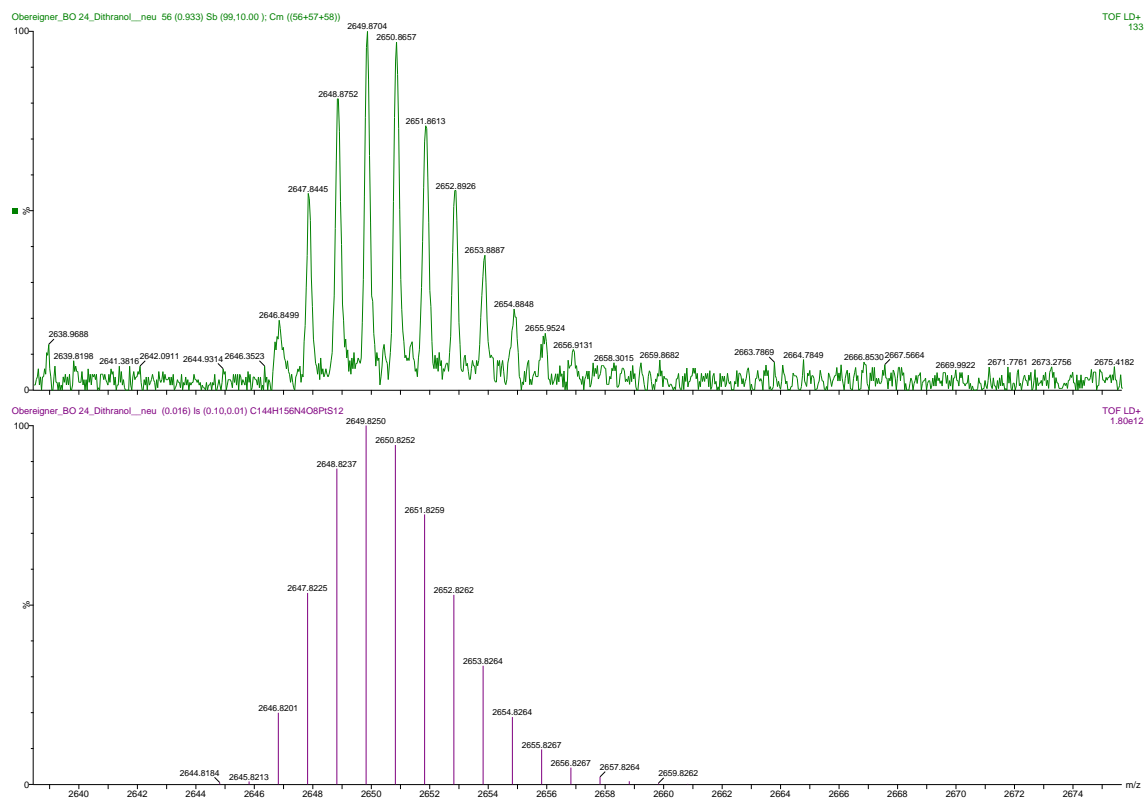


Figure A 3. MALDI-TOF MS of Pt(II) tetra(((2-hexylthio)thioxomethyl)thiopropionatemethylphenyl) *meso*-tetraphenyl tetra(*tert*-butyl)-benzoporphyrin (HTP<sub>4</sub> TPTBTBP Pt). Calculated  $m/z$  [ $M^+$ ] calc. for C<sub>144</sub>H<sub>156</sub>N<sub>4</sub>O<sub>8</sub>PtS<sub>12</sub>: 2649.8704; found, 2649.8250.

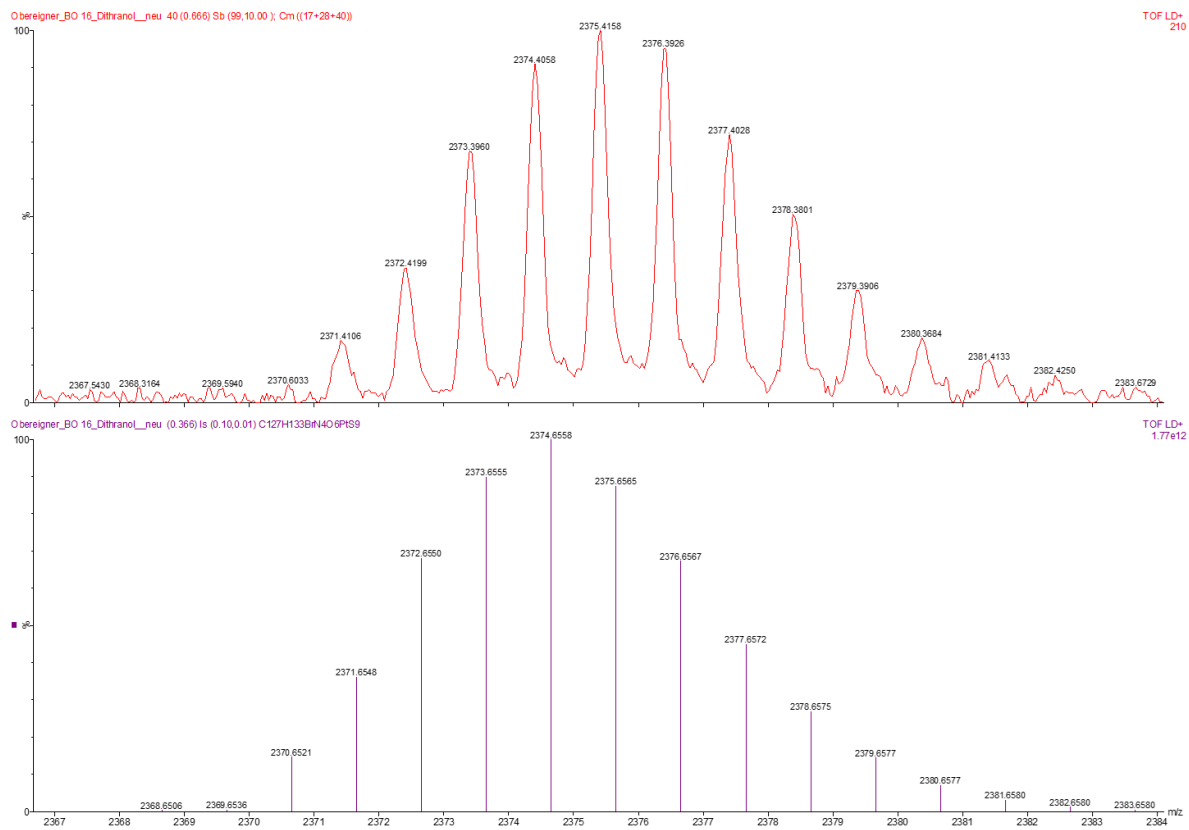


Figure A 4. MALDI-TOF MS of Pt(II) tri(((2-hexylthio)thioxomethyl)thiopropionatemethylphenyl) monobromo *meso*-tetraphenyl tetra(*tert*-butyl)-benzoporphyrin (Br HTP<sub>3</sub> TPT-BTBP Pt). Calculated m/z [M<sup>+</sup>] calc. for C<sub>127</sub>H<sub>133</sub>BrN<sub>4</sub>O<sub>6</sub>PtS<sub>9</sub>: 2374.6558; found, 2375.4158.

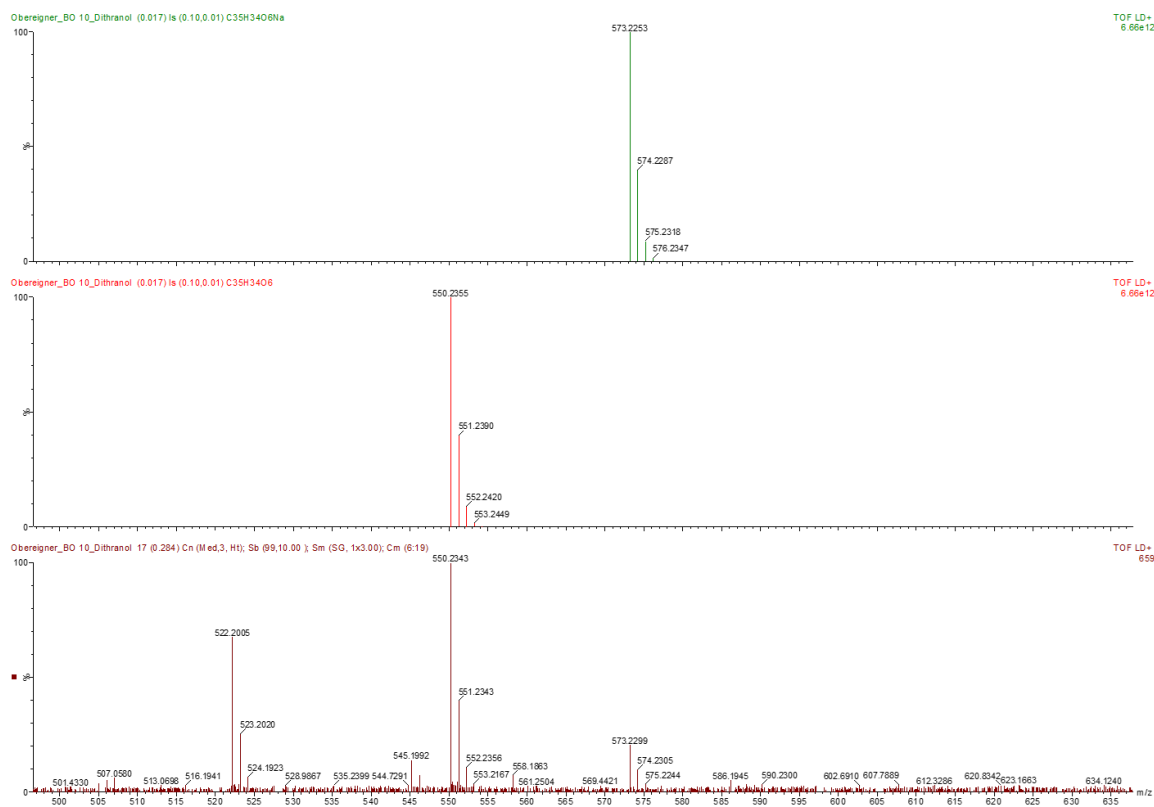


Figure A 5. MALDI-TOF MS of 3-(6-(acryloyloxy)hexyl)9-butyl perylene-3,9-dicarboxylate ( $PDE_{mon}$ ). Calculated  $m/z$  [ $M^+$ ] calc. for  $C_{127}H_{133}BrN_4O_6PtS_9$ : 550.2355; found, 550.2343.

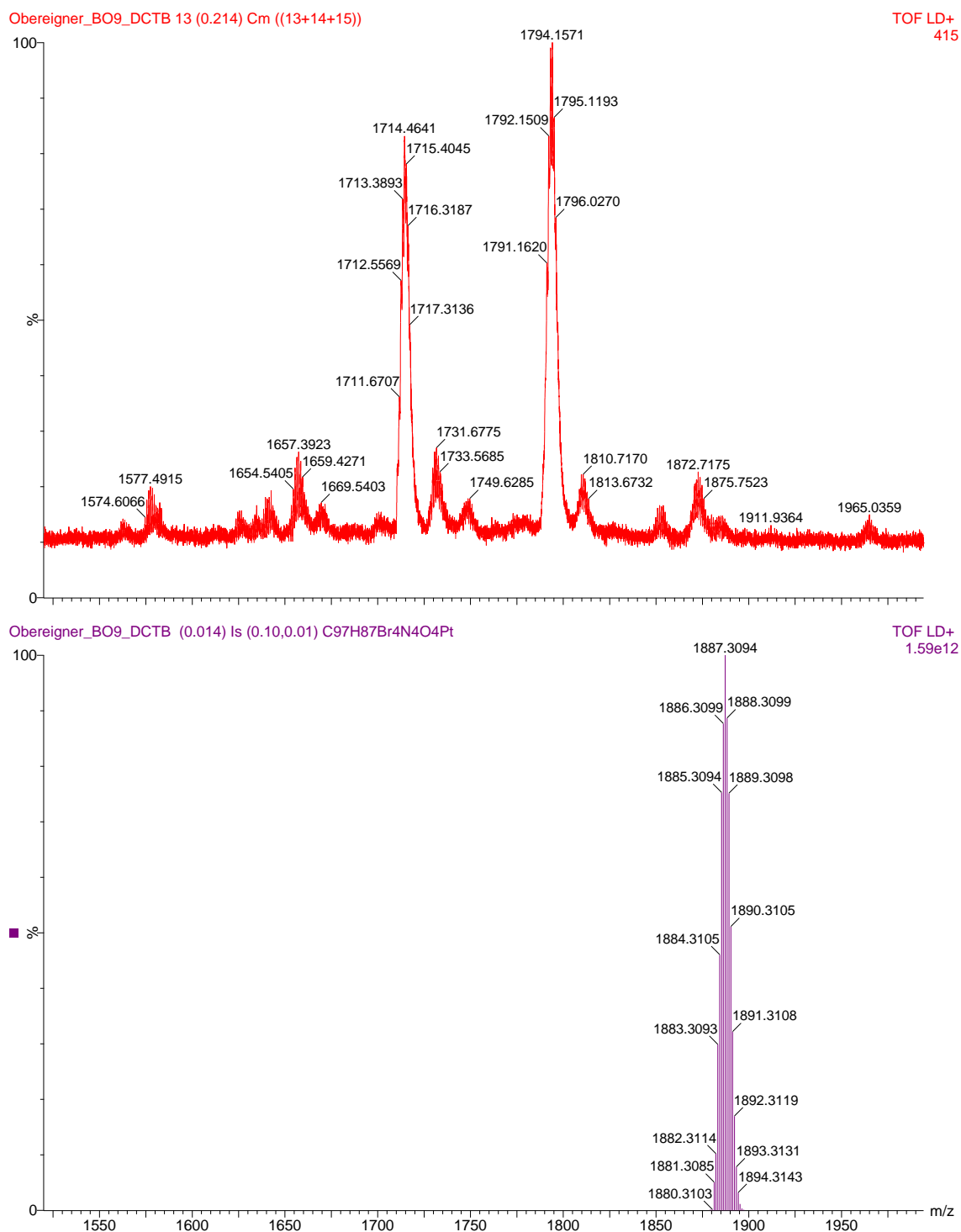


Figure A 6. MALDI-TOF MS of dibromo di(2-bromopropanoatemethylphenyl) *meso*-tetraphenyl tetra(*tert*-butyl)-benzoporphyrin (Br<sub>2</sub> BPMP<sub>2</sub> TPTBTBP Pt). Calculated m/z [M<sup>+</sup>] calc. for C<sub>97</sub>H<sub>87</sub>Br<sub>4</sub>N<sub>4</sub>O<sub>4</sub>Pt: 1887.3094; found, 1794.1571.

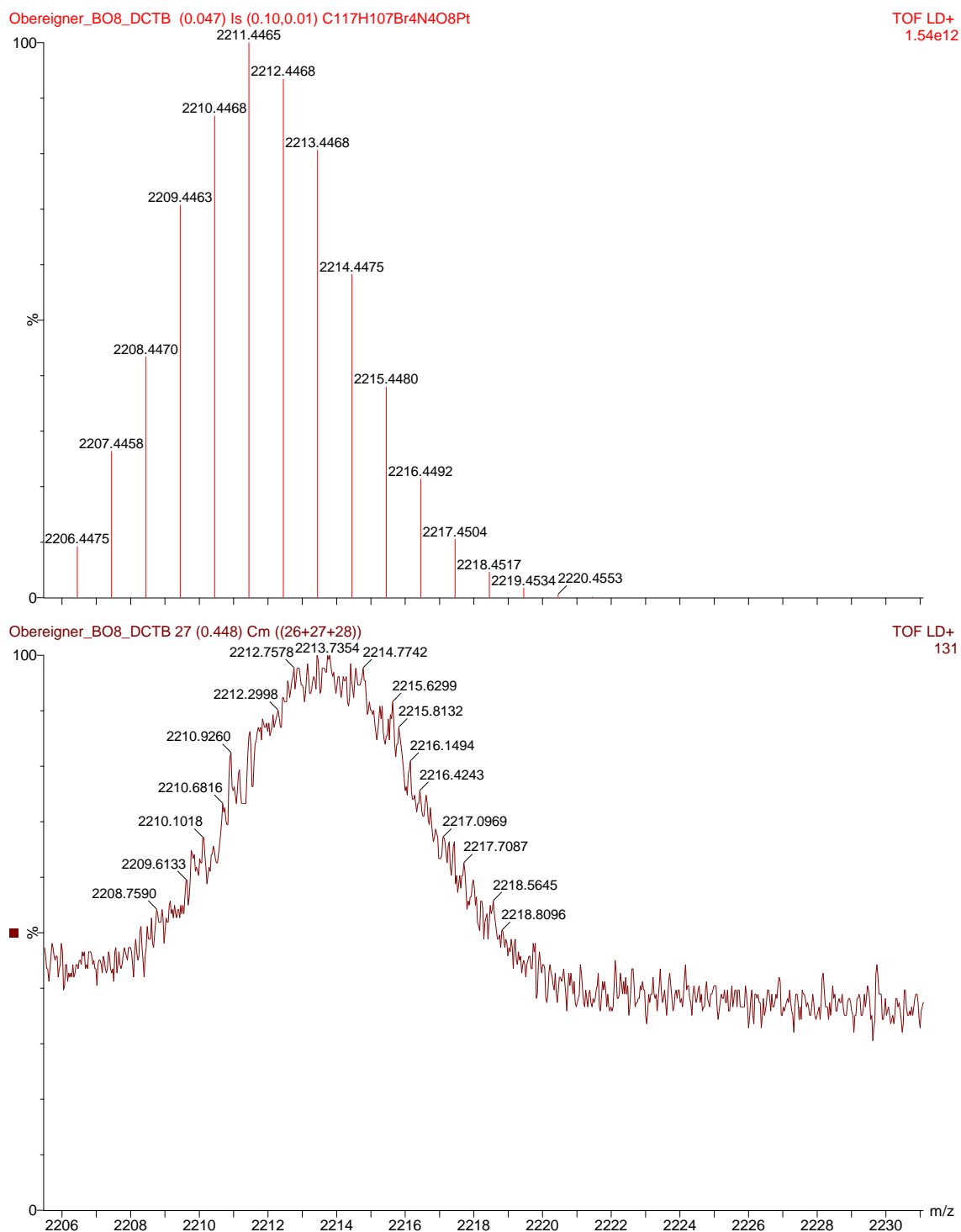


Figure A 7. MALDI-TOF MS of tetra(2-bromopropanoatemethylphenyl) *meso*-tetraphenyl tetra(*tert*-butyl)-benzoporphyrin (BPMP<sub>4</sub> TPTBTBP Pt). Calculated m/z [M<sup>+</sup>] calc. for C<sub>117</sub>H<sub>107</sub>Br<sub>4</sub>N<sub>4</sub>O<sub>8</sub>Pt: 2211.4465; found, 2213.7354.

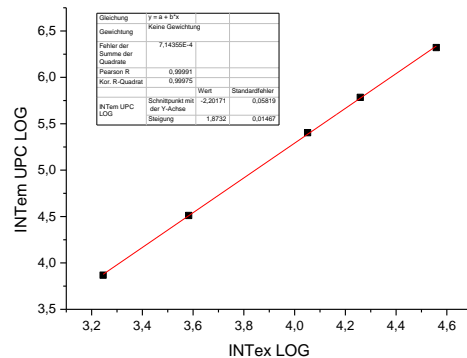
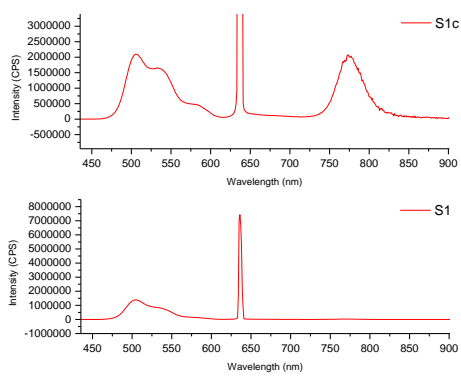


Figure A 8. TTA-UC spectrum of *polymer I* and the corresponding double logarithmic plot of energy dependent UC measurements (excitation with a laser diode:  $36\ 200\ \mu\text{mol s}^{-1}\ \text{m}^{-2}$ ).

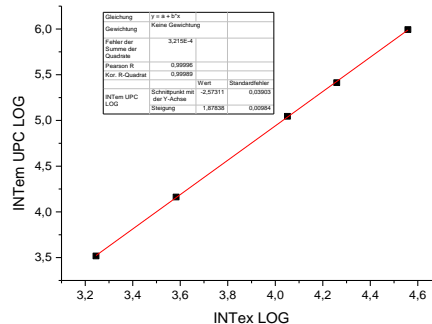
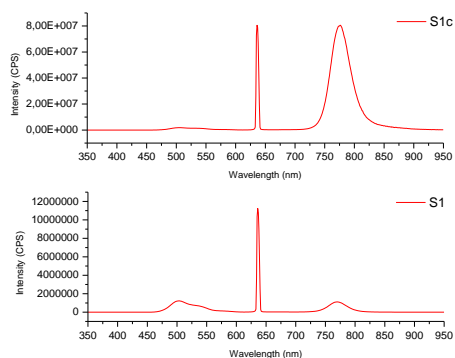


Figure A 9. TTA-UC spectrum of *polymer II* and the corresponding double logarithmic plot of energy dependent UC measurements (excitation with a laser diode:  $36\ 200\ \mu\text{mol s}^{-1}\ \text{m}^{-2}$ ).

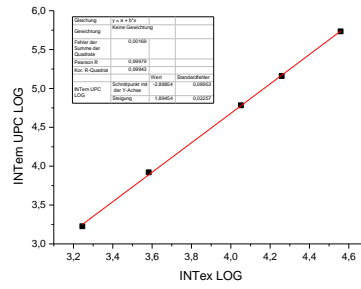
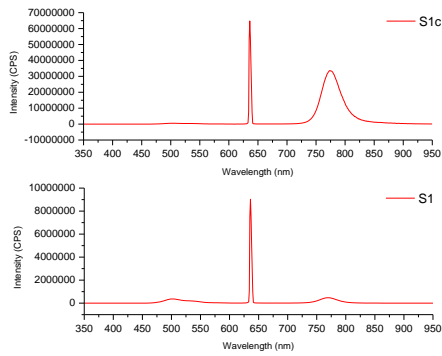


Figure A 10. TTA-UC spectrum of *polymer III* and the corresponding double logarithmic plot of energy dependent UC measurements (excitation with a laser diode:  $36\ 200\ \mu\text{mol s}^{-1}\ \text{m}^{-2}$ ).

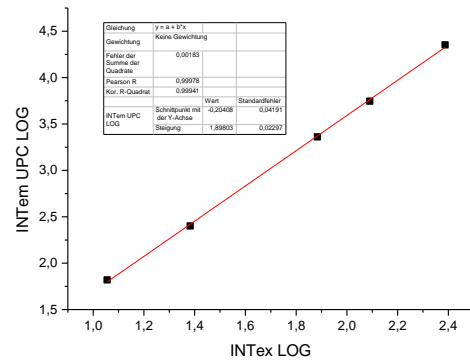
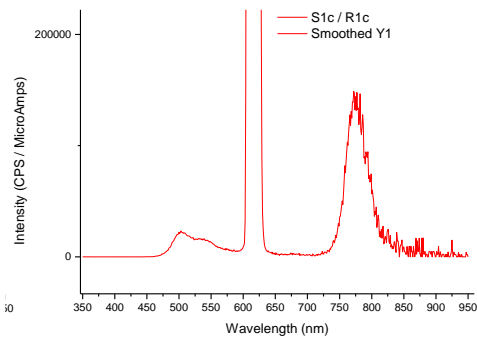


Figure A 11. TTA-UC spectrum of *polymer I* and the corresponding double logarithmic plot of energy dependent UC measurements (excitation with a 450W Xe lamp:  $244\ \mu\text{mol s}^{-1}\ \text{m}^{-2}$ ).

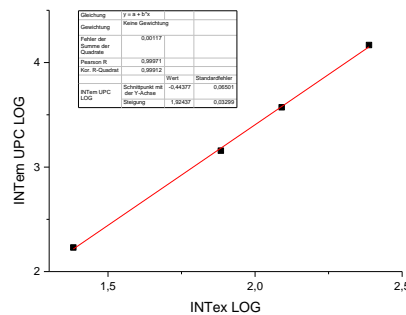
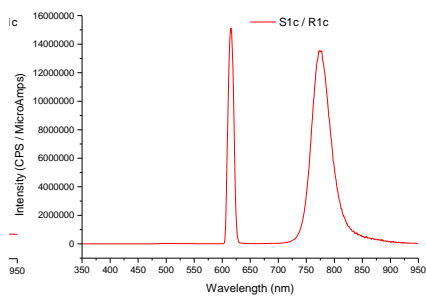


Figure A 12. TTA-UC spectrum of *polymer II* and the corresponding double logarithmic plot of energy dependent UC measurements (excitation with a 450W Xe lamp:  $244\ \mu\text{mol s}^{-1}\ \text{m}^{-2}$ ).

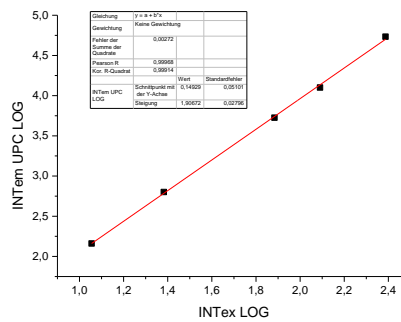
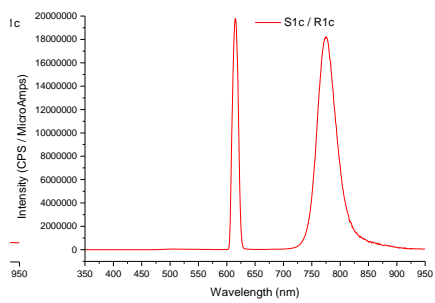


Figure A 13. TTA-UC spectrum of *polymer III* and the corresponding double logarithmic plot of energy dependent UC measurements (excitation with a 450W Xe lamp:  $244 \mu\text{mol s}^{-1} \text{m}^{-2}$ ).